



Faculty of Pharmacy, Nutritional Sciences and Health Care

Department of Pharmaceutical Sciences

“B. Telesio-Doctoral School of Science and Technique”

Mesophases and Molecular Materials

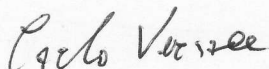
CHIM/02

XXIV cycle, PhD thesis

**Behavior and effects of additives
in liquid crystal compounds**

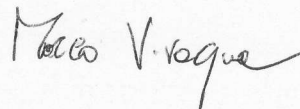
School Director
Prof. Roberto BARTOLINO

Curriculum Coordinator
Prof. Carlo VERSACE



Supervisor
Prof. Fiore P. NICOLETTA

Candidate
Marco VIVACQUA



Academic Year: 2010/2011

Author's e-mail: marco.vivacqua@unical.it
marco.wh2o@gmail.com

Author's address:
Department of Pharmaceutical Sciences
University of Calabria
Via Pietro Bucci, Ed. Polifunzionale
87036 Arcavacata di Rende, Cosenza

ph.: +39 0984 493266
ph.: +39 0984 466478
cell: +39 349 3253095

PLEDGE AGAINST PLAGIARISM

I, Marco Vivacqua, hereby confirm that the work submitted in this report is my own and that I have not violated the University of Calabria's policy on plagiarism.

Signature Marco Vivacqua

Date: 30/11/2011

Table of contents

Preface	1
<i>General Introduction, Aims and Organization of this Thesis</i>	1
1 <i>General Introduction</i>	1
2 <i>Aims of this thesis</i>	3
3 <i>Organization of this thesis</i>	3
Chapter 1- Liquid Crystal	5
1.1 <i>Liquid Crystals</i>	5
1.1.1 <i>Introduction</i>	5
1.1.2 <i>Chemical properties of liquid crystals</i>	10
1.1.3 <i>Phases of Liquid Crystal</i>	13
1.1.3.1 <i>Nematic Phase</i>	13
1.1.3.2 <i>Cholesteric Phase</i>	14
1.1.3.3 <i>Smectic Phase</i>	15
1.1.3.4 <i>Columnar Phase</i>	17
1.1.4 <i>Birefringence in Liquid Crystals</i>	17
1.1.5 <i>External Influences on Liquid Crystals</i>	18
1.1.6 <i>Liquid Crystal in nature</i>	21
1.2 <i>Polymer Liquid Crystals</i>	22
1.2.1 <i>Introduction</i>	22
1.2.2 <i>Main Chain Polymer Liquid Crystals</i>	23
1.2.3 <i>Side Chain Polymer Liquid Crystals</i>	24
1.2.4 <i>Phases of Polymer Liquid Crystals</i>	25
1.2.5 <i>Polymer-dispersed liquid crystals (PDLCs)</i>	26
1.2.6 <i>Applications of Polymer Liquid Crystals</i>	28
<i>References</i>	28

Chapter 2-Additives	30
2.1 Electrochromism	30
2.1.1 Electrochromism in Liquid Crystal.....	33
References	35
2.2 Ionic liquids	37
2.2.1 Property of Ionic liquid.....	38
References	39
2.3 Magnetism.....	40
References	45
2.4 Magnetic Particles	47
2.4.1. Magnetic Particles in biomedicine.....	48
2.4.2. Protection and Functionalization of MNPs.....	51
References	54
2.5 Ferrofluids.....	58
2.5.1 Applications	59
2.6 Lipoprotein.....	61
2.6.1 Cholesterol	62
2.6.2 Cholesterol as cause of vascular diseases	66
Reference	67
2.7 Liposomes	69
2.7.1 Types of liposomes.....	71
2.7.2 Manufacturing.....	72
2.7.3 Applications	72
References	74
Chapter 3-Results	76
3.1 Liquid crystals governing the electromigration	76
3.1.1 Materials and Preparation of Sample.....	78
3.1.2 Results and discussion.....	81
3.1.3 Conclusion	98
References	99
3.2 Liquid crystals governing the diffusion of magnetic particles	101
3.2.1 Materials and Preparation of Sample.....	102

3.2.2 Results and discussion.....	104
3.2.3 Conclusion.....	109
References	110
3.3 Liquid crystals that enhance the stability of surrounding environment (Fréedericksz Transition)....	112
3.3.1 Materials and Preparation of Sample.....	113
3.3.2 Results and discussion.....	116
3.3.3 Conclusion.....	123
References	123
3.4 Liquid crystals that improve the conductivity through the visible light.....	125
3.4.1 Materials and Preparation of Sample.....	128
3.4.2 Results and discussion.....	129
3.4.3 Conclusion.....	137
References	138
3.5 Lyotropic Liquid crystals and Ferrofluids in nonlinear optics.....	140
3.5.1 Materials and Preparation of Sample.....	141
3.5.2 Theoretical Background.....	143
3.5.2.1 Electronic nonlinear optical process	143
3.5.2.2 Thermal Lens.....	147
3.5.3 Experimental setup: The Z-scan technique	148
3.5.4 Results and discussion.....	153
3.5.5 Conclusion.....	162
References	162
3.6 Lyotropic liquid crystals as drug delivery system of doxorubicin.....	165
3.6.1 Materials and Preparation of niosomes	167
3.6.2 Qualitative/Quantitative measurement	168
3.6.2.1 Size and distribution analysis.....	168
3.6.2.2 Transmission electron microscopy (TEM)	168
3.6.2.3 Drug entrapment efficiency.....	168
3.6.2.4 Assay of magnetite	169
3.6.2.5 In vitro release studies.....	169
3.6.3 Results and discussion.....	169
3.6.4 Conclusion.....	172
References	173

Preface

General Introduction, Aims and Organization of this Thesis

1. General Introduction

The search for new exciting topics has led researchers to exploit any type of material.

Several studies have been done over the years to improve the characteristics of the materials and to expand the applications in the everyday life. Among these materials, one of the most spectacular examples for its impact on of citizens and for the fundamental nature of the issues present in their study, is that of liquid crystals.

The term “liquid crystal” was adopted by the international scientific community and, more recently, by the general public, even though his name will bring an apparent contradiction Due to their intrinsic characteristics between solid and liquid, these materials have been extensively studied and used for the implementation of systems and devices in medicine and technology.

Liquid crystals are systems of immense interest, due to the numerous physical phenomena involved, like phase transitions leading to rich polymorphism, ferroelectricity, nonlinear dynamics, etc.

The synergic combination of liquid crystals technology with polymeric science, drug delivery concepts and material technology offers new way to concept and develop new useful materials.

Thinking in this direction, it becomes crucial the need to study the interactions between liquid crystals and other materials.

In particular, from the simple idea of a slow release of the drug, are emerging new ways on controlling the pharmacokinetics and pharmacodynamics through

external factor (pH, Temperature, electric and magnetic field) based on interdisciplinary approaches that combine polymer science, pharmaceuticals, physical chemistry, and molecular biology.

The lyotropic liquid crystals, for example, are an interesting “*Drug Delivery System*” (DDS), since they are capable of incorporating large amounts of molecules or active ingredients with different physico-chemical properties.

Exploiting its biocompatibility and ability to incorporate other molecules, lyotropic liquid crystals can be loaded with magnetic particles and driven in specific tissues to treat e.g. a tumor. In this context, the use of new techniques for the recognition and specific treatment of cancer cells, could avoid invasive operations in areas difficult to reach.

On the other hand, even the thermotropic liquid crystals, to date neglected as DDS, could be very attractive. In fact, these could potentially affect the transport of active ingredients due to the different configuration of the director induced by surface treatments, applications of external fields or by the increase in temperature.

The discovery of liquid crystals from the audience, is mainly due to its applications in technology, in fact, besides applications in the medical field, the liquid crystal devices are very present in modern technology, just thinking of electro-optical devices, LCD screens, electronic displays (due to fast switching times) or surface temperature detectors. Among these many effort are working to improve the properties of *smart windows* devices to reduce the environmental impact produced by the heating and cooling of our buildings.

The constant search for new devices based on liquid crystals, evidenced by the number of papers that continue to publish, means that some aspects of liquid crystals are still undiscovered and that this technology still has much to offer the scientific community.

2 Aims of this thesis

The present thesis was realized in the Physical chemistry group, Department of Pharmaceutical Sciences (University of Calabria) and deals about the development of liquid crystals devices for technological and pharmaceutical applications. In particular, it is wanted focus the work on observation of the behavior of liquid crystals (thermotropic and lyotropic) mixed with other molecules, when subjected to external stimuli. Moreover, the research of possible applications, especially in the field of pharmaceutical technology, has led me to the study of biocompatible systems that can be used in medicine. For this reason, part of my work, based on biocompatible systems, was carried out during an interesting and fruitful scientific visiting at the Complex Fluids Group (Universidade de Sao Paulo) in the Physical Institute under the supervision of Professor Dr. Antonio Martins Figueiredo Neto and Dr. Daniel. Espinosa.

3 Organization of this thesis

The present thesis is divided into three self-contained chapter.

In the first two chapters will describe the characteristics of the materials used. In the first chapter an overview will be made on the different types and physico-chemical properties of liquid crystals.

In the second chapter will be introduced the physical-chemical phenomena observed during the experiments, and then we will describe all the additives used in the course of my research.

In the third chapter will be discussed the results of the experiments conducted and the instrumental setup used.

Due to the multitude projects, chapter three is divided into six self-contained sections.

The first section named: "Liquid crystals governing the electromigration" will be studied and characterized the spread of electrochromic molecules dissolved in the liquid crystal, so that by staining these testify to the spread from one electrode to

another. Also describes how to change the transmission time based on the orientation of the director in the sample and the life cycle of the device.

In the second paragraph will be taken into account the effect of magnetic field on magnetic particles. As in the previous section, we will describe the diffusion times of particles in the various liquid crystal' alignments.

The purpose of these two sections is to study the diffusion of various molecules in the liquid crystal in such a way to obtain all the information needed to create a device for the programmed release of drugs

The third section will describe as elongated molecules and magnetic particles, can stabilize the liquid crystal system, thereby raising the value of the threshold voltage able to generate a change in orientation of the director. (Freedericksz Transition)

The competition between surface anchoring and electric field re-orientation is often used in liquid crystal devices.

In the fourth section, will describe the study and characterization of a reverse mode PDLC, able to increase its electrical conductivity when exposed to visible light radiation. The purpose of this section is to create smart windows devices that are transparent when no power is applied and turn to opaque when required. Furthermore, the increase of the conductivity in the presence of visible light reduce the environmental impact, with a considerable saving of energy.

The fifth part, instead, contains all the experiments performed during my scientific visiting in the Universidade de São Paulo aimed at the development of the study of nonlinear optics (absorption and refraction), through the Z-scan technique, of oil- and water-based ferrofluid and cholesterol. The study of these compounds may be useful for future applications of biotechnology and drug delivery systems.

The last part of this chapter concerns the preparation of magneto liposomes Doxorubicin-based for the treatment of cancer. In this section are described the analytical method to obtain magnetic liposomes and the release studies *in vitro*.

1

Liquid Crystal

1.1 Liquid Crystals

1.1.1 Introduction

Although applications of liquid crystals in displays have been spread more widely in the early 70s of the twentieth century, the study of liquid crystals began in 1888 when an Austrian botanist named Friedrich Reinitzer observed that a material known as cholesteryl benzoate (a cholesterol derivative) (Fig. 1.1) had two distinct melting points.^[1]

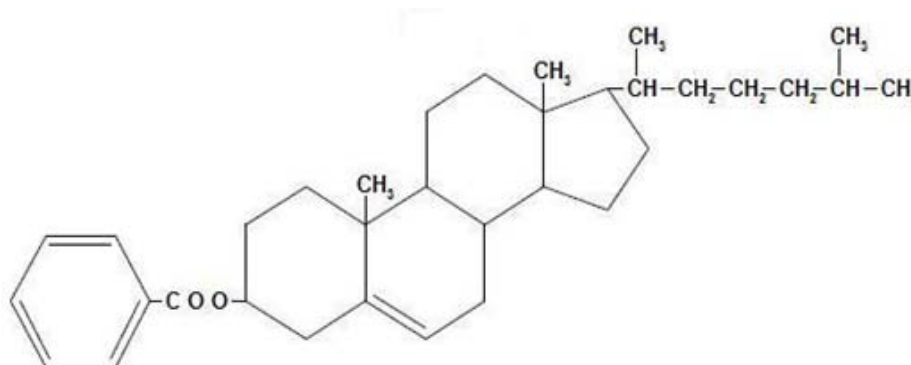


Fig. 1.1 Molecular structure of cholesteryl benzoate

In his experiments Reinitzer had observed, depending on the temperature, the thermo-optical properties of this material: firstly, the material transitioned from solid crystalline to “translucent liquid” or milky state, and, then, at higher temperature, this state transitioned “translucent liquid” to a “clear liquid”. In addition, he noted

that a thin film of material, even in liquid state, reflected light of characteristic colors, which depended on the temperature. For these studies Reinitzer is often referred to as the discoverer of a new phase of matter: liquid crystalline phase.

Up to date liquid crystals are playing an important role in modern technology. In fact, the liquid crystal technology has had a great effect in many areas of science and engineering, as well as technological device. The applications of this kind of materials are still being discovered and continue to provide effective solutions to various problems.

The most common application of liquid crystal technology is that of liquid crystal displays (LCDs), but very important and practical applications have been developed in different areas such as medicine and electronics.

Actually the term “liquid crystal” (or mesophase) means a state in which matter has an internal order and physic-chemical properties between those of a conventional liquid and those of a solid crystal. For instance, a LC may flow like a liquid, but its molecules may be oriented in a crystal-like way.

To understand the physical and chemical properties of the liquid crystal we must briefly describe the various states of matter and the fundamental concepts of order.^[2]

In the solid phase molecules are highly ordered, organized spatially in a well-defined positions (Fig. 1.2). They have both orientational and positional order, but little freedom to move. The molecules are forced to occupy specific sites in a lattice point and their molecular axis specific directions. Thus the solids maintain their shape due to strong intermolecular forces. We say that these constituents have long-range positional order.

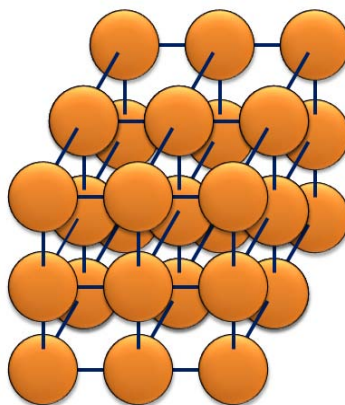


Fig. 1.2 Arrangement of molecules in a solid

On the other hand, the basic constituents in an isotropic liquid have no long-range positional order. The molecules do not have an intrinsic order, possess translational and rotational freedom, bump against each other, and are always in motion (Fig. 1.3). The molecules in a liquid spread randomly through the sample, with the molecular axes arranged in space with no orientational order. They are said isotropic, because there have no privileged directions in space that contains the liquid, and their properties are the same in any investigated direction.

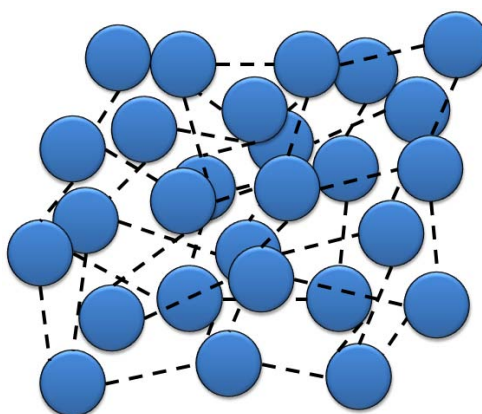


Fig. 1.3 Arrangement of molecules in a liquid

It is clear that by varying the temperature you can see a transition from one phase to another.

In materials, that form liquid crystals, the intermolecular forces, typical of crystalline solids, do not have the same strength in all directions. When a material is heated, the increased molecular motion produces a molecular reorganization. To fix the ideas let us consider a substance consisting of molecules with the shape of a

stick (like a cigar). Substances that have molecules of this type may pose between the crystalline solid state (usually at low temperatures) and the isotropic liquid (usually at high temperatures) (Figure 1.4).

Here, if we identify the centers of mass of individual molecules, we would see that these centers of mass would have a spatial arrangement as that present in liquid, but there is not any kind of long-range positional order as in the case of solids.



Fig. 1.4 Arrangement of molecules in a liquid crystal

The molecules are still in layers, but within each layer they occupy random positions, although they remain more or less parallel. Molecules within the layers can slide around each other and the layers can slide one over another. This molecular mobility produces the fluidity of a typical liquid phase.

Thus, there is an orientational ordering, but non-positional one. In other words, if we refer to a preferred orientation of the molecules can be said that another molecule (far away from that of reference) will also have its major axis oriented on the one specific way.

The distinguishing feature of the liquid crystalline phase is the tendency of the molecules (mesogens) to orient themselves along a particular preferred direction in space, called the director \mathbf{n} (Fig. 1.5).

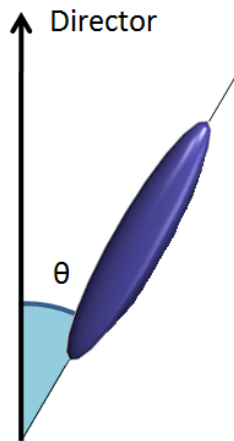


Fig. 1.5 Orientation of liquid crystal molecule along the axis

The order of liquid crystals can be altered by mechanical, magnetic or electric forces. The liquid crystal materials generally have several common characteristics:

- an anisotropic molecular structure (stick, disc, etc.);
- stiffness along the axis;
- strong dipoles and / or easily polarizable substituents.

To accurately measure the degree of order of a material, an order parameter (S) is calculated. Traditionally, the order parameter for a uniaxial material is defined as follows:

$$S = \frac{1}{2} \langle 3 \cos^2 \theta - 1 \rangle \quad (1)$$

where θ is the angle between the director and the long axis of each molecule. The brackets denote a thermal average performed on all molecules in the sample liquid-crystalline.

In an isotropic liquid the molecules have random orientations, the values of θ can vary from 0 to 360° with equal probability, and so the average of the cosine terms is zero. In this case the order parameter is equal to zero.

For a perfect crystal, however, the molecules are aligned along the director (i.e. $\theta = 0$) and therefore the order parameter is 1. Typical values for the order parameter of a liquid crystal varies between 0.3 and 0.9, the exact value is a function of temperature as a consequence of molecular motion.

1.1.2 Chemical properties of liquid crystals

From a chemical point of view, it is possible to classify liquid crystals into two main categories:^[3]

- *Thermotropic Liquid Crystal*
- *Lyotropic Liquid Crystal*

The *thermotropic* liquid crystals are compounds in which variations in temperature determine the transitions of the liquid-crystalline phase (thermally induced). There is no formation of molecular aggregates. These molecules may have a rod (most common), disk or arc shape. The thermotropic mesophases are generally due to the existence of anisotropic dispersion forces and intermolecular interactions.

The discotic phase are generally formed by disk-like molecules, composed of a core of adjacent aromatic rings. This allows a two-dimensional columnar arrangement. The rod-shaped molecules have an elongated geometry which allows a preferential alignment along a preferred direction

An example of rod-like liquid crystal with low molar mass, 5CB, is shown in Figure 1.6.

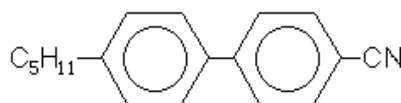


Fig. 1.6 Molecular structure of 5CB

It is characterized by a rigid structure due to the interconnection of two rigid cyclic units, that induce to have a planar linear conformation.

Generally, the liquid crystals have a molecular structure with aromatic rings connected in order to obtain a long chain. In addition, there will be units that contain multiple bonds such as - (CH=N) -, - N=N-, - (CH=CH)_n-, - CH=N-N=CH-, etc. that limit the freedom of rotation. These groups can be conjugated with the phenyl rings which increase the anisotropic polarizability of the compounds.

Thermotropic liquid crystal phases are principally divided into three groups as follows:

1. *disordered or anisotropic plastic crystals* (soft crystals): the molecules have long range positional order, but also exhibit rapid dynamic motions.
2. *smectic and columnar discotic mesophases*: the molecules do not possess long range translational order, yet they retain layer ordering (in the case of smectics) or columnar ordering (in the case of discotics). Again the molecules are in dynamic motion.
3. *nematic phases*: the molecules are only orientationally ordered and exhibit rapid and diffuse molecular motion.

The *lyotropic* liquid crystals (LLCs), on the other hand, are mixtures of amphiphilic molecules and solvents that under certain conditions of temperature, pressure and relative concentration of different components, show the formation of superstructures - molecular aggregates - which are organized in space, showing some degrees of order.

The lyotropic molecules are typically amphiphilic, meaning they are composed of both lyophilic parts (similar to the solvent) and lyophobic (rejecting the solvent).

Self-aggregation phenomena govern the formation of micellar structures, where the hydrophilic heads and the hydrophobic tails, respectively, interact “attracting the water” and “rejecting water”. The amphiphilic molecules are arranged in a way to minimize contact between the polar region of the molecule and the polar solvent. The aggregates are called micelles when they have small dimensions (tens of nanometers) and characterized by flat or elongated shapes. For these compounds both the concentration of the solution and the temperature determine the stability of liquid-crystalline phase. If the concentration of the solution is increased and/or the solution is cooled, the micelles increase in size and eventually merge.

When lyotropic molecules are dispersed in a solvent they can form one or more phases depending on the size of the polar head groups, the number of aliphatic chains present in the amphiphile, and the nature (polarity) of the solvent.

The phases are dependent on the concentration of solvent and the degree of curvature produced by the packing arrangements of the amphiphilic molecules.

We can distinguish:

A *lyotropic nematic phase*, composed of stick micelles with a long-range orientational order (LOO) respect to the axis of symmetry of the micelle, but no long-range positional order (LPO). (Fig. 1.7)

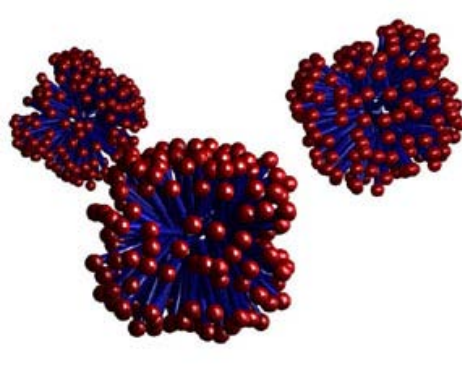


Fig. 1.7 Arrangement of molecules in lyotropic nematic phase (micelle)

A *lamellar phase* (micelles with laminated disc indefinitely extended) usually has a bilayered structure as structural unit and shows LPO in one dimension (normal to the layers) and LOO within the layer. (Fig. 1.8)

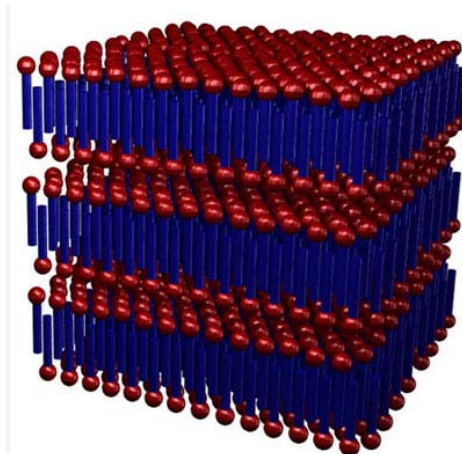


Fig. 1.8 Arrangement of molecules in lyotropic lamellar phase

A *hexagonal phase* (hexagonal shell of sticks micelles) shows LPO in two dimensions (normal to the axis of symmetry of the rods). (Fig.1.9)

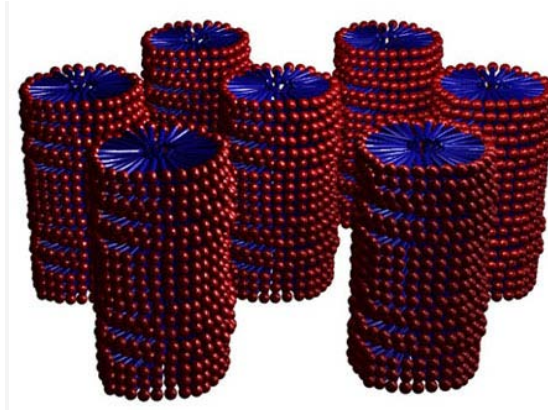


Fig. 1.9 Arrangement of molecules in lyotropic hexagonal phase

A cubic phase, (cubic envelope of spherical micelles) shows LPO in three dimensions.

The hexagonal phase can exist in a normal form, when the solvent is polar and the extremes of molecules protrude outwards (respect to the axis of symmetry) and in a reverse form, when the solvent is lipophilic and the extremes of molecules projecting inward.^[4]

1.1.3 Phases of Liquid Crystal

There are different liquid-crystalline phases, depending on the degree order.

1.1.3.1 Nematic Phase

The molecules in the nematic phase have no positional order, but on average are oriented along a particular direction (*director*).^[3,5]

Consequently, there is macroscopic anisotropy in many material properties such as dielectric constant and refractive index. The nematic phase is used in many liquid crystal devices, because the average orientation can be changed easily with an electric field and the polarization of the light will follow the molecular orientation based on how it changes through a sample.^[4]

When the temperature increases, we can see a transition from a solid (Fig. 1.10a) to a nematic phase (Fig. 1.10b) where the matter has orientational order but no positional order and, finally, to isotropic phase where the molecules have random orientation (Fig. 1.10c).

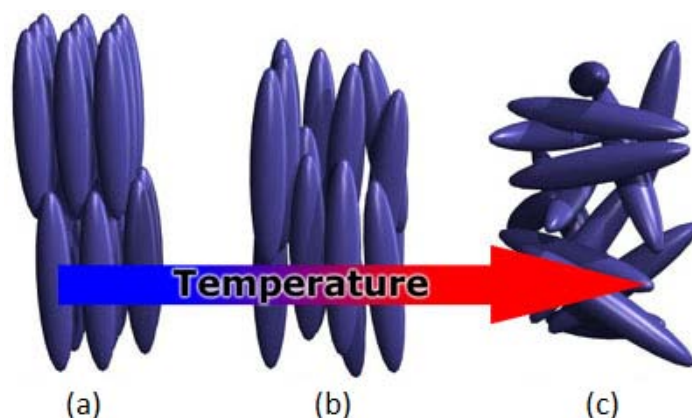


Fig. 1.10 Liquid crystal molecules in the solid (a), in the nematic (b) and in the isotropic (c) phase

1.1.3.2 Cholesteric Phase

A particular kind of nematic liquid crystal is known as chiral nematic (or *cholesteric*). It is composed typically of nematic molecules that contain a chiral center which produces intermolecular forces that favor the alignment between the molecular planes at a slight angle to each other. Each nematic plane (2D nematic phase) is slightly rotated respect to the previous one. Therefore, instead of a fixed director, as in the nematic phase, the cholesteric director turns around for the entire sample (Fig.1.11). Many cholesterol esters present this behavior, hence the name cholesteric.



Fig. 1.11 Orientation of the director in a cholesteric phase

An important characteristic of the cholesteric mesophase is the *pitch*. The

pitch, p , is defined as the distance that the director does through a complete turn of the helix as shown in Figure 1.12.

Another important property of the helical structure of the chiral phase is its ability to selectively reflect a wavelength equal to the length of the pitch, so that a color will be reflected when the step length falls in the visible spectrum. The effect depends on the temperature. A gradual change in temperature results in a change in orientation between successive layers of the director (shown above), which changes the length of the pitch and the wavelength of reflected light. Similarly, decreasing the temperature of the device, the step size of the chiral liquid crystal increases. Consequently, it is possible to build liquid crystal thermometers that display the temperature based on the reflected color.

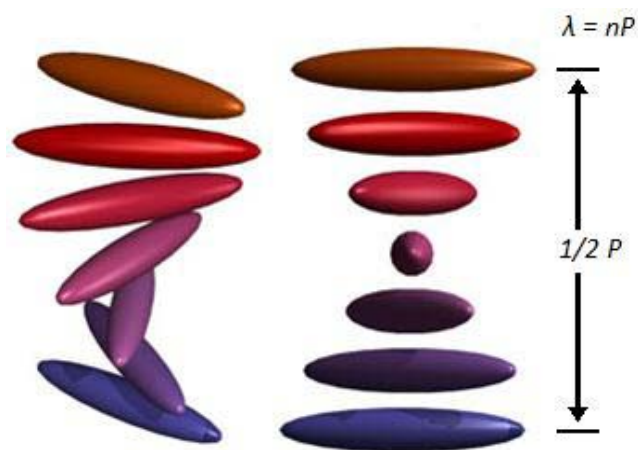


Fig. 1.12 Pitch in a cholesteric phase

1.1.3.3 Smectic Phase

The smectic phase is typical of the liquid crystal at low temperatures. In this mesophase the molecules retain their nematic orientational order, but gain a positional order. In smectic phase, the molecules are still in parallel layers, although they are free to move within each layer, but now they are oriented perpendicular, or nearly so, to the layers. It is possible to distinguish different categories of smectic phases depending on the orientation of molecules within the layers.

In smectic-A the director is perpendicular to the layers and there is a particular positional order in layers (Fig. 1.13).

In smectic-C the molecules are arranged as in smectic-A, but the director is inclined at a fixed angle respect to the normal smectic layer (Fig. 1.14).

As in the nematic phase the mesophase smectic-C can have a chiral form indicated as C*. Similarly to smectic-C the director in smectic-C* phases makes an angle of inclination respect to the smectic layer, but this angle rotates from layer to layer forming a helix as shown in Figure 1.15. The director of the mesophase smectic-C* is not parallel or perpendicular to the layers and turns of one layer to the next.



Fig. 1.13 Arrangement of molecules in the smectic-A phase



Fig. 1.14 Arrangement of molecules in the smectic-C phase

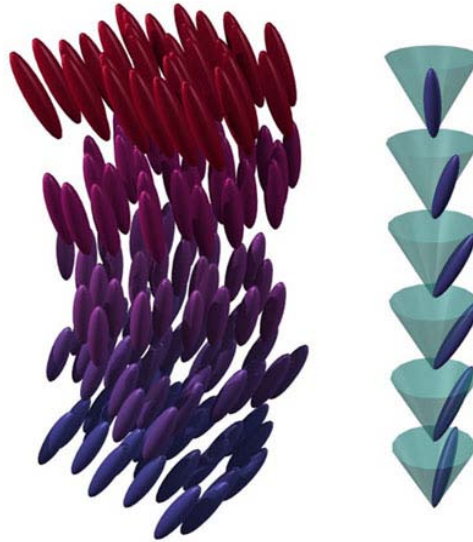


Fig. 1.15 Arrangement of molecules in the smectic-C* phase

1.1.3.4 Columnar Phase

The columnar liquid crystals are different from previous types because they are shaped like disks instead of long rods. This mesophase is characterized by columns of stacked molecules. The columns together form a two-dimensional crystal alignment. The arrangement of molecules within the columns and the arrangement of the columns themselves leads to new mesophase. (Fig. 1.16)



Fig. 1.16 Columnar phase

1.1.4 Birefringence in Liquid Crystals

Liquid crystals are birefringent due to their *anisotropic* nature. That is, they demonstrate double refraction. When a polarized light beam passes through a liquid crystal material, the light is splitted into two components traveling at different speeds: the fastest (for positive anisotropy) is perpendicular to the director of the liquid (called the ordinary ray), the slowest is parallel to the latter (called the extraordinary ray). Because the two components travel at different

velocities, the waves get out of phase. When the rays are recombined as they exit the birefringent material, the polarization state has changed due to the induced phase difference. Of course, the length of the sample plays an important role because the phase shift accumulates as long as the light propagates in the birefringent material. Any polarization state can be produced with the right combination of the birefringence and the length of the samples. The birefringence of a material is defined as the difference, Δn , of the refraction index for the ordinary and extraordinary rays.

Since the refraction index is defined as the ratio of the speed of light in vacuum to that in the material, the ordinary refractive index, n_o , is:

$$n_o = \frac{c}{v_{\perp}} \quad (2)$$

and the extraordinary one, n_e , is:

$$n_e = \frac{c}{v_{\parallel}} \quad (3)$$

where c , v_{\perp} and v_{\parallel} are, respectively, the speed of light in vacuum and in liquid crystal for a direction perpendicular and parallel to the director. The maximum value for the birefringence is $\Delta n = n_e - n_o$. The condition $n_e > n_o$ describes a positive uniaxial material.

1.1.5 External Influences on Liquid Crystals

Liquid crystals are used in a variety of applications because an external perturbation can cause significant changes in their macroscopic properties.^[3-6]

Both electric and magnetic fields can be used to induce these changes. Furthermore, special surface treatments can be used to force specific orientations of the director or texture.

The term texture refers to the orientation of liquid crystal molecules in the vicinity of a surface. Each liquid crystal mesophase can form its own characteristic textures, which are useful in identification.

If mesogenic materials are confined between closely spaced plates with rubbed surfaces and oriented with rubbing directions parallel, the entire liquid crystal sample can be oriented in a *planar* texture (Fig. 1.17).

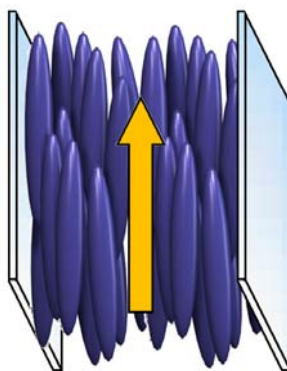


Fig. 1.17 Director is parallel to the surface in planar texture

Mesogens can also be oriented normal to a surface with the use of appropriate polymer films, or in the presence of an electric field applied normal to the surface, giving rise to the *homeotropic texture*, as illustrated in Fig. 1.18.

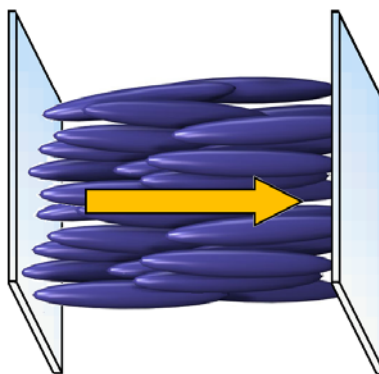


Fig. 1.18 Director is perpendicular to the surface in homeotropic texture.

The ability of the director to align along an external field is caused by the electric nature of the molecules. Permanent electric dipoles result when one end of a molecule has a net positive charge while the other end has a net negative charge. When an external electric field is applied to the liquid crystal, the dipole molecules tend to orient themselves along the direction of the field. (Fig. 1.19)

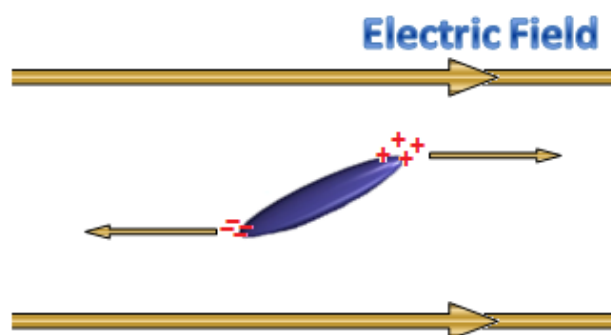


Fig. 1.19 Representation of a molecular dipole that tends to orient along the direction of the applied external electric field

Even if a molecule does not form a permanent dipole, it can still be influenced by an electric field. In fact, the field produces slight re-arrangement of electrons and protons in molecules such that an induced electric dipole results. The effects of magnetic fields on liquid crystal molecules are analogous to electric fields. Because magnetic fields are generated by moving electric charges, permanent magnetic dipoles are produced by electrons moving about atoms. When a magnetic field is applied, the molecules will tend to align with or against the field.

In the absence of an external field, the director of a liquid crystal is free to point in any direction. It is possible, however, to force the director to point in a specific direction by introducing an outside agent to the system, for example a thin polymer coating on glass substrate, or just rubbing the substrate in a specific direction. In fact, it is observed that liquid crystal molecules in contact with that surface align along with the rubbing direction.

The competition between surface anchoring and electric field re-orientation is often used in liquid crystal devices. Consider the case in which liquid crystal molecules are aligned parallel to the surface and an electric field is applied perpendicular to the cell as in Fig.1.20. At first, as the electric field increases in magnitude, no change occurs in alignment. However at a threshold magnitude of electric field, deformation occurs.

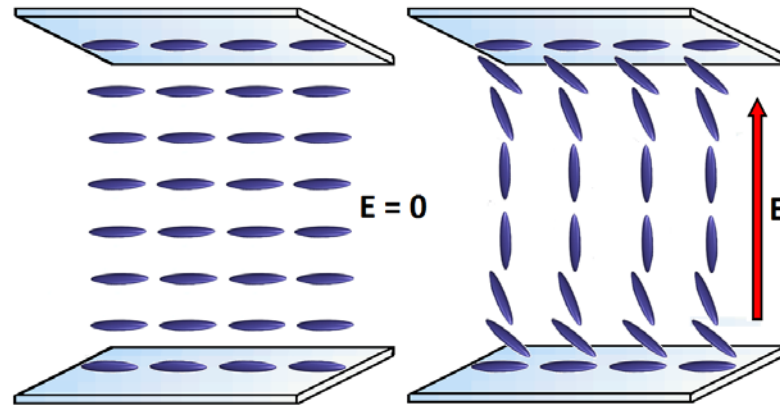


Fig. 1.20 Schematic representation of a Freedericksz transition

Deformation occurs where the director changes its orientation from one molecule to the next. The occurrence of such a change from an aligned to a deformed state is called a *Freedericksz transition*^[3,7] and can also be produced by the application of a magnetic field of sufficient strength.

1.1.6 Liquid Crystal in nature

Living organisms are composed of many types of molecules immersed in a “sea” of water. This simple observation would suggest the possibility that lyotropic liquid crystals are present within our body. And in fact there are many substances that form the mesophase as: steroids, glycolipids and phospholipids, for example. Moreover, the high degree of organization of molecules in complex structures inside our cells (for example the cell nucleus, mitochondria and many other cell organelles) can remember the typical order of some liquid crystals.^[8]

The cell membrane (Fig. 1.21), which separates the external environment from that inside, consists of a double layer of phospholipids. It is a classic example of a lyotropic lamellar liquid crystal. The phospholipids, in fact, are very similar to lyotropic molecules, because they have a polar head (with phosphorus units) and a non polar tail, consisting of two long-chain lipid (hydrophobic). The bilayer structure, shown in Figure 1.21, is of great importance for many functions: from the regulation of the flow of substances, between the exterior and interior of the cell, to the proper functioning of proteins such as enzymes and proteins channel.

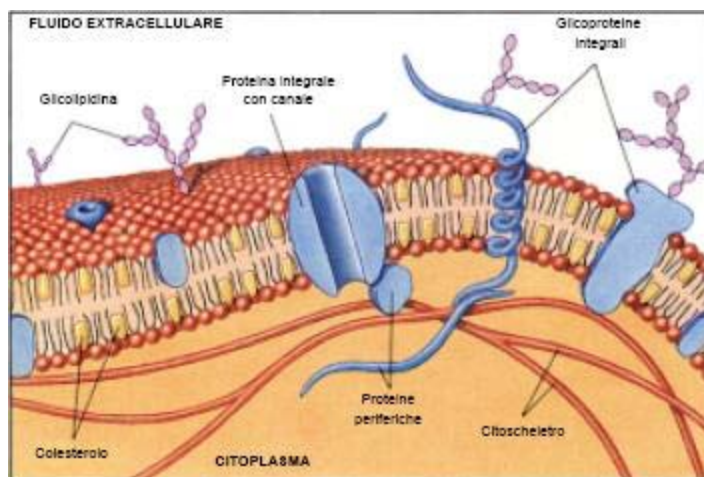


Fig. 1.21 Membrana cellulare e struttura a doppio strato

The realization of all these functions is made possible by the double-layer laminated structure, which ensures fluidity and flexibility combined with a great organization. Other liquid-crystalline structures found in nature are the liposomes. These are special vesicles, or spheroidal aggregates delimited by a double layer of lipids, similar to cell membranes. These vesicles are very important in nature because they are the base for understanding the processes of fusion between cells.

1.2 Polymer Liquid Crystals ^[9]

1.2.1 Introduction

Polymer liquid crystals (PLCs) are a class of materials that combine the properties of polymers with those of liquid crystals. These “hybrids” show the same mesophases characteristic of ordinary liquid crystals, yet retain many of the useful and versatile properties of polymers. To ensure that the normally flexible polymers may exhibit the characteristics of the liquid crystal, rod-like or disk-like elements must be included into their chains.

The arrangement of mesogen plays an important role in determining the type of PLC that may form. Main-chain polymer liquid crystals, MC-PLCs, are formed when mesogens are part of the main chain of a polymer. Conversely, side chain polymer liquid crystals (referred to as SC-PLCs) are formed when mesogens are

connected as side chains to the polymer by a flexible “bridge molecule” called spacer (Fig. 1.22).

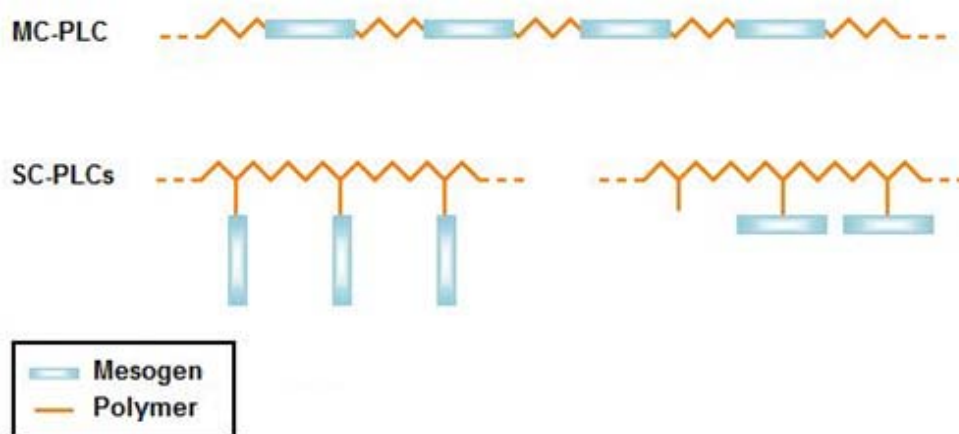


Fig. 1.22 Examples of two types of liquid-crystalline polymers

Other factors that influence the nature of the mesomorphic polymers include the presence of long flexible spacers and the sequence of rigid and flexible units along the backbone.

1.2.2 Main Chain Polymer Liquid Crystals

Main chain polymer liquid crystals are formed when rigid elements are incorporated into the backbone of normally flexible polymers. These rigid regions along the chain allow the polymer to orient in a manner similar to common liquid crystals, and thus show liquid crystal characteristics. There are two distinct groups of MC-PLCs, which differ by the way to form the rigid regions.

The first group of MC-PLCs is characterized by rigid rod-like monomers. These monomers are commonly made up of many aromatic rings that provide its specific shape. (fig. 1.23).

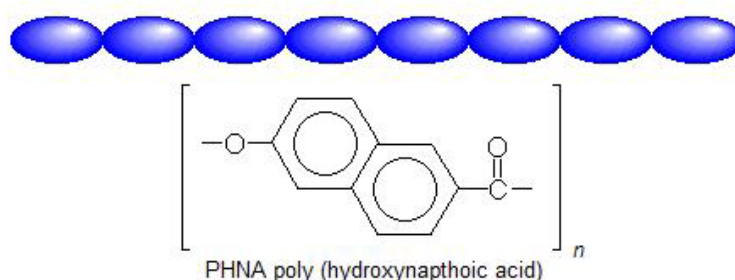


Fig. 1.23 Examples of MC-PLC

The second group of MC-PLCs incorporates a mesogen directly in the chain. Generally, mesogen units consist of two or more aromatic rings which give the necessary impediment that allows the polymer to display liquid crystal properties.

This group is different from the first because the mesogens are separated from the spacers (Fig. 1.24). Decoupling of the mesogen allows the independent movement of the molecules and facilitates the correct alignment.

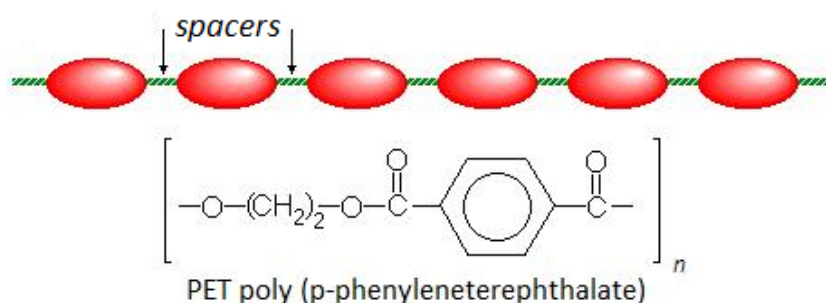


Fig. 1.24 Example of MC-PLC. Flexible spacers are composed by methylene groups

Temperature is a problem for MC-PLCs as sometimes liquid-crystalline behavior is above the polymer decomposition temperature. This problem can be avoided by random arrangement of monomers in the chain, creation of a random copolymer and introduction of defects in the chain structure.

All these changes disturb the regularity of the chains and lower the melting temperature of the polymer.

1.2.3 Side Chain Polymer Liquid Crystals

Side chain polymer liquid crystals (SC-PLCs) are made up by mesogenic units linked to the polymer as side chains (Fig. 1.25).

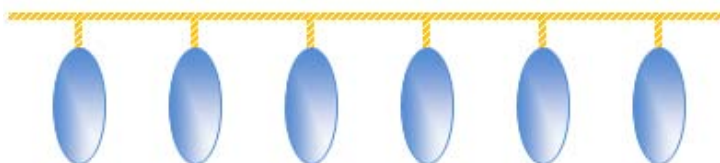


Fig. 1.25 Examples of SC-PLC

The SC-PLCs have three main structural elements making them versatile liquid crystals: the internal structure, the mesogen and the spacer.

The internal structure of a SC-PLCs is the unit to which the side chains are linked. The arrangement of the internal structure can be very important for the behavior of PLCs. Polymers with rigid internal structures generally have high glass transition temperatures and so mesophases are often difficult to observe.

The mesogen is the most important part of the SC-PLCs, because the alignment of this group causes the liquid crystal behavior.

The spacer allows the movement and the orientation of the side groups in the internal structure of the SC-PLCs. The length of the spacer has a fundamental effect on the temperature and phase transitions: in fact, the glass transition temperature decreases with increasing length of the spacer.

1.2.4 Phases of Polymer Liquid Crystals

The PLCs can show the same mesophases of ordinary liquid crystals. The SC-PLCs show a tendency to separate the internal structure from the mesogenic side groups. This occurs in the smectic phase: the mesogenic groups and backbone chains form individual layers (fig. 1.26).

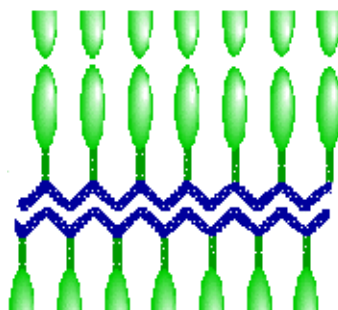


Fig.1.26 Examples of alignment of PLCs

Many SC-PLCs give rise to “double comb” configuration (Fig. 1.27).

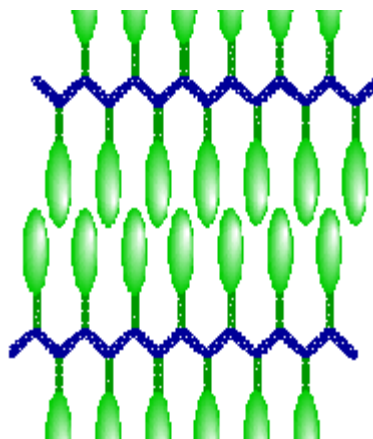


Fig. 1.27 "Double comb" configuration

Atactic polymers cannot form this structure because the side chains are connected to the backbone in random directions.

1.2.5 Polymer-dispersed liquid crystals (PDLCs)

Polymer-dispersed liquid crystals (PDLCs) are a relatively new class of materials that hold promise for many applications ranging from switchable windows to projection displays.^[10] These materials, which are simply a combined application of polymers and liquid crystals, are the focus of extensive research in the display industry.

PDLCs are composite materials containing liquid crystal microdomains (droplets) dispersed in a solid polymer matrix.^[11,12] The resulting material is a sort of "Swiss cheese" polymer with liquid crystal droplets filling the holes. These tiny droplets (a few microns for practical applications) are responsible for the unique behavior of the material. By changing the orientation of the liquid crystal molecules with an electric field, it is possible to vary the intensity of transmitted light, so they can be switched from an opaque to a transparent state by application of a suitable switching field (Fig. 1.28).

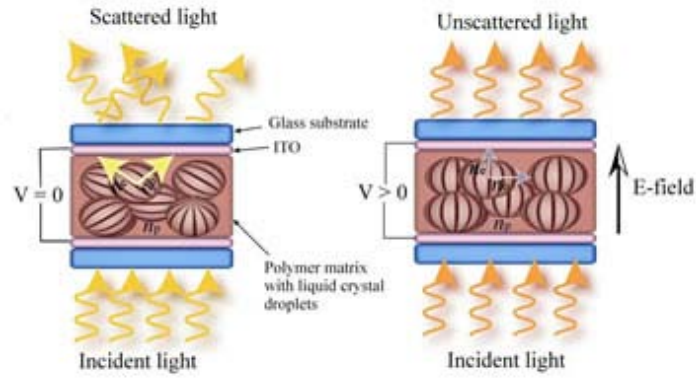


Fig.1.28 A PDLC device

The PDLC properties are influenced by the size and morphology (shape) of the droplets, the polymer type, used liquid crystal, polymerization procedure rate.

The configuration of the liquid crystal droplets in a polymer matrix is the focus of many researches. Many different configurations have been observed and depend on droplet size and shape, surface anchoring, and applied fields.

The radial configuration occurs when the liquid crystal molecules are anchored with their long axes perpendicular to the droplet walls (Fig. 1.29a). A point defect is in the center of the droplet.

The axial configuration of the liquid crystal droplets also occurs when the molecules are oriented perpendicularly to the droplet wall, but with a weak surface anchoring. This configuration creates a line defect that runs around the equator of the spherical droplet, as seen in Fig. 1.29b. When an electric field is applied to a radial droplet, the molecules adopt the axial configuration. The radial configuration is restored when the field is removed.

The bipolar configuration is obtained by a tangential anchoring of the liquid crystal molecules. Two point defects are present at the droplet poles as shown in Fig 1.29c.

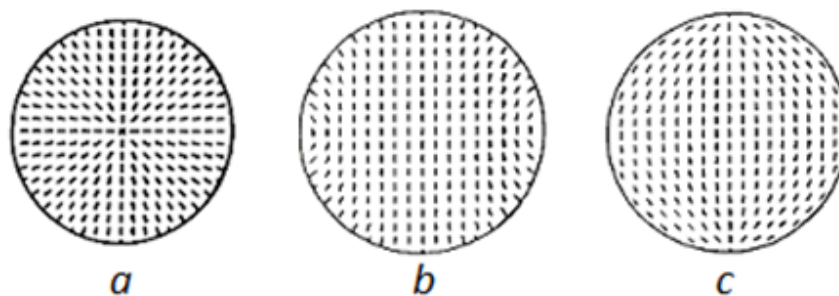


Fig.1.29 Configuration of the LC droplets in a PDLCs: Radial (a), Axial (b) and Bipolar (c)

1.2.6 Applications of Polymer Liquid Crystals

The applications of PLCs vary from the production of high resistance materials to the use in optical devices.

For examples, Kevlar, which is used to make bullet-proof vests, is an application of PLCs for strong light weight materials.

In the display industry polymer liquid crystals are characterized by relatively slow “response times” to electric fields. Polymer-dispersed liquid crystals hold potential for a variety of electro-optic applications ranging from displays to light shutters.

PDLC windows are based on the ability of the nematic director in the liquid crystal droplets to align under an electric field. In a typical application, a thin PDLC film (about 25 microns thick) is cast between two substrates coated with a very thin layer of conducting indium tin oxide (ITO).

Transmission of light through a PDLC window depends primarily on scattering, which in turn depends on the difference in refractive index between droplets and their environment. In the field OFF conditions the random droplet orientation provides significant differences in indices and hence a strong scattering. The cell appears opaque. When an electric field is applied, the droplet directors align along the field direction.

References

- [1] F. Reinitzer, *Monatsh. Chem.*, v. 9, 421, (1888).

- [2] P. J. Collings and M. Hird, *“Introduction to Liquid Crystals: Chemistry and Physics”*, Taylor and Francis, (1997).
- [3] P.G. de Gennes and J. Prost, *“The Physics of Liquid Crystals”*, Clarendon Press, Oxford University Press, (1993).
- [4] P. W. Atkins, *“Physical Chemistry”*, Oxford University Press, Oxford (1994, 5th edition).
- [5] S. J. Elston and J. R. Sambles, *“The Optics of Thermotropic Liquid Crystals”*, Taylor and Francis, (1997).
- [6] L. M. Blinov and V. G. Chigrinov, *“Electrooptic Effects in Liquid Crystal Materials”*, Springer-Verlag, (1996).
- [7] S. Chandrasekhar, *“Liquid Crystals”*, Cambridge University Press, (1992)
- [8] I. W. Hamley *“Introduction to Soft Matter. Polymers Colloids, Amphiphiles and Liquid Crystals”*, chapter 5, Wiley & Sons Ltd, (2000).
- [9] <http://plc.cwru.edu/tutorial/enhanced/files/textbook.htm>
- [10] P.S. Drzaic, *“Liquid Crystal Dispersions”* World Scientific, Singapore (1995).
- [11] J.L. Fergason, U.S. Patent 4 435 047 (1984)
- [12] J.W. Doane, G. Chidichimo, N.A. Vaz, U.S. Patent 4 688 900 (1987)

2

Additives

2.1 Electrochromism

Electrochromism is defined as a reversible and visible change in transmittance of a material, as a result of electrochemical oxidation and/or reduction.^[1] The electro-active species change their optical absorption bands due to a gain or a loss of an electron. After applying an electric field-current (dc field), which allows the transfer of the electron to the electrode work, the devices become colorful and persist in this condition until it is applied an opposite electrical impulse, or a competitive reaction occurs.

Without the application of an external electric field, electrochromic devices generally present themselves transparent (OFF state). Thanks to a subsequent application of a low voltage, the electrochromic device undergoes a color change (ON state) (Fig. 2.1).

In these systems, the chemical reaction is oxidation, a reaction in which the molecules of a compound lose an electron. Ions allow the change from transparent to colored state in the intermediate electrochromic layer. By applying a source of energy to the conductive oxide layers, the potential difference transports ions from their storage medium to electrochromic materials, through the conductive layer. This transfer enables the coloration of glasses.

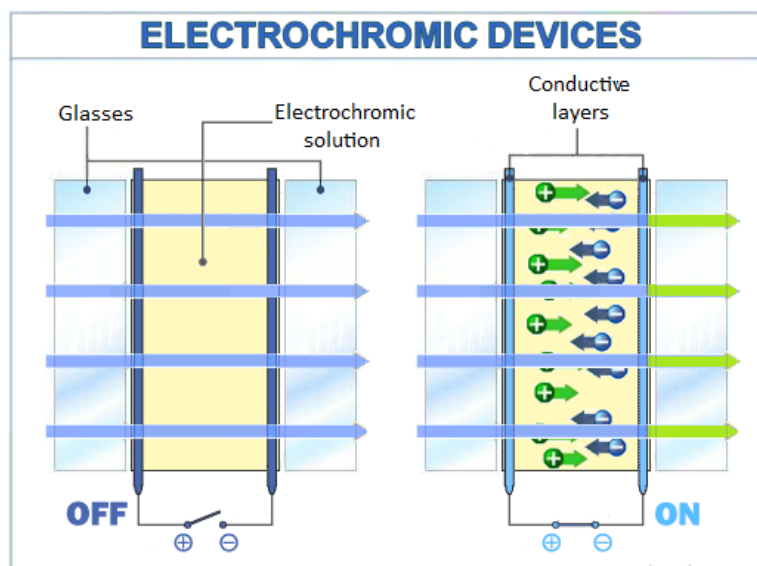


Fig. 2.1 Scheme of an electrochromic device in the OFF and ON state

Following the removal of the electric signal, the ions are removed from the electrochromic layers and return to the storage medium. As a result, the device regains its transparency.

The ionic diffusion involved here, or the inherent absorption rate or loss of the electrons, will determine the speed of color change. The species is colored during the redox reaction is often called electro-chromophore or electrochromic material.^[2] The colored state, which occurs after the transfer of electrons, persists, due to the memory effect. An adequate current, opposite in direction, reverses the electrochemical process and the display returns to the colorless or bleached state.

The electrochromic have many advantages:

- They consume little energy in the production of images that, once formed, persist with little or no addition of energy due to the so-called "memory effect";
- Large electrodes or many small electrodes^[3] can be used. In general, there is no theoretical limit to the size.

The initial development of the electrochromic devices was directed toward applications now used by liquid crystal display, that is, small displays, such as watches, clock slides or screens of personal computers. The anti-glare electrochromic mirrors in cars are another important application.^[4,5]

Electrochromic sunglasses can be darkened at will, unlike the photochromic lenses.

In addition, entire electrochromic windows can be tinted to reduce light into a room, office or otherwise in a windshield of a car. ^[6]

It is well known that visible light can be considered as a set of electromagnetic waves of wavelengths ranging from 420 nm (violet) to 700 nm (red) or as a set of photon energies from 4.7×10^{-19} J (purple) to 2.8×10^{-19} J (red).

The color is subjective visual impression of the eye involving the retinal response to certain wavelengths of impinging light. The resulting colors depend on the material absorption and reflection. In white light, the perceived color of a material is the complementary color of the light that it absorbs (Fig. 2.2). ^[7]

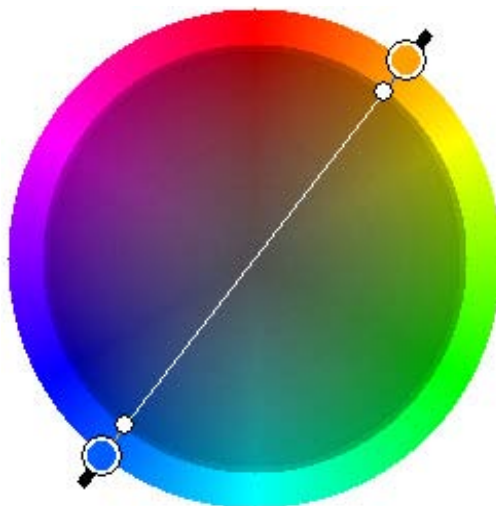


Fig.2.2 The color wheel

A quantitative measure of the color intensity change is the contrast ratio, CR, defined as:

$$CR = \frac{R_0}{R_x} \quad (4)$$

where R_x is the intensity of light diffusely reflected in the colored state and R_0 is the intensity of light diffusely reflected in the bleached state. ^[8]

The right side of equation 4 can be replaced with $e^{2\alpha l}$ where α is the linear absorption coefficient and l is the film thickness. The factor 2 is due to the fact that the photons pass twice through the colored layers.

The time taken to color an electrochromic device from its colorless state (or vice versa) is called reaction time, τ .

In electrochromic windows or mirrors, reaction times of the order of seconds (minutes for windows) can be accepted, but they must be shorter for optical devices or television screens. Recently a display that show an ultra-fast color change has been presented.^[9,10]

The use of indium tin oxide, ITO, as transparent conducting electrodes limits the response time, because of its moderate conductivity.^[11]

When a device continually alternates states of electrochromic coloring and bleaching, device damage may occur due to physical changes in solid phases or secondary chemical reactions.

The life cycle of an electrochromic device is a measure of its stability, because it represents the number of cycles prior to its degradation. An important item of the manufacturers is obviously to raise the life cycle of electrochromic devices.

Tracy and al.^[12] showed that the most important cause of device degradation is the combination of continuous cycles of coloration/discoloration, high temperatures and irradiation.

2.1.1 Electrochromism in Liquid Crystal

Recently, the behavior of Electrolyte / Liquid Crystal Dispersions, ELCD, was studied.^[13,14] ELCD show independent electro-optical and electrochromic properties, characterized by bright colors and fast coloring and bleaching times.

Liquid crystals, doped with a small amount of quaternary ammonium salts^[15] or ionic liquid, show a reversible color change when a dc electric field is applied.^[16,17]

The colorful species will occur at the cathode, and electrochromism is observed in both the liquid crystal and isotropic state.

In particular, the color density increases linearly with the current, the dominant electrochemical reaction for the discoloration is a first-order reaction.

Lately, it was found that liquid crystals that host electrochromic molecules can

provide a change of color due to the electrochromic reactions at the electrodes.^[13,18] The samples appear initially transparent but they will be characterized by different colors depending on the liquid crystal used after an application of a dc electric current (2 Volts) (Fig. 2.3).

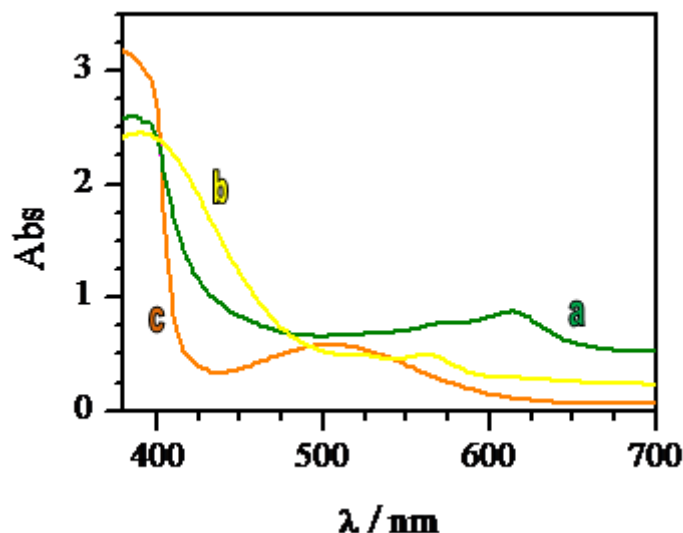
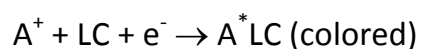


Fig. 2.3 Absorption in the ON state by ELCD with different LC: a)E7, b)E49, c)ZLI4788-000

The increase of electrolyte concentration in the samples causes a decrease in the rise and decay times due to more rapid formation and disappearance of the local fields acting on the cell.^[19]

The absorption reaches a plateau in a few seconds, depending on the electrolyte concentration and the application time of the dc current. Removing the field, the sample bleaches spontaneously in about ten seconds, depending on the electrolyte concentrations.

According to the mechanism coloring/discoloration proposed by Nakamura and al.^[24] the application of a dc current in the ELCD causes the motion of the ions of the ammonium salt (or ionic liquid) A^+ to the cathode, where the following reaction between A^+ and the liquid crystal (LC) occurs:



giving a colored complex.

At the same time the molecules of halide, Ha_2 , are produced at the anode. These molecules diffuse and react with the colored species, resulting in

discoloration of the sample when the dc external field is removed, according to the following reaction:



References

- [1] T. Rades, Y. Padmadisastra, C. C. Müller-Goymann, *Pharmazie*, **51**, 846, (1996)
- [2] M. -A. De Paoli and W. A. Gazotti, *Macromol. Symp.*, **189**, 83 (2002)
- [3] G. G. Wallace, G. M. Spinks, L. A. P. Kane-Maguire and P. R. Teasdale, "Conductive Electroactive Polymers 2nd edition", CRC Press. (2003)
- [4] H. J. Byker, U.S. Patent No 4,902,108 (1990)
- [5] T. Nagamura, Y. Isoda and K. Sakai; *Polym. Int.*, **27**, 125 (1992)
- [6] F. G. K. Baucke, *Schott Information*, **1**, 11 (1983)
- [7] F. G. K. Baucke; *Solar Energy Mater.*, **16**, 67 (1987)
- [8] R. B. Goldner, F. O. Arntz, G. Berera, T. E. Haas, G. Wei, K. K. Wong and P. C. Yu; *Solid State Ionics*, **53-56**, 617 (1997)
- [9] T. Oi; *Ann. Rev. Mater. Sci.*, **16**, 185 (1986)
- [10] F. B. Kaufmann, *Conference Record: Biennial Display Research Conference*, 23 I.E.E.E. (1978)
- [11] D. Cummins, G. Boschloo, M. Ryan, D. Corr, S. N. Rao, D. Fitzmaurice; *J. Phys. Chem. B*, **104**, 11449 (2000)
- [12] N. Sbar, M. Badding, R. Budziak, K. Cortez, L. Laby, L. Michalski, T. Ngo, S. Schulz and K. Urbanik; *Solar Energy Materials and Solar Cells*, **56**, 321(1999)
- [13] F. P. Nicoletta, G. Chidichimo, D. Cupelli, G. De Filipo, M. De Benedittis, B. Gabriele, G. Salerno, A. Fazio; *Advanced Functional Materials*, **15**, 995 (2005)

- [14] F. P. Nicoletta, D. Cupelli, G. De Filpo, G. Chidichimo; *Applied Physics Letters*, **84**, 4260 (2004).
- [15] C. Fairhurst, S. Fuller, J. Gray, M. C. Holmes, G. J. T. Tiddy, “Lyotropic Surfactant Liquid Crystals”, In “*Handbook of Liquid Crystals*”, D. Demus, J. Goodby, G. W. Gray, H.-W. Spies, V. Vill, Eds.; Wiley-VCH: Weinheim; **3**, CVII, 341, (1998)
- [16] H. Meng, D. Tucker, S. Chaffins, Y. Chien, R. Helgeson, B. Dunn, and F. Wudl, *Adv. Mater.*, **15**, 146 (2003)
- [17] A. A. Argun, P. -H. Aubert, B. C. Thompson, I. Schwenderman, C. L. Gaupp, J. Hwang, N. J. Pinto, D. B. Tarmer, A. G. Mac Diarmid and J. R. Reynolds, *Chem. Mater.*, **16**, 440, (2004)
- [18] G. Chidichimo, D. Cupelli, M. De Benedittis, G. De Filpo, J. Lanzo, F. P. Nicoletta, B. Gabriele, G. Salerno, L. Veltri; World Patent, WO2006008776 (2006).
- [19] K. Nakamura, K. Nakada, Y. Ito and E. Koishi, *J. Appl. Phys.*, **57**, 135, (1985)

2.2 Ionic liquids^[1]

Ionic liquids, IL, are salts, that are in a liquid state at low temperatures, and are formed by organic cations (usually imidazole, pyridine, phosphonium and ammonium ions) and inorganic anions.

Ionic liquids have a high thermal stability as they have a melting point below 100°C and boiling points above 200°C. Furthermore, they are good solvents and poorly volatile, since they have a negligible vapor pressure.

Research in the field of ILs began in 1982 with the study of J. S. Wilkes on the synthesis of aluminium chloride ILs. ILs stable in air and in mixtures were produced only in '90s, while few years ago specific ILs (or third generation) have been synthesized (Fig. 2.4).^[1,2]

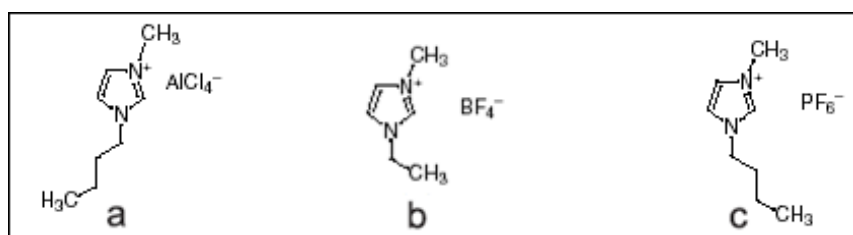


Fig. 2.4 Three examples of ILs of different generations: a) Aluminium chloride ILs, b) ILs stable in air and in mixtures, c) specific ILs

If one considers the various combinations of all cations and anions, it could be possible to create up to 10^8 types of ionic liquids (Fig. 2.5): about 1000 different ionic liquids are described in the literature, and approximately 300 are commercially available.^[3]

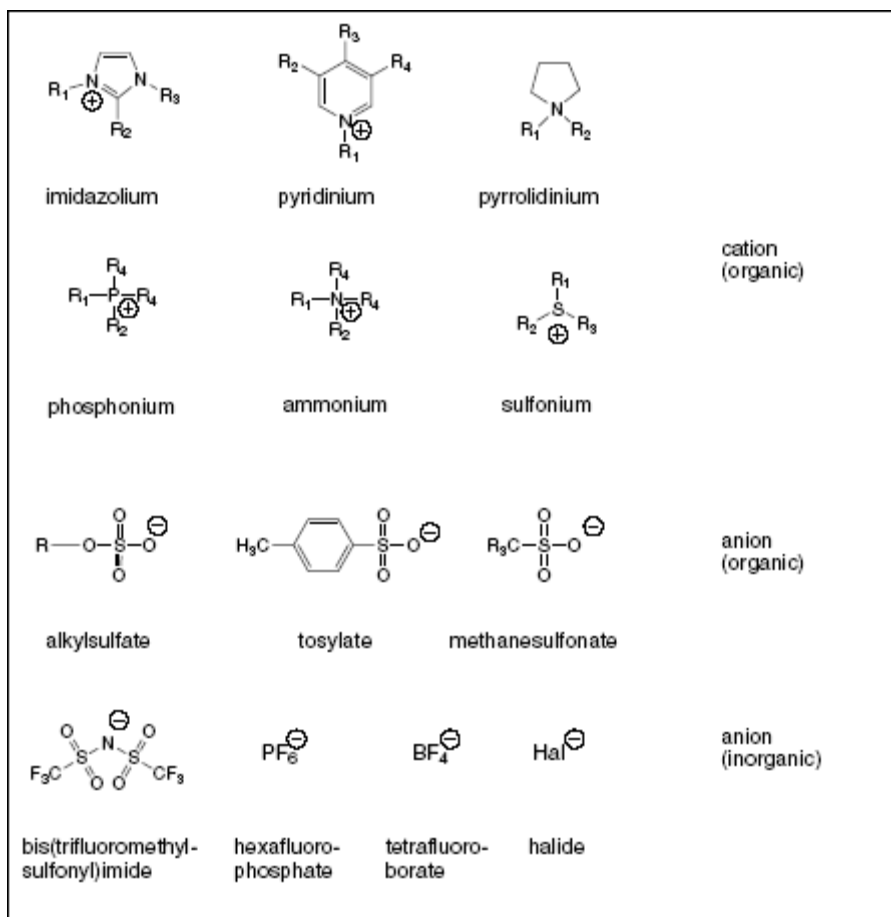


Fig. 2.5 Typical structures of ionic liquids ^[3]

2.2.1 Property of Ionic liquid ^[4]

An ionic liquid must have the following characteristics:

- Not volatile;
- Not flammable;
- High chemical, thermal and electrochemical stability;
- Liquid phase in a wide temperature range;
- Dissolution of many organic and inorganic compounds;
- Variable miscibility with water and organic solvents.

The stability largely depends on the used type of cation and anion.

Many studies have demonstrated that ionic liquids, in contrast to organic solvents, do not alter the integrity of cell membranes. This property is very useful in medicine and bio-pharmaceutics, opening new possibilities in building strategies for new pharmaceutical formulations. ^[5-8]

References

- [1] V. Busico, P. Cernicchiaro, P. Corradini, M. Vacatello, *J. Phys. Chem.*, **87**, 1631, (1983)
- [2] J. D. Gault, H. A. Gallardo, H. J. Müller, *Mol. Cryst. Liq. Cryst.*, **130**, 163, (1985)
- [3] Welton, T., *Chem.Rev*, **99**, 2071, (1999)
- [4] Dupont, J., *J.Braz.Chem.Soc*, **15**, 341, (2004)
- [5] Q. Yang, D.D Dionysiou, *Journal of Photochemistry and Photobiology, A: Chemistry*, **165**, 229, (2004)
- [6] www.ionicliquids-merck.de
- [7] H. B. Zhang, X. H. Zhou, J. F. Dong, G.Y. Zhang and C.X. Wang, *Sci China Ser B-Chem*, **50**, 238, (2007)
- [8] M. D. Baumann, A. J. Daugulis, P. G. Jessop, *Appl. Microbiol Biotechnol* **67**, 131, (2005)

2.3 Magnetism

Magnetism is a property of materials that respond at an atomic or subatomic level to an applied magnetic field.

Magnetism has been known and exploited for centuries. The first known natural magnets, “loadstones” (magnetic iron oxides) were discovered by the ancient Chinese and Greek civilizations. These materials were found to point always in one direction when allowed to rotate freely. This led to the development of the magnetic compass. In the seventeenth century it was discovered that the earth itself is a giant magnet with north and south poles; and in the early nineteenth century the relationship between magnetism and electricity was established. Then a more theoretical understanding of magnetism and electricity has begun to emerge (Fig. 2.6).

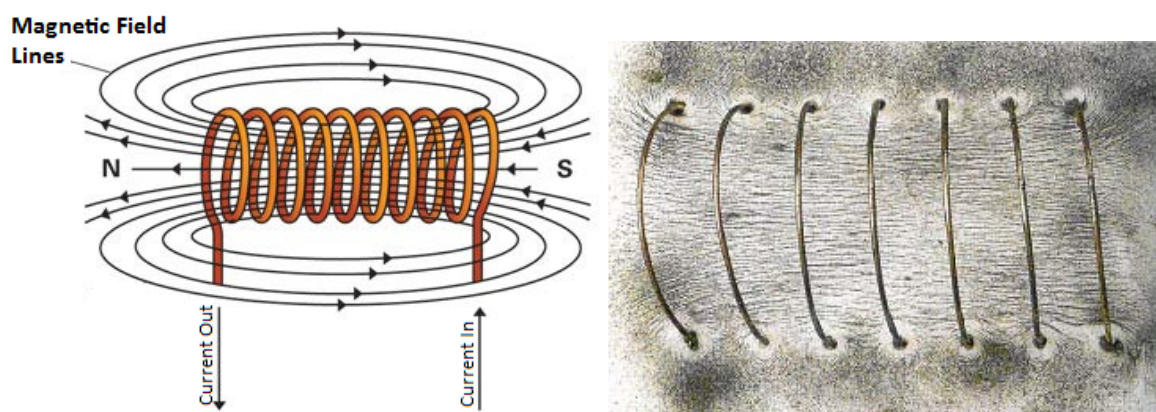


Fig. 2.6 Magnetic field produced by a solenoid

The twentieth century witnessed the magnetic applications in a wide range of areas such as electronics, nuclear magnetic resonance spectroscopy and materials science.

Magnetism arises from two sources:

- Electric currents or, more generally, moving electric charges;
- Many particles have nonzero “intrinsic” (or “spin”) magnetic moments.

Sources of magnetism are: electrons’ motions around the nucleus, electrons’ intrinsic magnetic moments, nuclear magnetic moments but they are typically

smaller than the electrons' ones, so they are negligible in the context of the magnetization of materials.

Either spontaneously, or owing to an applied external magnetic field, each electronic magnetic moments will be, on average, lined up. Then the material can produce a net total magnetic field, which can potentially be quite strong.

The magnetic behavior of a material depends on its structure, particularly its electron configuration, and also on the temperature. At high temperatures, random thermal motion destroys the alignment.

Ferromagnetism is the most familiar type of magnetism. Although elemental iron is traditionally considered as the “stuff of magnets”, many other materials exhibit magnetic properties including nickel and cobalt^[1], and more recently, even organic materials^[2]. Nonetheless, many applications are still based on iron even if the magnetic strength of iron magnets is relatively low.

The term *magnet* is typically reserved to objects that produce their own persistent magnetic field even in the absence of an applied magnetic field. Only certain classes of materials can do this. Most materials produce a magnetic field in response to an applied magnetic field.

Several forms of magnetic behavior have been observed in different materials, including:

- **Ferromagnetic** and **ferrimagnetic** materials are normally thought magnetic materials; they are attracted by a magnet. These materials retain magnetization and become magnets; a common example is a refrigerator magnet. Ferrimagnetic materials have weaker magnetic properties than ferromagnetics. The difference between ferro- and ferrimagnetic materials is related to their microscopic structures.
- **Paramagnetic** substances, such as platinum, aluminium, and oxygen, are weakly attracted by a magnet. This attraction is 10^5 times weaker than that of ferromagnetic materials, so it can be detected only by using sensitive instruments or extremely strong magnets (Fig. 2.7). Magnetic ferrofluids, although they are made of tiny ferromagnetic particles suspended in

liquid, are sometimes considered paramagnetic since they cannot be magnetized.

- **Superparamagnetism** appears in small ferromagnetic or ferrimagnetic nanoparticles. In sufficiently small nanoparticles, magnetization can randomly flip its direction under the influence of temperature. The Curie temperature, T_c , is an important parameter that characterizes the ferromagnetic materials: above of T_c the material lose the spontaneous magnetization. The paramagnetism is thus an intrinsic property, while the superparamagnetic depends on external conditions such as temperature or size. Furthermore, their magnetic susceptibility is much larger than the one of paramagnets.
- **Diamagnetic** means repelled by both poles. Compared to paramagnetic and ferromagnetic substances, diamagnetic substances, such as carbon, copper, water, and plastic, are even more weakly repelled by a magnet. The permeability of diamagnetic materials is less than the permeability of a vacuum.

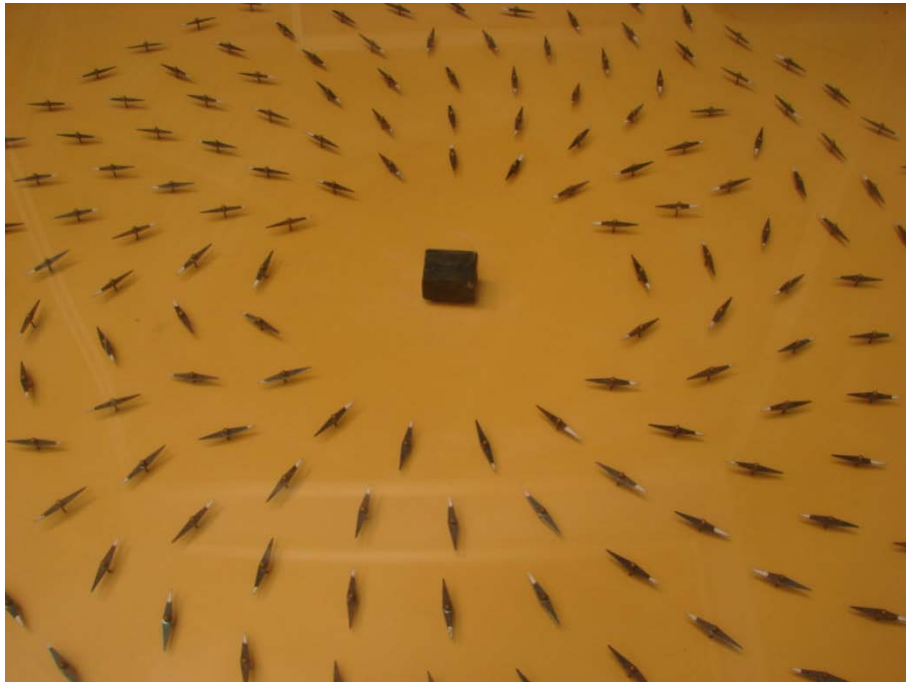


Fig. 2.7 Magnetic needles that feel a magnetic field

If a magnetic material is placed in a magnetic field of strength H , the individual

atomic moments in the material contribute to its overall response, resulting in the magnetic induction $\mathbf{B} = \mu_0(\mathbf{H} + \mathbf{M})$, where μ_0 is the permeability of free space, and the magnetization $\mathbf{M} = \mathbf{m}/V$ is the magnetic moment per unit volume, where \mathbf{m} is the magnetic moment of a volume V of the material.

Materials may be conveniently classified in terms of their volumetric magnetic susceptibility, χ , where $\mathbf{M} = \chi\mathbf{H}$ describes the magnetization induced in a material by \mathbf{H} . In SI units, χ is dimensionless, \mathbf{B} is expressed in Tesla (T), and both \mathbf{M} and \mathbf{H} are expressed in A/m.

Magnetic beads have additional advantages: having embedded magnetic entities, they can be magnetically manipulated using permanent magnets or electromagnets, independent of normal microfluidic or biological processes. This additional degree of freedom is the basis of a still improved exposure of the functionalized bead surface to the surrounding liquid, due to the increased relative motion of the bead with respect to the fluid. It is important to note that a magnetic field gradient is required to exert a translation force, because a uniform field solely gives rise to a torque, but no translational action. The magnetic force acting on a point-like magnetic dipole or “magnetic moment” \mathbf{m} in a magnetic induction \mathbf{B} can be written as a function of the derivative of the magnetic induction:^[3-7]

$$\mathbf{F}_m = \frac{1}{\mu_0}(\mathbf{m} \cdot \nabla)\mathbf{B} \tag{5}$$

As an example, for a constant moment \mathbf{m} in the x -direction, leading to $\mathbf{m} \cdot \nabla = m_x((\partial)/(\partial x))$, a force will be exerted on the moment, provided there is a magnetic field gradient in the x -direction.

The susceptibility of a particle is also called effective susceptibility and is related to the intrinsic susceptibility of the material χ_{mat} by $\chi = \chi_{\text{mat}}/(1 + N_d\chi_{\text{mat}})$, with N_d the demagnetization factor (1/3 for a spherical particle).^[8]

In case of superparamagnetic particles in a biological medium, one can describe the moment at small fields by the linear relation $\mathbf{m} = V\mu_0 \mathbf{M} = V\mu_0\Delta\chi\mathbf{H}$, with \mathbf{M} the magnetization of the particle and $\Delta\chi$ the difference in magnetic

susceptibility between the magnetic particle and the surrounding liquid medium. Using the relation $\mathbf{B} = \mu_0\mathbf{H}$, eq 5 for a superparamagnetic particle in the linear susceptibility regime becomes:

$$\mathbf{F}_m = \frac{V\Delta\chi}{\mu_0}(\mathbf{B}\cdot\nabla)\mathbf{B} \quad (6)$$

The magnetic moment of a superparamagnetic nanoparticle generally is smaller than that of a larger ferromagnetic microparticle. Hence, the magnetic force on a superparamagnetic particle will be smaller, which will result in slower magnetic separation processes. However, the advantage of superparamagnetic particles is the possibility to simply “switch off” the magnetic effects by removing the magnetic induction field.

In many applications, a magnetically labeled material is separated from a liquid solution by passing the fluid mixture through a region with a magnetic field gradient that can immobilize the tagged material via magnetic forces. For in vivo applications, magnetic particles can be transported by the blood flow and locally retained with the help of an external magnet. In other applications, there is a magnetic translational driving force, and the liquid solution is static. In the equilibrium state, the magnetic force \mathbf{F}_m is opposed to the hydrodynamic drag force \mathbf{F}_d acting on the magnetic particle.

The hydrodynamic drag force is a consequence of the velocity difference between the magnetic particle and the liquid Δv and, for a spherical particle with radius r , is given by:^[9]

$$\mathbf{F}_d = 6\pi\eta r\Delta v f_D \quad (7)$$

where η is the viscosity of the medium surrounding the particle (for water, $\eta = 8.9 \times 10^{-4}$ N s/m²). f_D is the drag coefficient of the particle and incorporates the influence of a solid wall in the vicinity of the moving particle.^[10,11]

In a microfluidic system, a particle may be moving under influence of the applied magnetic forces, so that the viscous force of eq 7 will vary along the particle trajectory. Equalizing eqs 6 and 7 permits one to determine the maximum

flow rate that a particle can withstand when exposed to a magnetic immobilization force, or the maximum particle flow rate that can be generated by a magnetic force in a surrounding static liquid:

$$\Delta v = \frac{2r^2 \Delta\chi (\mathbf{B} \cdot \nabla) \mathbf{B}}{9\mu_0 \eta f_D} \equiv \frac{1}{\mu_0 f_D} \xi (\mathbf{B} \cdot \nabla) \mathbf{B} \quad (8)$$

with

$$\xi \equiv \frac{2r^2 \Delta\chi}{9\eta} = \frac{V \Delta\chi}{6\pi r \eta} \quad (9)$$

the “magnetophoretic mobility” of the particle, a parameter describing how magnetically manipulable the particle is. The quantity $(\mathbf{B} \cdot \nabla) \mathbf{B}$ can be a strongly varying function in space, which implies a similar spatial variation for Δv .

References

- [1] C.H. Setchell; *J. Chem. Tech. Biothec.*, **35B**, 175 (1985)
- [2] J.S. Miller, A.J. Epstein; *Chem. Commun.*, **13**, 1319 (1998)
- [3] R. Becker; *Electromagnetic Fields and Interactions*; Dover: New York, (1982)
- [4] S. Chikazumi; “*Physics of Magnetism*”, R.E. Krieger Publishing Co.: Malabar, FL, (1964)
- [5] U. Häfeli, W. Schütt, J. Teller, M. Zborowski; “*Scientific and Clinical Applications of Magnetic Carriers*”; Plenum Press: New York, (1997)
- [6] Y. Moser, T. Lehnert, M.A.M. Gijs; *Appl. Phys. Lett.* 022505 (2009)
- [7] S.S. Shevkoplyas, A.C. Siegel, R.M. Westervelt, M.G. Prentiss, G.M. Whitesides; *Lab Chip* **7**, 1294 (2007)
- [8] Jackson, J. *Classical Electrodynamics*; Wiley: New York, (1998)
- [9] F.M. White; *Fluid Mechanics*; McGraw-Hill: New York, (1999)
- [10] H. Faxen; *Ann. Phys.* **68**, 89 (1922)

- [11] R. Wirix-Speetjens, W. Fyen, K.D. Xu, J. De Boeck, G. Borghs; *IEEE Trans. Magn.* **41**, 4128, (2005)

2.4 Magnetic Particles

Intense interest in magnetic nanoparticles that are superparamagnetic^[1-4] has arisen from their potential applications ranging from clinical diagnostics to industrial processes.

Magnetic nanoparticles (MNPs) have been employed for magnetic spin-based data storage,^[5-7] proposed as contrast agents for the treatment of localized radiation in MRI^[8-11], used in anti-angiogenic therapy to induce vascular occlusion in tumors^[12] and hypothermia treatment of cancer cells.^[13] In 1960 Freeman et al. proposed that the magnetic nanoparticles could be transported through the vascular system and focused through a magnetic field in an area of the body,^[14] but the idea of using magnetic nanoparticles as carriers for therapeutic substances dates back only to 1970.^[15] Since then, several strategies have been proposed to transport therapeutic substances in a specific site, such as near a tumor.^[16] Today the scientific community is trying to exploit the intrinsic properties of magnetic nanoparticles to overcome the limitations associated with conventional therapies in the treatment of cancer,^[17] such as chemotherapy, surgery, radiotherapy and immunotherapy that are limited by the accessibility to the tumor site, the risk of operating on a vital organ, the lack of selectivity toward cancer cells.^[16]

The magnetic nanoparticles due to their unique physical properties represent the largest class of nanoscale materials with the potential to revolutionize the current clinical diagnostic and therapeutic technique, because they have dimensions with a magnitude similar to those of many biomolecules, so are capable of interacting with biological species both in vitro and in vivo.

Some naturally occurring iron oxides such as magnetite (Fe_3O_4) and maghemite ($\gamma\text{Fe}_2\text{O}_3$) possess magnetic properties which have been exploited in various applications such as sewage treatment.

Although often referred to as magnetic, such materials are more strictly termed paramagnetic (and superparamagnetic). This means that these materials are attracted by a magnetic field, but do not retain the magnetism when the field is removed. This property is particularly useful for biochemical applications.^[18,19]

The colloidal iron oxide nanoparticles have been extensively studied for biomedical applications, due to their excellent biocompatibility and easy to synthesis.

Typically composed of magnetite or maghemite nanocrystals protected by a polymer coating, these ferrite nanoparticles form with oxygen ions a cubic lattice crystal structure with the iron ions located to the interstices. In addition to their magnetic properties, also biodegradability and biocompatibility have contributed to their diffusion in biomedical applications. Regarding the metabolism of the ferric ions nanoparticles are added to the body's iron stores, enabling safe use in vivo.^[20]

Depending on the methods of synthesis, the magnetization can vary greatly even in particles of similar size due to the incorporation of impurities, which can disrupt the crystal structure and surface effects.^[21]

To improve the magnetic properties MFe_2O_4 compounds have been developed where M can be Mn, Fe, Co and Ni.^[22] It has been shown, for example, that MFe_2O_4 nanoparticles are non-toxic in vitro and possess a higher magnetic susceptibility than magnetite nanoparticles, suggesting the possible use as ultra-sensitive probe in MRI.^[23]

2.4.1. Magnetic Particles in biomedicine

The use of magnetic bead solutions for biomedical applications, but excluding microfluidic applications, has been reviewed several times.^[24-28]

An important in vivo application is the use of magnetic beads to produce a distortion in the magnetic field at a given site under examination via MRI. The presence of magnetic beads strongly alters the cell contrast, enabling visualization of hitherto impossible objects. Another in vivo application lies in the production of controlled heating: a high-frequency magnetic field can be used to selectively warm a given area and destroy malignant tissue by hyperthermia. Magnetic beads can also play a role of vector in drug targeting and can be magnetically guided to the desired location. (Fig. 2.8)

For in vitro applications, the possibility of the specific labeling of cells or biomolecules with magnetic microbeads has led to advanced developments in cell manipulation and biomolecule separation, DNA sequencing, and biomolecule selection and purification.

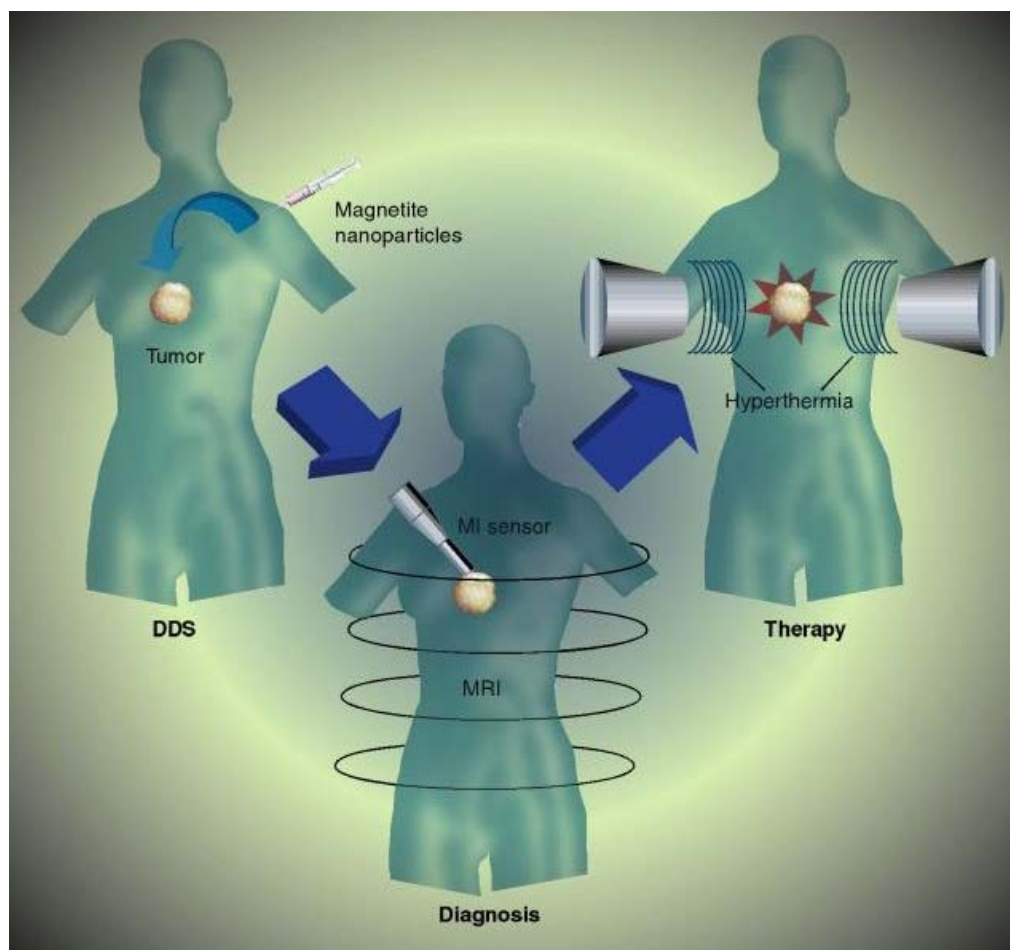


Fig. 2.8 Magnetic particles in biomedicine

In MRI, image contrast is a result of the different signal intensities that each tissue produces in response to a particular sequence of applied radio frequency pulses. This response depends on the proton density and magnetic relaxation times of the tissue. Target-specific superparamagnetic particles can serve as a dramatic source of contrast and have become an indispensable tool for the non-invasive study of biological processes with MRI. Superparamagnetic particles change the local rate at which protons decay from their excited state to the ground state.

When biocompatible dextran- or starch-coated particles selectively bind to

healthy or diseased cells, they generate a local magnetic dipole in the large field of the MRI setup which, by a change in the local proton relaxation time, is at the basis of the imaging contrast between the different types of cells.^[29-32]

There is also a size effect: for example, nanoparticles with diameters of ca 30 nm or more are rapidly collected by the liver and spleen, while particles with sizes of ca 10 nm or less are not so easily recognized. The smaller particles, therefore, have a longer half-life time in the blood and are collected by certain types of cells in the lymph nodes and the bone marrow.^[33]

Hyperthermia is one of the most promising approaches in cancer therapy: it consists in heating and destroying the target tissue to temperatures between 42°C and 46°C. Various methods are employed in hyperthermia, such as the use of hot water, capacitive heating, and inductive heating of malignant cells.^[34-39]

The problem with hyperthermia is the difficulty of local heating of only the tumor region until the required temperature is reached, without damaging the surrounding normal tissue. Magnetic particle hyperthermia is appealing because it offers a way to ensure that only the intended target tissue is heated. The concept is based on the principle that a magnetic particle can generate heat by hysteresis loss when placed in a high-frequency (~1 MHz) magnetic field.^[35]

Intracellular hyperthermia using dextran nanoparticles dates from 1979.^[38] The principle of heating with superparamagnetic particles (that show no magnetic hysteresis at low frequencies) by an AC field has been reviewed by Rosensweig^[39]: the heat dissipation results from the orientational relaxation of the particles having thermal fluctuations in a viscous medium.^[40] A number of studies have demonstrated the therapeutic efficacy of this form of treatment in animal models^[41], but the application of this technology to human patients is just starting.^[42]

A disadvantage of most chemotherapies is that they are relatively non-specific and induce secondary effects in the healthy tissue. In magnetically targeted therapy, a cytotoxic drug is attached to biocompatible magnetic carriers that are

injected into the patient via the circulatory system. When the particles have entered the bloodstream, external high-gradient magnetic fields are used to concentrate the complex at a specific target site within the body.^[43]

Once the drug carrier is concentrated at the target, the drug can be released either via enzymatic activity or changes in physiological conditions, such as pH or temperature^[44], and be taken up by the tumor cells. An overview of the clinical applications of magnetic drug targeting was given by Lubbe et al.^[45]

Agglomerates of superparamagnetic particles larger than 1 μm were shown to be more effective in withstanding flow dynamics within the circulatory system. In most cases, the magnetic field gradient is generated by a strong permanent magnet, such as NdFeB, fixed outside the body on the target site. Limitations of the technique are: (1) possibility of embolization of blood vessels in the target region due to the accumulation of magnetic carriers; (2) difficulties in scaling up from animal models due to the larger distances between the target site and the magnet; (3) the fact that, once the drug is released, it is no longer attracted to the magnetic field; and (4) toxic responses to the magnetic carriers.^[27]

In addition, the magnetic carriers have been used in clinical trials to target cytotoxic drugs (doxorubicin) in tumors such as sarcoma.^[46]

2.4.2. Protection and Functionalization of MNPs

Nanoparticles have a significant tendency to agglomerate (coalesce) due to their high surface energy. The electrostatic colloidal stabilization, which results from the repulsion of surface charges on the nanoparticles, it is usually not enough to prevent the aggregation in biological solutions due to the presence of salts or other electrolytes that can neutralize these charges.^[47]

Maintaining the stability of magnetic beads for a long time without agglomeration or precipitation problems is a prerequisite for applications. Especially pure metallic particles are subjected to oxidation or degradation, but also magnetite nanoparticles are not very stable under ambient conditions, and can be easily oxidized to maghemite or dissolved in an acid medium.

Particle protection results in magnetic beads having a core-shell structure, where the role of the shell is to protect the magnetic core against environmental influence. Also, some particle compounds, in particular cobalt, are considered extremely toxic, and thus its leakage into liquid media must be avoided. Several coating strategies exist, coating the magnetic nanoparticles with organic shells containing surfactants and polymers, with inorganic compounds like silica, with carbon, with precious metals. Besides simply coating individual magnetic nanoparticles, it is also possible to embed a number of magnetic nanoparticles or magnetic material in a polymer or silica matrix to form composites. This way, one can synthesize microbeads that, due to a higher magnetic content, are more easy and rapid to manipulate magnetically than the primary magnetic nanoparticles. Such types of beads (size around 1 μm) are therefore often used in microfluidic systems.

Electrostatic or steric repulsions can be used to keep the nanoparticles dispersed in a non-agglomerated colloidal state. the stability of ferrofluids^[48] results from a control of surface charges and the use of specific surfactants; both water- and oil-based ferrofluids are available. Surfactants or polymers can be chemically linked to or physically adsorbed to the magnetic nanoparticles, creating repulsive forces (due to steric hindrance) that balance the attractive magnetic, electrostatic, and van der Waals forces. Polymers containing functional groups, such as carboxylic acids, phosphates, and sulfates, can bind to the surface of iron oxide,^[49] while surface modified magnetic nanoparticles with certain biocompatible polymers are intensively studied for magnetic-field-directed drug targeting^[50] and as contrast agents for magnetic resonance imaging.^[51,52]

Biodegradable or non-biodegradable (organic and inorganic) coatings can be used to avoid the removal, to delay the identification and uptake by macrophages of the RES (reticulo-endothelial system). PEG is the most common coating: it is a neutral linear polyester, which attached to the surface of nanoparticles creates a shielding effect or "stealth", retards the action of the RES and prolongs circulation time. PEG shows a low toxicity and immunogenicity, and is excreted through the

kidneys.

Silica coatings are attractive due to their relatively good stability under aqueous conditions, their easy surface modification, and control of interparticle interactions via the variation of shell thickness.

The coating thickness can be varied by tuning the concentration of ammonium and the ratio of tetraethoxysilane (TEOS) to water. Silica-coated magnetic nanoparticles (Fig. 2.9) are hydrophilic and can be easily functionalized with several groups.^[53] Direct silica deposition on pure metal nanoparticles is complicated because of the lack of hydroxyl groups on the metal surfaces. Another problem is the oxidation of metals like iron or cobalt in the presence of dissolved oxygen in the reaction medium. Although silica coatings are in general robust, silica is unstable under basic conditions and, in addition, may contain pores through which oxygen can diffuse.

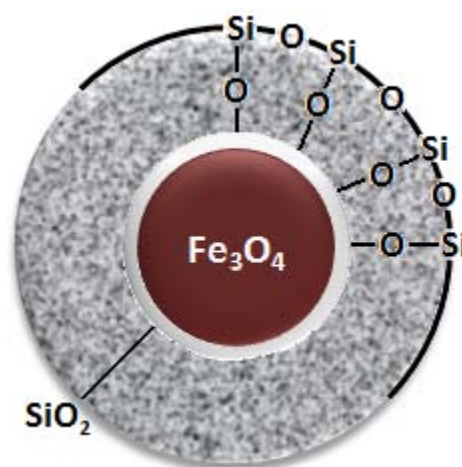


Fig. 2.9 Silica-coated magnetic nanoparticles

Another interesting feature is the porosity of the silica: it can be used to accommodate a drug avoiding the adsorption of larger molecules. For example, albumin, which has an effective spherical radius of about 40 Å, can be inserted into these micropores, whereas molecules larger than 4 nm would be excluded. Finally, the silica is heat resistant, has a large surface area and has good mechanical strength.

A shell around a magnetic nanoparticle or a matrix protect the particle against

degradation, but they can also be used to functionalize the bead surface with specific molecules. Ligands as targeting agents, permeation enhancers, proteins, optical dyes and therapeutic agents can be conjugated to the surface or embedded within these nanostructures.

The targeted units, for example, can be responsible for specific ligand-receptor interaction and the presence of receptors on the membrane can enhance the targeted release and facilitate the transfer to interior thereof through a receptor-mediated endocytosis.

Silica-coated beads can be used as-prepared to recover and purify the total DNA content of a lysed cell solution.^[54]

References

- [1] C.P. Bean, J.D.J. Livingstone; *Appl. Phys.*, 30, 120S (1959)
- [2] G.A. Held, G. Grinstein, H. Doyle, S. Sun, C.B. Murray; *Phys. Rev. B*, 64, 012408-1 (2001)
- [3] S.N. Molotkov, S.S. Nazin; *Phys. Low-Dimens. Struct.*, 10, 85 (1997)
- [4] P. Poddar, T. Fried, G. Markovich; *Phys. Rev. B*, 65, 172405-1 (2002)
- [5] M.H. Kryder; *MRS Bull.*, 21, 17 (1996)
- [6] D. Weller, A. Moser; *IEEE Trans. Magn.*, 35, 4423 (1999)
- [7] S. Sun, D. Weller; *J. Magn. Soc. Jpn.*, 25, 1434.(2001)
- [8] S.H. Koenig, K.E. Kellar; *Academic Radiology*, 3, 273 (1996)
- [9] S.A. Corr, S.J. Byrne, R. Tekoriute, C.J. Meledandri, M.L. Grougham, C. Kerskens, L. O'Dwyer, Y.K. Gun'ko; *J. Am. Chem. Soc.*, 130, 4214 (2008)
- [10] O. Veiseh, C. Sun, J. Gunn, N. Kohler, P. Gabikian, D. Lee, N. Bhattarai, R. Ellenbogen, R. Sze, A. Hallahan, J. Olson, M. Zhang; *Nano Lett.*, 5, 1003 (2005)
- [11] P.H. Meyers; *Am. J. Roentgenology Radium Ther. Nucl. Med.*, 90, 1668 (1963)
- [12] J.F. Alksne, A.G. Fingerhut; *Bull. Neurol. Soc.*, 30, 153 (1965)

- [13] I. Hilger, W. Andra, R. Hergt, R. Hiergeist, H. Schubert, W.A. Kaiser; *Radiology*, 218, 570 (2001)
- [14] M.W. Freeman, A. Arrot, J.H.L. Watson; *J. Appl. Phys.*, 31, S404 (1960)
- [15] K.J. Widder, A.E. Senyei, D.G. Scarpelli; *Proc. Soc. Exp. Biol. Med*, 58, 141 (1978)
- [16] M. Arruebo, R. Fernandez-Pacheco, M.R. Ibarra, J. Santamaria; *Nano Today Review*, 2, 22 (2007)
- [17] S.Conroy, S.H.L. Jerry, Z. Miqin; *Adv. Drug Delivery Rev.*, 60, 1252 (2008)
- [18] I. Safarik, M. Safarikova, S.J. Forsythe; *J. Appl Bacterial*, 78, 575 (1995)
- [19] A. Sinclair; "To beads or not to beads - application of magnetic bead technology", *The Scientists*, 12, 13 (1998)
- [20] R. Weissleder, D.D. Stark, B.L. Engestald, B.R. Bacon, C.C. Compton, D.L. White, P. Jacobs, J. Lewis; *American J. of Roentgenology*, 152, 167 (1989)
- [21] A.K. Gupta, M. Gupta; *Biomaterials*, 6, 3995 (2005)
- [22] M.A. Willard, L.K. Kurihara, E.E. Carpenter, S. Calvin, V.G. Harris; *International Materials Review*, 49, 125 (2004)
- [23] G. Baldi, D. Bonacchi, M.G. Franchini, D. Gentili, G. Lorenzi, A. Ricci, C. Ravagli; *Langmuir*, 23, 4026 (2007)
- [24] J. Roger, J.N. Pons, R. Massart, A. Halbreich, J.C. Bacri; *Eur Phys J Appl Phys*, 5, 321 (1999)
- [25] I. Safarik, M. Safarikova; *Monatsh Chem* 133(6):737–759(2002)
- [26] M. Shinkai; *J Biosci Bioeng* 94(6):606–613 (2002)
- [27] Q.A. Pankhurst, J. Connolly, S.K. Jones, J. Dobson; *J Phys D–Appl Phys* 36(13):R167–R181(2003)
- [28] L.A. Bauer, N.S. Birenbaum, G.J. Meyer; *J Mater Chem* 14(4):517–526 (2004)

- [29] R. Lawaczeck, H. Bauer, T. Frenzel, M. Hasegawa, Y. Ito, K. Kito, N. Miwa, H. Tsutsui, H. Volger, H.J. Weinmann; *Acta Radiologica* 38(4):584–597 (1997)
- [30] D.K. Kim, Y. Zhang, J. Kehr, T. Klason, B. Bjelke, M. Muhammed; *J Magnetism Magn Mater* 225(1–2):256–261 (2001)
- [31] D.K. Kim, Y. Zhang, W. Voit, K.V. Kao, J. Kehr, B. Bjelke, M. Muhammed; *Scripta Materialia* 44(8–9):1713–1717(2001)
- [32] D.K. Kim, M. Mikhaylova, F.H. Wang, J. Kehr, B. Bjelke, Y. Zhang, T. Tsakalagos, M. Muhammed; *Chem Mater* 15(23):4343–4351 (2003)
- [33] S.G. Ruehm, C. Corot, P. Vogt, S. Kolb, J.F. Debatin; *Circulation* 103(3):415–422 (2001)
- [34] R. Cavalier, E.C. Ciocatto, B.C. Giovanel, C. Heidelbe, R.O. Johnson, M. Margotti, B. Mondovi, G. Moricca, A. Rossifan; *Cancer* 20(9):1351 (1967)
- [35] P.R. Stauffer, T.C. Cetas, A.M. Fletcher, D.W. Deyoung, M.W. Dewhirst, J.R. Oleson, R.B. Roemer; *IEEE Trans Biomed Eng* 31(1):76–90 (1984)
- [36] J.C. Lin, Y.J. Wang; *Int J Hyperthermia* 3(1):37–47(1987)
- [37] N. Ikeda, O. Hayashida, H. Kameda, H. Ito, T. Matsuda; *Int J Hyperthermia* 10(4):553–561 (1994)
- [38] R.T. Gordon, J.R. Hines, D. Gordon; *Med Hypotheses* 5(1):83–102 (1979)
- [39] R.E. Rosensweig; *J Magnetism Magn Mater* 252(1–3):370–374 (2002)
- [40] R. Hergt, W. Andra, C.G. d’Ambly, I. Hilger, W.A. Kaiser, U. Richter, H.G. Schmidt; *IEEE Trans Magn* 34(5):3745–3754 (1998)
- [41] P. Moroz, S.K. Jones, B.N. Gray; *Int J Hyperthermia* 18(4):267–284 (2002)
- [42] A. Jordan, R. Scholz, K. Maier-Hauff, M. Johannsen, P. Wust, J. Nadobny, H. Schirra, H. Schmidt, S. Deger, S. Loening, W. Lanksch, R. Felix; *J Magnetism Magn Mater* 225 (1–2): 118–126 (2001)
- [43] J. Dobson, *Drug Development Research*, 67, 55 (2006)

- [44] C. Alexiou; *Clin Cancer Res* 7(11):257 (2001)
- [45] A.S. Lubbe, C. Alexiou, C. Bergemann; *J Surg Res* 95(2):200–206 (2001)
- [46] K.J. Widder, R.M. Morris, G.A. Poore, D.P. Howard, A.E. Seneyei, *Eur. J. Cancer Clin. Oncol.*, 19, 9 (1983)
- [47] C.C. Berry, A.S.G. Curtis, *Journal of Physics D.*, 36, R198 (2003)
- [48] S.S. Papell; U.S. Patent 3215572, (1965)
- [49] R.M. Cornell, U. Schertmann; “*The Iron Oxides: Structure, Properties, Reactions, Occurrence and Uses*”, VCH: Weinheim, (1996)
- [50] A. Petri-Fink, M. Chastellain, L. Juillerat-Jeanneret, A. Ferrari, H. Hofmann; *Biomaterials*, 26, 2685 (2005)
- [51] R. Lawaczeck, H. Bauer; T. Frenzel, M. Hasegawa, Y. Ito, K. Kito, N. Miwa, H. Tsutsui, H. Volger, H.J. Weinmann; *Acta Radiol.*, 38, 584 (1997)
- [52] D.K. Kim, Y. Zhang, J. Kehr, T. Klason, B. Bjelke, M.J. Muhammed; *Magn. Mater.*, 225, 256 (2001)
- [53] A. Ulman; *Chem. Rev.*, 96, 1533 (1996)
- [54] U. Lehmann, C. Vandevyver, V.K. Parashar; M.A.M. Gijs; *Angew. Chem., Int. Ed.*, 45, 3062 (2006)

2.5 Ferrofluids

Ferrofluids are colloidal liquids made of nanoscale ferromagnetic, or ferrimagnetic, particles suspended in a carrier fluid (usually an organic solvent or water) which becomes strongly magnetized in the presence of a magnetic field.

Particles, with an average size of about 100 Å (10 nm), are coated with a stabilizing dispersing agent (surfactant) which prevents particle agglomeration even when a strong magnetic field gradient is applied. However, the surfactant tends to break down over time (a few years), and eventually the nano-particles will agglomerate, and they will separate out and no longer contribute to the fluid's magnetic response.

Ferrofluids were originally discovered in the 1960s at the NASA Research Center, where scientists were investigating different possible methods of controlling liquids in space. The benefits of a magnetic fluid were immediately obvious: the location of the fluid could be precisely controlled through the application of a magnetic field, and, by varying the strength of the field, the fluids could be forced to flow. Researchers have prepared ferrofluids containing small particles of ferromagnetic metals, such as cobalt and iron, but the most work has been conducted on ferrofluids containing small particles of magnetite, Fe_3O_4 .

In the absence of a magnetic field, the magnetic moments of the particles are randomly distributed and the fluid has no net magnetization. When a magnetic field is applied to a ferrofluid, the magnetic moments of the particles orient along the field lines almost instantly. The magnetization of the ferrofluid responds immediately to the changes in the applied magnetic field and when the applied field is removed, the moments randomize quickly. Some ferrofluids are attracted by magnetic fields that they will stand up along magnetic field lines, forming an array of spikes (Fig. 2.10).

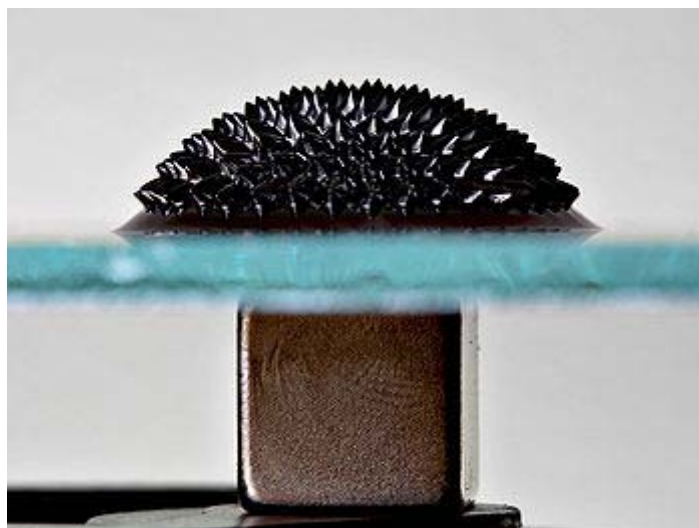


Fig. 2.10 Magnetic lines of force shown by ferrofluid

In a field gradient the whole fluid responds as a homogeneous magnetic liquid which moves to the region of highest flux. This means that ferrofluids can be precisely positioned and controlled by an external magnetic field. For these reason they are classified as superparamagnets rather than ferromagnets.

2.5.1 Applications

Although the array of spikes on the surface of the ferrofluid is spectacular, this property is not particularly useful. However, ferrofluids have found a wide variety of applications, including use in rotating shaft seals. A ferrofluid can behave as a liquid O-ring where a rotating shaft enters either a low- or high-pressure chamber. The ferrofluid is held in place by permanent magnets and forms a tight seal, eliminating most of the friction produced in a traditional mechanical seal. These rotating shaft seals are found in rotating anode X-ray generators and in vacuum chambers used in the semiconductor industry. Ferrofluid seals are used in high-speed computer disk drives to eliminate harmful dust particles or other impurities that can cause the data-reading heads to crash into the disks.

Another application of ferrofluids is the improving the performance of loudspeakers. In a loudspeaker, electric energy is sent through a coil located in the center of a circular permanent magnet. The magnetic field induced by the electric energy causes the coil to vibrate and thus produces sound and heat. Bathing the

electric coil in a ferrofluid, which is held in place by circular permanent magnets, dampens unwanted resonances and also provides a mechanism to dissipate heat from excess energy supplied to the coil. Both of these factors lead to an overall improved sound quality.

Finally, there is much hope for future biomedical applications of ferrofluids. For example, researchers are attempting to design ferrofluids that can carry medications to specific locations in the body through the use of applied magnetic fields. Other ongoing work is investigating the use of ferrofluids as contrast agents for magnetic resonance imaging.

2.6 Lipoprotein

Lipoproteins are *biochemical assemblies* that contain both proteins and lipids. Lipids or their derivatives may be covalently or non-covalently bound to proteins. Many enzymes, transporters, structural proteins, antigens, adhesins and toxins are lipoproteins. Examples include the high density (HDL) and low density (LDL) lipoproteins, which enable fats to be carried in the blood stream.

Lipoproteins have hydrophilic groups of phospholipids, cholesterol and apoproteins directed outward. Such characteristics makes them soluble in the salt water-based blood pool. Triglyceride-fats and cholesterol esters are internally carried, shielded from the water by the phospholipid monolayer and apoproteins.

Lipoproteins may be classified in five major groups as follows:^[1]

- Chylomicrons, which carry triglycerides (fat) from the intestines to the liver, skeletal muscle, and adipose tissue.
- Very-low-density lipoproteins (VLDL), which carry triacylglycerol from the liver to adipose tissue.
- Intermediate-density lipoproteins (IDL), that are intermediate between VLDL and LDL. They are not usually detectable in the blood.
- Low-density lipoproteins (LDL), that carry cholesterol from the liver to cells of the body. LDLs are sometimes referred to as the "bad cholesterol" lipoprotein.
- High-density lipoproteins (HDL), which collect cholesterol from the body's tissues, and bring it back to the liver. HDLs are sometimes referred to as the "good cholesterol" lipoprotein.

Class	Density (g/mL)	Diameter (nm)
HDL	>1.063	5–15
LDL	1.019–1.063	18–28
IDL	1.006–1.019	25–50
VLDL	0.95–1.006	30–80
Chylomicrons	<0.95	100-1000

Table 2.1 Features of main Lipoproteins

2.6.1 Cholesterol

The name cholesterol originates from the Greek *chole-* (bile) and *stereos* (solid), and the chemical suffix *-ol* for an alcohol (Fig. 2.11).

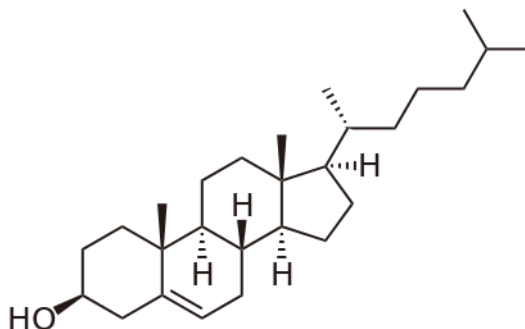


Fig.2.11 Chemical structure of cholesterol

Cholesterol is a waxy steroid of fat that is produced in the liver or intestines. It is used to produce hormones and cell membranes and is transported in the blood plasma of all mammals. It is an essential structural component of mammalian cell membranes and is required to establish proper membrane permeability and fluidity. In addition, cholesterol is an important component for the manufacture of bile acids, steroid hormones, and vitamin D. Cholesterol is the principal sterol synthesized by animals; however, small quantities can be synthesized in other eukaryotes such as plants and fungi.

Since cholesterol is only slightly soluble in water (it is insoluble in blood), it is transported in the circulatory system within lipoproteins.

Phospholipids and cholesterol, being amphipathic, are transported in the surface monolayer of the lipoprotein particle (Fig 2.5.1). For these features it can also be considered as a *Lyotropic Liquid Crystal*.

Although cholesterol is important and necessary for mammals, high levels of cholesterol in the blood have been linked to damage to arteries and are potentially linked to diseases such as those associated with the cardiovascular system.

The cholesterol within all the various lipoproteins is identical, although some cholesterol is carried as the "free" alcohol and some is carried as fatty acyl esters referred to as cholesterol esters. However, the different lipoproteins contain

apolipoproteins, which serve as ligands for specific receptors on cell membranes. In this way, the lipoprotein particles are molecular addresses that determine the start- and end-points for cholesterol transport.

Cholesterol comes from two sources: our body and food. Liver and other cells in our body make about 75 percent of blood cholesterol. The other 25 percent comes from the foods we eat.

Among cholesterol it can be distinguished the so called "good" and "bad" cholesterol.

HDL is the "good" cholesterol which helps keep the LDL (bad) cholesterol, from getting lodged into artery walls. A healthy level of HDL may also protect against heart attack and stroke, while low levels of HDL (less than 40 mg/dL for men and less than 50 mg/dL for women) have been shown to increase the risk of heart disease.

LDL molecules, therefore, are the major carriers of cholesterol in the blood, and each one contains approximately 1,500 molecules of cholesterol ester. The shell of the LDL molecule contains just one molecule of apolipoprotein B100, which is recognized by the LDL receptor in peripheral tissues. Upon binding of apolipoprotein B100, many LDL receptors become localized in clathrin-coated pits. Both the LDL and its receptor are internalized by endocytosis to form a vesicle within the cell. The vesicle then fuses with a lysosome, which has an enzyme called lysosomal acid lipase that hydrolyzes the cholesterol esters. Now within the cell, the cholesterol can be used for membrane biosynthesis or esterified and stored within the cell (Fig. 2.12).

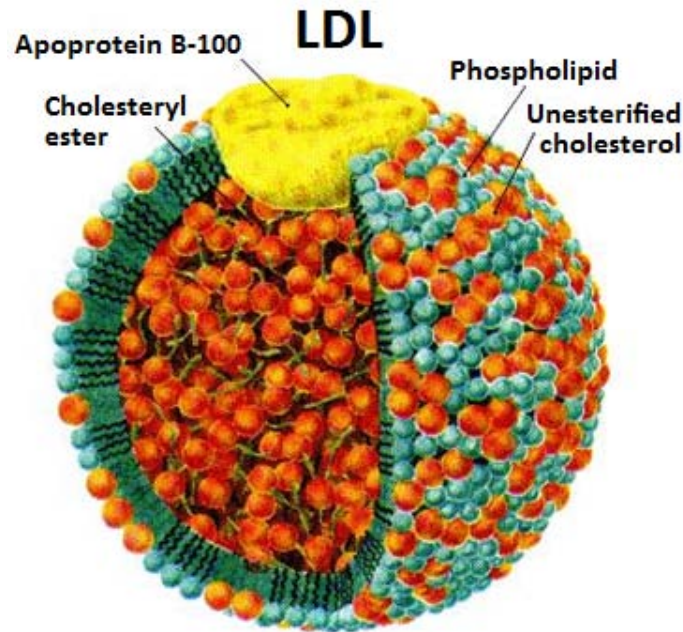


Fig.2.12 LDL organization

When the cell has abundant cholesterol, LDL receptor synthesis is blocked so new cholesterol in the form of LDL molecules cannot be taken up. On the converse, more LDL receptors are made when the cell is deficient in cholesterol. When this system is deregulated, many LDL molecules appear in the blood without receptors on the peripheral tissues. These LDL molecules are oxidized and taken up by macrophages, which become engorged and form *foam cells*. These cells often become trapped in the walls of blood vessels and contribute to atherosclerotic plaque formation (Fig. 2.13).^[2]

Also, HDL particles are thought to transport cholesterol back to the liver for excretion or to other tissues that use cholesterol to synthesize hormones in a process known as *reverse cholesterol transport* (RCT).^[3] Having large numbers of HDL particles correlates with better health outcomes.^[4] In contrast, having small numbers of large HDL particles is independently associated with atheromatous disease progression within the arteries.

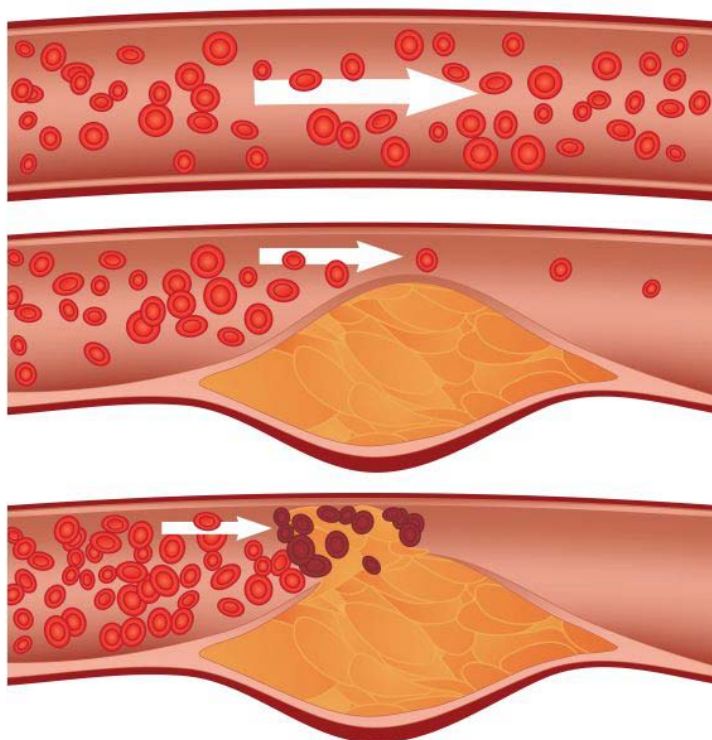


Fig.2.13 Atherosclerotic plaque formation steps

Cholesterol-rich microemulsion (LDE) binds to low-density lipoprotein (LDL) receptors. It is selectively taken up by malignant cells that overexpress those receptors and may be used as vehicle for antineoplastic agents.^[5,6]

LDE roughly resembles the LDL lipidic structure, is made without proteins, but when injected into the blood stream it acquires several small molecular weight apolipoproteins, including apoE. ApoE endows LDE particles to bind to the LDL receptors, since those receptors recognize not only the apoB present in LDL, but also apoE that is not found in the LDL fraction. LDE may be used as a probe to verify LDL intravascular metabolism and removal and LDL receptor function.^[7]

Cholesterol, as already said, is susceptible to oxidation and easily forms oxygenated derivatives known as *oxysterols*. Three different mechanisms can form oxysterols: autoxidation, secondary oxidation to lipid peroxidation, and cholesterol-metabolizing enzyme oxidation. A great interest in oxysterols arose when they were shown to exert inhibitory actions on cholesterol biosynthesis.^[8]

Cholesterol is also oxidized by the liver into a variety of bile acids.^[9] These, in turn, are conjugated with glycine, taurine, glucuronic acid, or sulfate. A mixture of

conjugated and nonconjugated bile acids, along with cholesterol itself, is excreted from the liver into the bile. Approximately 95% of the bile acids are reabsorbed from the intestines, and the remainder are lost in the feces.^[10]

2.6.2 Cholesterol as cause of vascular diseases

The cause and progression of vascular diseases is intimately related to the health of the inner arterial walls. However a barrage of atherogenic factors, if left unchecked, damages the delicate endothelial cells. This damage leads to endothelial dysfunction and ultimately allows lipids and toxins to penetrate the endothelial layer and enter the smooth muscle cells. This results in the initiation of an oxidative and inflammatory cascade that culminates in the development of plaque deposits. Subsequently, these plaques begin to calcify and, over time, become prone to rupture. If a plaque deposit ruptures, the result is oftentimes a deadly blood clot.

Numerous factors that directly contribute to endothelial dysfunctions have been identified and aging individuals can easily assess their risk for vascular disease through blood testing. The results of these blood tests can then be used to develop targeted intervention strategies to modify levels of risk factors that do not fall within an optimal range. Atherogenic factors are:

- **Elevated LDL cholesterol.** When too much LDL cholesterol circulates in the blood, it can slowly build up in the inner walls of the arteries that feed the heart and brain. Together with other substances, it creates *foam cells*, which form the core of a plaque hard deposit that can narrow the arteries and make them less flexible. Oxidized LDL cholesterol (LDL that has been exposed to free radicals) within the endothelium also triggers an inflammatory process that accelerates vascular disease. Life Extension recommends keeping LDL cholesterol levels below 80 mg/dL.
- **Low HDL cholesterol.** HDL protects against vascular diseases by transporting cholesterol from the blood vessel wall back to the liver for disposal through a process known as *reverse cholesterol transport*. If HDL

levels are low, then reverse cholesterol transport becomes inefficient, allowing for increased accumulation of cholesterol in the vessel wall. HDL levels of at least 50-60 mg/dL are recommended for optimal vascular protection.

- **Elevated triglycerides.** Triglycerides interact with LDL cholesterol to form a particularly dangerous sub-type of LDL known as *small-dense LDL*. Small-dense LDL particles penetrate the endothelial layer and contribute to plaque formation much more efficiently than larger, more buoyant LDL particles. Life Extension recommends keeping fasting triglycerides below 80 mg/dL to limit the formation of small-dense LDL particles.
- **Oxidized LDL.** The oxidation of **LDL** results in severe vascular damage. Thousands of studies now reveal how oxidized LDL contributes to the entire atherogenic process from start to finish. Commercial blood tests are not yet available at affordable prices to measure oxidized LDL. Aging individuals should assume their endogenous antioxidant levels (superoxide dismutase, catalase, and glutathione) are being depleted and that the oxidation of their LDL is progressively worsening (Matsuura, 2008). Many of the nutrient suggestions in this protocol afford considerable protection against LDL oxidation.
- **Hypertension.** High blood pressure is known to aggravate endothelial dysfunctions and leading researchers have identified the endothelium as an “end organ” for damage caused by high blood pressure. Life Extension suggests a target optimal blood pressure of 115/75 mmHg (or lower).

Reference

- [1] Garrett & Grisham; “*Biochemistry*” 2nd Ed. *Harcourt Brace, Custom Publishers* (1995)
- [2] J.L. Tymoczko, S.B. Tymoczko, S. Lubert, B.J. Mark; *Biochemistry. San Francisco: W.H. Freeman. 726* (2002)

- [3] G.F. Lewis, D.J. Rader; *Circ. Res.*, 96, 1221(2005)
- [4] D.J. Gordon, J.L. Probstfield, R.J. Garrison, J.D. Neaton, W.P. Castelli, J.D. Knoke, D.R. Jacobs, S. Bangdiwala, H.A. Tyroler; *Circulation*, 79,8 (1989)
- [5] S.R. Graziani, F.A. Igreja, R. Hegg, C. Meneghetti, L.I. Brandizzi, R. Barboza, R.F. Amâncio, J.A. Pinotti, R.C. Maranhão; *Gynecol Oncol.*;85493 (2002)
- [6] A. Ades, J.P. Carvalho, , R.F. Amancio, J.S. Souen, J.A. Pinotti, R.C. Maranhão; *Gynecol Oncol.*, 82, 84 (2001)
- [7] R.D. Santos, W. Hueb, A.A. Oliveira, J.A.F. Ramires, R.C. Maranhão; *Journal of Lipid Research* 44, 464 (2003)
- [8] A.A. Kandutsch, H.W. Chen, H.J. Heiniger; *Science* 201 (4355): 498 (1978)
- [9] N.B. Javitt; *FASEB J.*, 8, 1308 (1994)
- [10] A.W. Wolkoff, D.E. Cohen; *Am. J. Physiol. Gastrointest. Liver Physiol.* 284 (2): G175–9 (2003)

2.7 Liposomes

Liposomes (from the Greek words: 'LIPO' meaning fat and 'Soma' meaning body) were first described in 1961 by British haematologist Bangham^[1-3]. Liposomes are lyotropic liquid crystals composed mainly by one or more amphiphilic bilayers that form hollow microspheres. (Fig. 2.14)

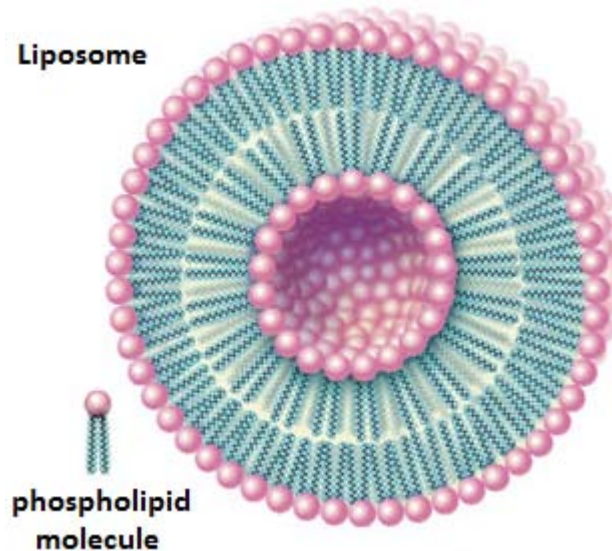


Fig. 2.14 Liposome

The interest of liposomes is related to their membrane that can be composed by naturally derived (consisting of cholesterol and phospholipids such as phosphatidyl-choline and *diacetyl-phosphate*) or other surfactants, whose structure, composition and proportions are virtually identical to the membrane of host cells. Phospholipids have a hydrophobic tail and a hydrophilic head, which, dissolving in water, rearrange in this way: the hydrophobic tails are attracted to each other, while the hydrophilic heads are arranged in contact with the outside environment and the internal aqueous (similar to micelles). Consequently, are formed lipid bilayers similar to the cells of the organism. A liposome can be formed at a variety of sizes as uni-lamellar or multi-lamellar construction. Though liposomes can vary in size from low micrometer range to tens of micrometers, unilamellar liposomes are typically in the lower size range.

can be filled with drugs, linked with various targeting ligands attached to their surface, and used to deliver drugs for cancer.^[4]

Since the 70s they were used as vehicles for drugs. The understanding of their behavior "in vivo" has allowed the creation of specific studies on the specific treatment of certain diseases. Naturally fat-soluble drugs are accommodated in the double layer, water-soluble drugs are encapsulated into the hydrophobic membrane, and drugs with mixed properties between the double layer and the interior. In this way liposome can carry both hydrophobic and hydrophilic molecules.

These liposomes are small deposits which may contain an antigen, an antibiotic, an allergen, a drug or a gene (gene therapy) and can be introduced into the body without causing immune rejection reactions. They can be administered intravenously, orally or intramuscularly.

To deliver the molecules to sites of action, the lipid bilayer can fuse with other bilayers such as the cell membrane, thus delivering the liposome contents, which would normally be unable to diffuse through the membrane.

Liposomes can also be designed to deliver drugs in other ways. For example, to decrease the degradation rate of the liposomes and slow down the release of its contents, it possible to act changing their composition and size. It can also increase the affinity of liposomes for a given tissue by changing their composition, the electric charge, or even adding receptors or antigens, which increases the concentration of drug in the target organ.

Liposomes that contain low (or high) pH can be constructed such that dissolved aqueous drugs will be charged in solution (i.e., the pH is outside the drug's isoelectric point range). As the pH naturally neutralizes within the liposome (protons can pass through some membranes), the drug will also be neutralized, allowing it to freely pass through a membrane. These liposomes work to deliver drug by diffusion rather than by direct cell fusion. In addition to gene and drug delivery applications, liposomes can be used as carriers for the delivery of dyes to textiles,^[5] pesticides to plants, enzymes and nutritional supplements to foods, and

cosmetics to the skin.^[6]

On the other hand, liposomes have several disadvantages as drug delivery carriers because they are subject to oxidative degradation and must be stored and handled in a nitrogen atmosphere.

2.7.1 Types of liposomes

The main component of liposomes is phosphatidylcholine: They can be distinguished in:

- **Liposomes:** are small vesicles with a diameter of 50-500 nm surrounded by one or more phospholipid bilayer membranes. Inside there is material in aqueous phase. Liposomes have high affinity for the stratum corneum and make a deep epidermal hydration. The phospholipid liposomes are destroyed by phospholipid hydrolytic enzymes when they reach the stratum corneum. Liposomes larger than 200 nm are more easily recognized and captured by macrophages.
- **Niosomes:** are non-ionic surfactant-based liposomes. They are an evolution of the liposomes, where the phospholipids of the membrane lipids consist of non-ionic synthetic amphiphiles. Niosomes are smaller than 200 nanometers, equivalent to the intercellular space present in the corneal layer.

The non-ionic liposomes are more stable than phospholipid ones, moreover, they are not destroyed by phospholipid hydrolytic enzymes on stratum corneum, and finally, being non-ionic surfactants, niosomes are less toxic than vesicles produced with ionic surfactants.

Liposomes can be classified according to their different and more relevant characteristics: size, lamellarity (number of lipid bilayers that make up the liposome) and the preparation method. These parameters, as well as specify the differences between the liposomes, affect important features, such as: stability, pharmacokinetics, bioavailability.

There are three types of liposomes: **MLV** (multilamellar vesicles), **SUV** (Small

Unilamellar Vesicles) and **LUV** (Large Unilamellar Vesicles), which are used to deliver different types of drugs.

2.7.2 Manufacturing

Formation of liposomes and nanoliposomes is not a spontaneous process. Lipid vesicles are formed when phospholipids such as lecithin are placed in water and, consequently, form one bilayer or a series of bilayers, each separated by water molecules, once enough energy is supplied.^[7]

Liposomes can be prepared by disrupting biological membranes, for example by sonication of phospholipids in water.^[8]

Sonication is generally considered a "gross" method of preparation as it can damage the structure of the drug to be encapsulated. Newer methods such as extrusion and Mozafari method^[9] are employed to produce materials for human use.

The correct choice of liposome preparation method depends on the following parameters:^[10,11]

1. the physico-chemical characteristics of the material to be entrapped and those of the liposomal ingredients;
2. the nature of the medium, in which the lipid vesicles are dispersed;
3. the effective concentration of the entrapped substance and its potential toxicity;
4. additional processes involved during application/delivery of the vesicles;
5. optimum size, polydispersity and shelf-life of the vesicles for the intended application;
6. batch-to-batch reproducibility and possibility of large-scale production of safe and efficient liposomal products

2.7.3 Applications

The cosmetic industry has been the first to use extensively the liposomes.

The benefits of cosmetic preparations containing liposomes can be summarized in four points:

- Basic constituents of the liposomes, either of natural origin (phospholipids or sphingolipids) or synthetic (non-ionic surfactants), are generally completely biocompatible without unwanted allergenic or toxic effects;
- Liposomes are able to incorporate and vehiculate both hydrophilic and lipophilic substances;
- Vehiculated substances are protected from the action of enzymes (proteases, nucleases) or denaturing environments (pH). In this way can be used very labile substances as nucleic acids, peptides and proteins;
- Liposomes are able to reduce the side effects of toxic agents or irritants.

An unfavorable element is the high cost equipment.

Liposomes are an imitation of the same liposomes that are formed in the Golgi bodies in epidermal cells. Liposomes, enveloped by vesicles (Odland bodies), are expelled from the granular cells of the epidermis, and from there back to the shiny layer that separates the still viable cells from dead cells (stratum corneum). Here the phospholipid bilayer is enzymatically destroyed with the formation of a useful protective barrier composed of ceramides, cholesterol and fatty acids.

Thanks to their high viscosity, liquid crystalline systems are also useful when the drug should be used in a specific area, for example subcutaneously or intramuscularly in the body cavity, the skin or mucous membranes of different surfaces.^[12] Nowadays, several companies are involved in biotechnology work exclusively with liposomes for development of different treatments: antibiotics, cancer, allergic sensitization, gene therapy, etc.

Another interesting property of liposomes is their natural ability to target cancer. The endothelial wall of all healthy human blood vessels is encapsulated by endothelial cells that are bound together by tight junctions. These tight junctions stop any large particles in the blood from leaking out of the vessel. Tumour vessels do not contain the same level of seal between cells and are diagnostically *leaky*. This ability is known as the Enhanced Permeability and Retention effect. Liposomes of certain sizes, typically less than 200 nm, can rapidly enter tumour sites from the blood, but are kept in the bloodstream by the endothelial wall in healthy tissue

vasculature. Anti-cancer drugs such as Doxorubicin, Camptothecin and Daunorubicin are currently being marketed in liposome delivery systems.

Doxorubicin is a drug that, although very active, has the problem of a low therapeutic index, which strongly limits its use. There are two major problems: acute toxicity in the bone marrow and cardiac toxicity both acute and chronic.

A solution to improve the therapeutic index is the inclusion of doxorubicin inside the liposomes, so that the effective dose is achieved gradually: when the bilayers are opened, secrete their contents directly into the cells. In this way, the toxicity was shown to be controlled, however, addressed indiscriminately to all cells. Liposomes also were soon recognized as foreign by the immune system and eliminated before they could complete their work.

A major success has been achieved by coating the liposomes with a film of polyethylene glycol (PEG), an inert substance that does not alert the immune system. In this way, the pegylated liposomes can move freely in the blood for 2-3 weeks without being destroyed, and then enter into cancer cells through the newly formed capillaries, used for spraying the areas of cancer.

The toxicity of conventional doxorubicin, thanks to transport by pegylated liposome, decreases sharply, while the drug effectiveness remains unchanged improving the quality of life of patients.

References

- [1] A.D. Bangham; R.W. Horne; *Journal of molecular biology*, **8**: 660–668. (1964)
- [2] R.W. Horne, A.D. Bangham, V.P. Whittaker; *Nature* **200**: 1340, (1963)
- [3] A.D. Bangham, R.W. Horne, A.M. Glauert, J.T. Dingle, J.A. Lucy; “*Action of saponin on biological cell membranes*” *Nature* 196: 952–955 (1962)
- [4] Kimball's Biology Pages, “Cell Membranes.”
- [5] H. Barani, M. Montazer; *Journal of Liposome Research*, 18 (3) 249-262 (2008)
- [6] L.A. Meure, R. Knott, N.R. Foster, F. Dehghani; *Langmuir*, 25, 326-337(2009)

- [7] M.R. Mozafari, S.M. Mortazavi; Nanoliposomes: From Fundamentals to Recent Developments. Trafford Publishing Ltd, Oxford, UK. (2005)
- [8] L. Stryer, "Biochemistry" 2nd ed, Freeman, San Francisco, (1981)
- [9] L.A. Meure, R. Knott, N.R. Foster, F. Dehghani; Langmuir, 25, 326-337 (2009)
- [10] A. Gomez-Hens, J.M. Fernandez-Romero; Trends Anal Chem 25:167–178 (2006)
- [11] M.R. Mozafari, C. Johnson, S. Hatziantoniou, C. Demetzos; Journal of Liposome Research. 18 (4), 309-327 (2008)
- [12] G. Zhang, X. Chen, Y. Xie, Y. Zhao and H. Qiu, Journal of Colloid and Interface Science 315, 601–606, (2007)

3

Results

The goal of these experiments are to observe how liquid crystals change its physical-chemical proprieties when additives are mixed up with them and how liquid crystals under external stimulus influence additives mixed. In fact when an external stimulus occurs (as thermal, electric and magnetic), we can observe in liquid crystals compounds, change of the T_{N-I} , change of the orientation, change of electrical conductivity and diffusion of particles.

In this chapter will be described and analyzed several studies of liquid crystal mixture observed during my PhD research.

3.1 Liquid crystals governing the electromigration

The study of the motion of particles, dispersed in a fluid medium while subjected to an electric field, has been a longstanding topic in science. The phenomenon, named electrophoresis, covers the rotational as well as the translation motion of particles and is used in a wide variety of applications ranging from analytical chemistry and biology^[1] all the way to display technologies^[2].

Nevertheless, electrophoresis is mainly discussed in relation to translational particle motion in isotropic liquids. For small amplitudes this motion proceeds with a velocity proportional to the electric field, $v=\mu E$, where μ is the electrophoretic mobility (Fig 3.1). For spherical particles the motion is directed parallel to the

direction of the applied electric field. Electric field induced particle motion in an isotropic matrix seems to be largely understood.

It is thus surprising that only very little work in this direction has been reported for liquid crystals. For all cases, it is important to notice that liquid crystals displays a strikingly rich variety of particle motions: rotation, translation, and irregular movement, all depending on the investigated liquid crystal phase, the applied external conditions and the aggregation status of the particles. From the literature it is known that liquid crystals can orient themselves according to external stimuli or specific treatment of the cells that contain them (**see chap. I**).

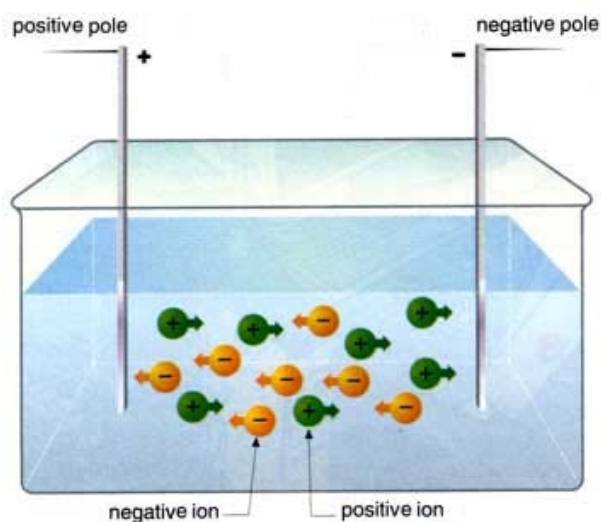


Fig. 3.1 Scheme of ion diffusion under electric field

Using this feature, typical of liquid crystals has been investigated the possibility of exploiting their properties to get “smart drug delivery systems”. In recent years, several studies have been conducted on the use of the mesophase for the controlled release of drugs.^[3-9]

The liquid crystalline phases are interesting “Drug Delivery System” (DDS), as they may be able to incorporate large amounts of active ingredients with different physico-chemical properties.^[10-15] In developing these formulations, the goal is to get systems that optimize the storage capacity and release of drugs, long-life and low toxicity.^[16] The active substance is involved in the microstructure of the system and can even influence it due to molecular interactions; this especially occurs if the drug possesses amphiphilic and/or mesogenic property.^[16]

The aim of this experiments are to observe the diffusion rate of a molecules as drugs model, to find out right mixtures of electrochromic solutions (liquid crystals and adequate additives), and determinate, through kinetics measurements (absorbance versus time), the transport properties as a function of time, frequency and intensity of the applied external field.

In particular, the idea is to create smart devices based on thermotropic liquid crystals for the release of active ingredients. The thermotropic liquid crystals are in fact the potential to affect transport and, consequently, the release of pharmacologically active molecules due to the different alignments (homeotropic, planar and isotropic) which may be a function of surface treatments, temperature and intensity of the applied external fields.

Additives used with liquid crystal must be considered as “molecular model” which will be later replaced with a pharmacologically active molecules with similar physical and chemical characteristics for their controlled release in the human body. For this reason, were initially viewed with a liquid crystal transition temperature T_{N-I} close to that of the human body and, in the first phase of the experiment, it chooses to use as liquid crystal the MBBA.

3.1.1 Materials and Preparation of Sample

To realize such systems were used mixtures of several materials in different liquid crystals. As model of active ingredients were chosen electrochromic molecules, that are capable of undergoing a color change once they arrive to the electrode in order to allow easy determination of the kinetic of transport by using UV-Vis spectroscopy.

In order to simplify the nomenclature were listed below abbreviations of the materials used during the trial.

As liquid crystal were used eutectic mixtures of **E7**, **E49**, **ZLI4788-000** provided by Merck and the liquid crystal **MBBA** (*N*-[4-Methoxybenzylidene]-4-butylaniline, 98%) provided by Sigma-Aldrich (Fig. 3.2), mixed up with different quaternary ammonium salts as *octadecyl-trimethylammoniumbromide* (**SA**) supplied by

Aldrich, *tetrahexylammonium tetrafluoroborate* (**SA2**) supplied by Fluka, or mixed with several ionic liquid as *1-Ethyl-3-methylimidazolium tetrafluoroborate* (**LI1**), *N-Butyl-4methylpyridinium tetrafluoroborate* (**LI2**), *1-Butyl-3-methylimidazolium methylsulfate* (**LI3**), *1-Ethyl-3-methylimidazolium bis (pentafluoroethyl)-phosphinate* (**LI4**), *1-Ethyl-3-methylimidazolium trifluoromethyl sulfonate* (**LI5**) provided by Merck (Fig. 3.3). In Table 3.1 are reported some Physico-chemical features of liquid crystals used.

Using these compounds, were prepared several samples of electrochromic solutions with different w/w% of additives in liquid crystals.

Have also been used and studied mixtures of ionic liquids with molecules of *Ethyl Viologen diperchlorate* (**EtV**) (cathodic species), mixture containing *Ethyl Viologen diperchlorate* ed *Ethylferrocene* (**AN**) (anodic species) and a mixture (**M1**) of *N,N-dimethyl-4,4'-azodianiline*, *Tetrachloroethane* (**TCE**), *Propylene carbonate* (**PPC**) and *Ethyl Viologen diperchlorate* in the following percentages in weight: 9% (5% *N,N-dimethyl-4,4'-azodianiline* + 95% TCE) + 84,6% PPC + 6,34 EtV.

Liquid Crystal	E49	E7	ZLI4788-000	MBBA
T_{S-N}	< -20°C	< -30°C	< -30°C	-
T_{N-I}	100°C	61°C	83°C	45°C
$\Delta\epsilon$ (1kHz, 20° C)	17	13,8	-5,7	-0,7
ϵ_{\parallel} (1 kHz, 20° C)	22,4	19	4,5	4,7
ϵ_{\perp} (1kHz, 20° C)	5,4	5,2	10,2	5,4
Δn (+ 20° C, 589 nm)	0,261	0,2253	0,164	0,22
n_o (+ 20° C, 589 nm)	1,527	1,5211	1,486	1,549
n_e (+ 20° C, 589 nm)	1,788	1,7464	1,65	1,769
Viscosity (cSt, 20°)	47	40	35	20,8
K1 (20°C, 10^{-12} N)	15,8	11,1	-	5,3
K3 (20°C, 10^{-12} N)	28,2	17,1	-	7,5

Table 3.1 Physic-chemical properties of liquid crystals used

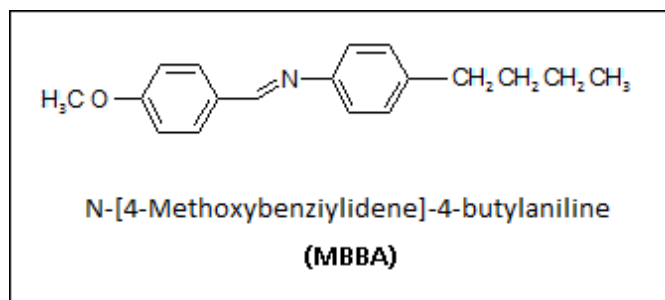


Fig 3.2 Structural formula of MBBA

A small amount of each mixtures was introduced by capillarity in cells having a thickness between 35-65 μ m. These cells have an electro-conductive layer, due to the presence of a thin layer of indium oxide (ITO, "indiumtin oxide") (Fig. 3.4).

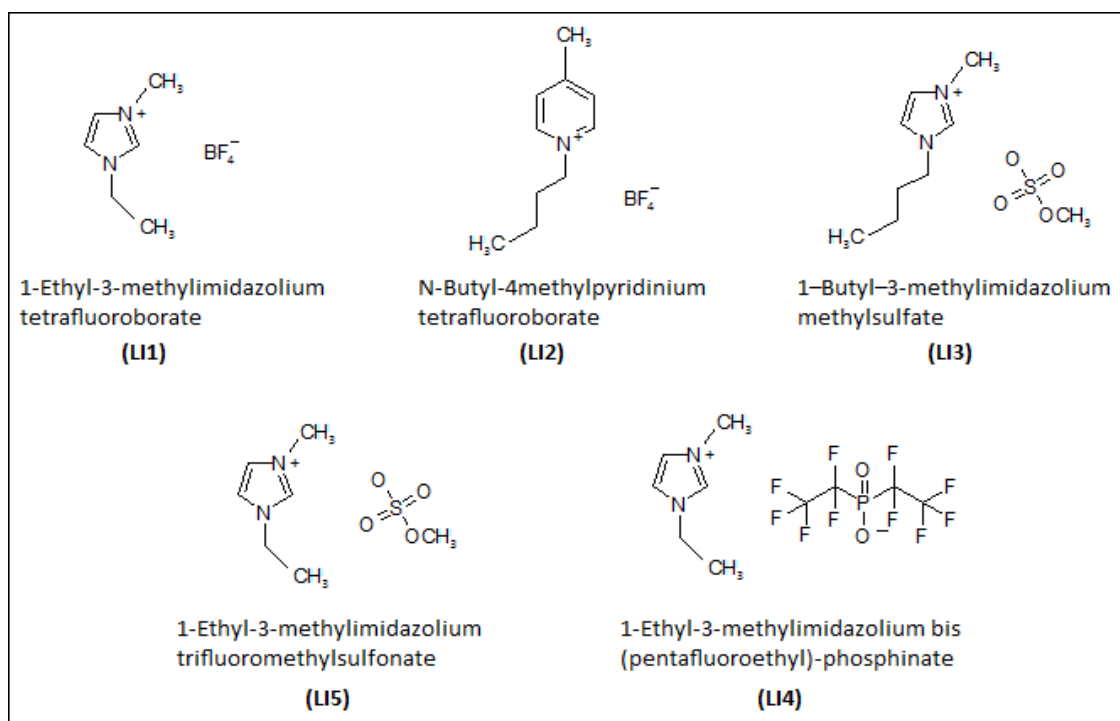


Fig 3.3 Structural formula of Ionic liquid used

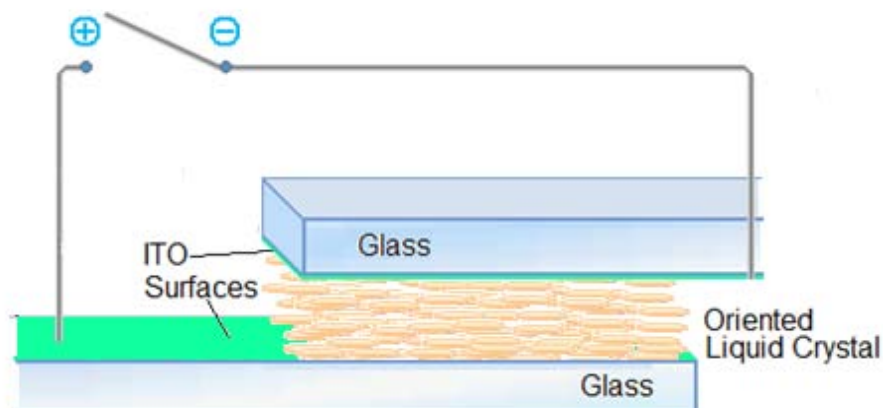


Fig. 3.4 Scheme of a cell filled with Liquid Crystal

Furthermore, to obtain an homeotropic alignment cells were prepared with an aligning layer (Fig. 4.7). The substrates were treated with a solution containing **DMOAP** (*Dimethyloctadecyl [3 - (trimethoxysilyl) propyl] ammonium chloride*), isopropanol and distilled water in a ratio of 1: 899: 100. After dipping and subsequent slow emergence in vertical position of glass slides from the solution, they have been placed in oven at a temperature of 120°C for about 30 minutes (Fig. 3.5).^[17]

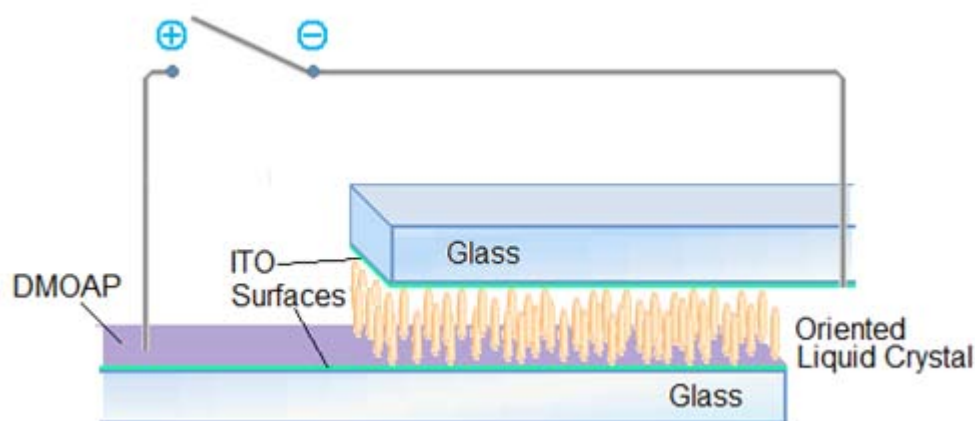


Fig. 3.5 Scheme of a homeotropic cell filled with Liquid Crystal

The samples prepared using the technique described above, were submitted to spectrophotometric measurements using a spectrophotometer UV-Visible Jasco V-550 190-900nm, in order to observe the optical properties of electrochromic mixtures, either by applying a dc field that in the absence of such field in a wavelengths range between 400nm and 800nm. Moreover were measured the colored and bleaching times as a result of certain dc fields.

In addition, were performed measurements to estimate the T_{N-I} of the various liquid crystal and different electrochromic mixtures through a Linkam LTS 350, able to vary the temperature of the samples in a controlled way (the state of the sample was monitored using an optical microscope polarized light).

3.1.2 Results and discussion

Following the studies developed by Nakamura^[18,19], various molecules of salt were dispersed in various liquid crystals, in concentration of 0.5% in weight, mixed

under mechanical agitation using a small magnet and in the absence of light sources at temperatures below 50°C.

Obtained for homogeneous mixtures, the solutions were introduced into cells and then analyzed by light microscopy to observe their physical and chemical properties. Moreover, these samples were heated by hot stage optical microscope to observe the temperature at which transitions from liquid crystal state to isotropic occur and vice versa. (Fig. 3.6 and 3.7)

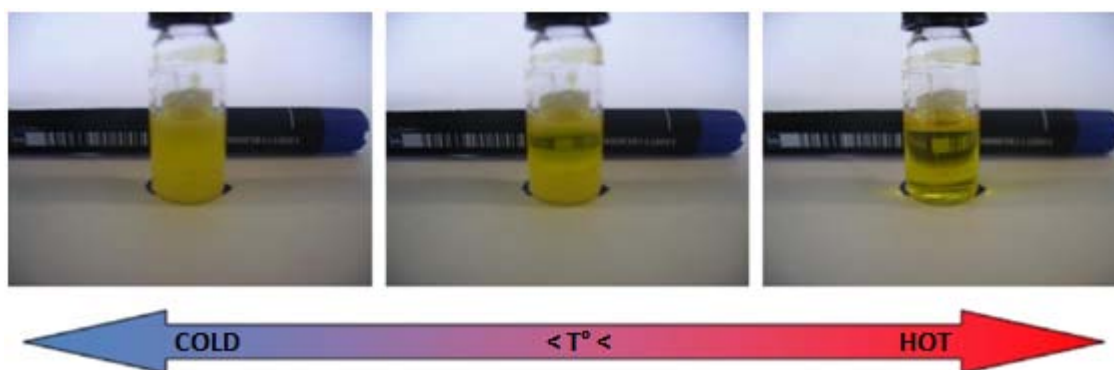


Fig. 3.6 Macroscopic observation of the transition from opaque to transparent, upon heating of the liquid crystal (MBBA)

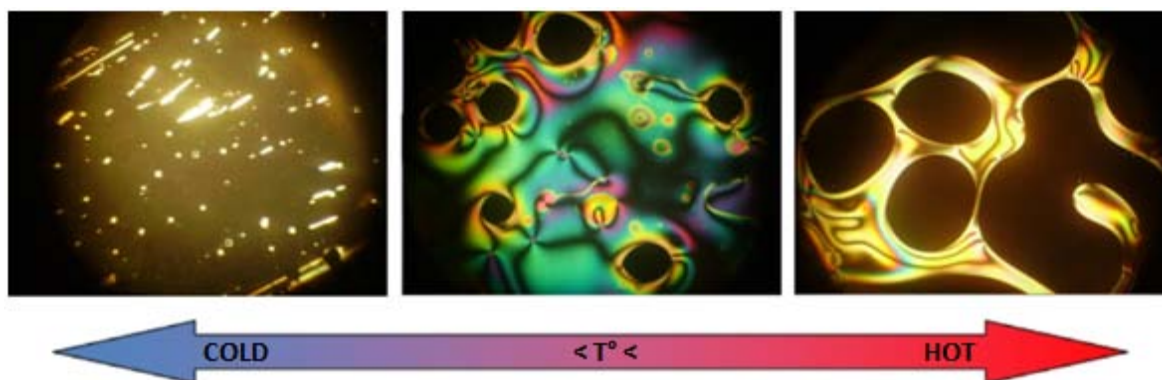


Fig. 3.7 Microscopic observation of the transition from planar to isotropic, upon heating of the liquid crystal (ZLI4788-000)

Determine the T_{N-I} of each sample was verified whether these mixtures were colored by the action of a dc electric field (starting at 0 V and gradually increasing the voltage).

The table below (Table 3.2) shows the color changes recorded.

The macroscopic remarks show that, by applying a dc field of 2 V and 100 μ A, only for the combination **ZLI4788-000/SA2**, a chromatic effect occurs.

Liquid Crystal	Additive	Chromatic transition by application of a dc field
MBBA	SA	none
	SA2	none
E49	SA	none
	SA2	none
E7	SA	None
ZLI4788-000	SA	None
	SA2	Grey → Pink

Table 3.2 Chromatic transition for each sample by application of a dc field

In search for possible chemical compounds that can give a color when dissolved in liquid crystals, it was decided to use the ethyl-viologen in concentration of 0.5% combined with 0.25% of an anodic species. The results obtained were not satisfactory, since no color transition is observed. Moreover, there was the presence of haze when applying a dc field 2V and 10 μ A, indicating that the use of these fields can generate “dynamic scattering” phenomena (confirmed by optical microscopic observations, electro-hydrodynamic instability) and not of weak chromatic effects (Table 3.3).

Liquid Crystal	Additive	Chromatic transition by application of a dc field
MBBA	EtV+AN	none
E49	EtV+AN	none

Table 3.3 Chromatic transition for each sample by application of a dc field

Subsequently, ionic liquids were used for their chemical “affinity” to the ammonium salts, since they contain a quaternary nitrogen (in the ionic liquid is present in a ring (Fig. 3.3)), and also, for their properties, especially its biocompatibility [20-23], as shown in chapter 2. Therefore we have used mixtures of 0.5% in weight of various ionic liquids and liquid crystals. The color changes due to dc fields are shown in the following Table 3.4.

At the same time it was thought to use a mixture of ionic liquid containing 1% by weight of ethyl-viologen, and the results are shown below (Table 3.5).

The color change described above in Tables 3.4 and 3.5, was observed after application of a dc field of 2 V and 100 μ A. Carrying out a comparison between the two tables, since the chromatic effects are almost identical, we can say that the EtV in the second case, is not responsible for the coloration of the sample and thus is the ionic liquid to give the effect of chromatic

Liquid Crystal	Additive	Chromatic transition by application of a dc field
MBBA	LI1	none
	LI2	Light Yellow \rightarrow Dark Yellow
	LI3	none
	LI4	none
	LI5	none
E7	LI1	none
	LI2	none
	LI3	none
	LI4	none
	LI5	none
ZLI4788-000	LI1	none
	LI2	none
	LI3	none
	LI4	Grey \rightarrow Pink
	LI5	none

Table 3.4 Chromatic transition for each sample by application of a dc field

Liquid Crystal	Additive	Chromatic transition by application of a dc field
MBBA	LI1+EtV	none
	LI2+EtV	Light Yellow \rightarrow Dark Yellow
	LI3+EtV	none
	LI4+EtV	none
	LI5+EtV	none
ZLI4788-000	LI1+EtV	none
	LI2+EtV	none
	LI3+EtV	none
	LI4+EtV	Grey \rightarrow Pink
	LI5+EtV	none

Table 3.5 Chromatic transition for each sample by application of a dc field

Therefore, for convenience, the two cases examined can be unified and will be analyzed only cases set out by the liquid crystal with the ionic liquid.

In search of a good electrochromic mix dissolved in MBBA, has studied the behavior of this with 3% in weight of the electrochromic mixture M1 defined in the previous section.

Liquid Crystal	Additive	Chromatic transition by application of a dc field
MBBA	M1	none

Table 3.6 Chromatic transition for each sample by application of a dc field

The result of this test did not lead to positive results because the mixture used in addition to not give any coloration, destroyed the nematic liquid crystal, separating the mixture in macroscopically visible droplets (Table 3.6).

Based on the reported results, the subsequent analysis will be focused on samples that had electrochromic response (Table 3.7).

Liquid Crystal	Additive	Chromatic transition by application of a dc field
MBBA	LI2	Light Yellow → Dark Yellow
ZLI4788-000	LI4	Grey → Pink
	SA2	Grey → Pink

Table 3.7 Samples where chromatic transition occurs by application of a dc field

Once chosen samples that under dc electric field give a visible transition of colors to naked eye, were carried out measurement of the “coloration observed” analyzing these samples using UV-Visible spectrophotometer.

By examining the sample containing **MBBA / LI2** and overlapping the graphs derived from the spectrophotometer examination of the sample in the absence and presence of the dc field, we obtained the plot shown in Figure 3.8.

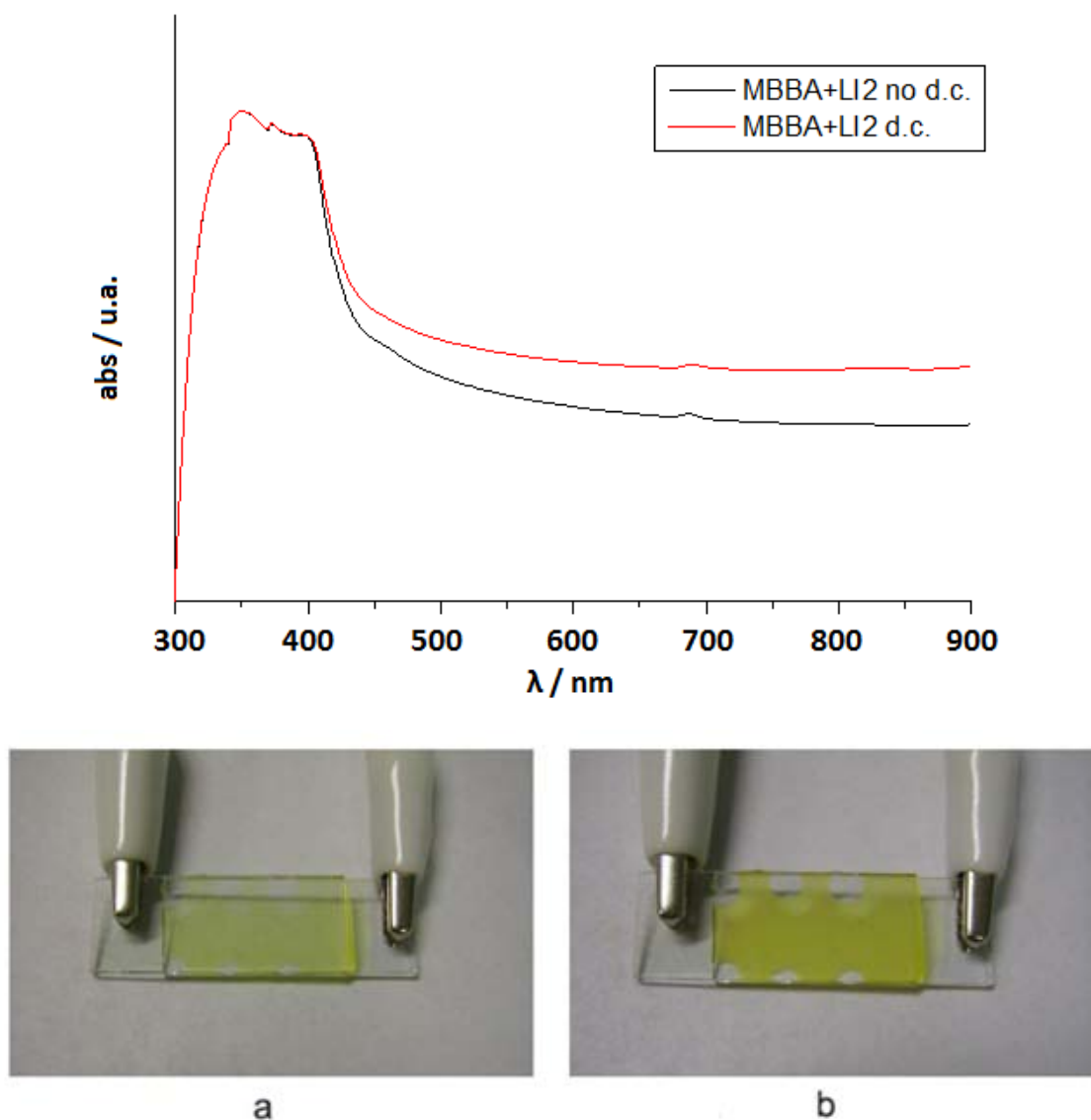


Fig. 3.8 Above: UV-Vis absorption spectrum of MBBA/LI2; Below: Macroscopic observation of the color transition of the mixture MBBA/LI2 when is applied (a) and not (b) a dc field

Figure 3.8 shows that the chromatic effect observed (transition from light yellow to dark yellow) is just an effect due to opacification of the mixture, caused by dynamic scattering. The phenomenon can be recognized visually from the almost parallel trend of the two curves that differ among themselves only at high wavelengths and, mainly, are not peaks that demonstrate the effective transition of color. In fact, there are no peaks by subtracting the two curves (Fig. 3.9).

This effect of parallelism is typical in phenomena of opacification of the samples, therefore it can say that the mixture does not have useful features for the creation of drug delivery systems.

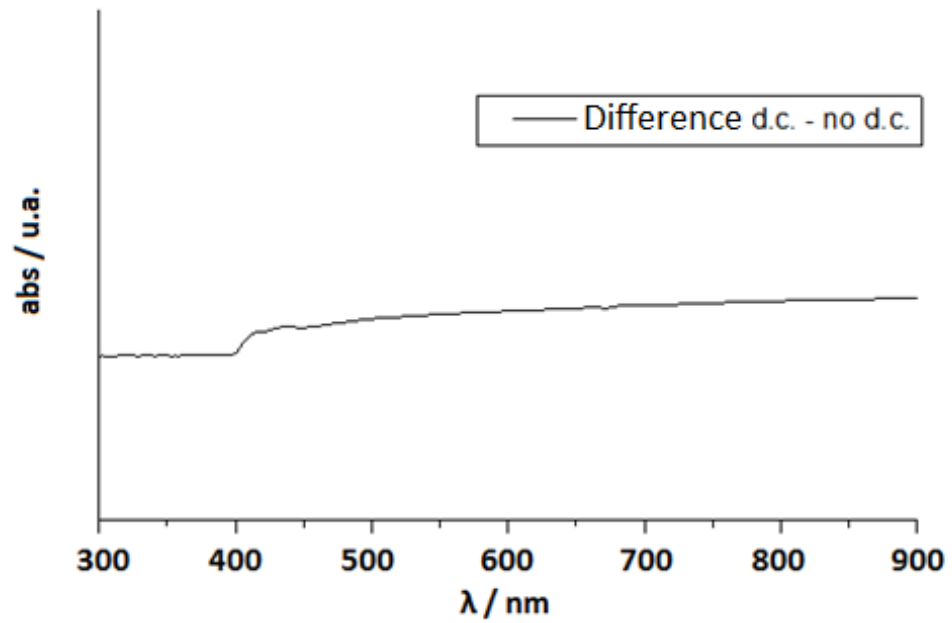
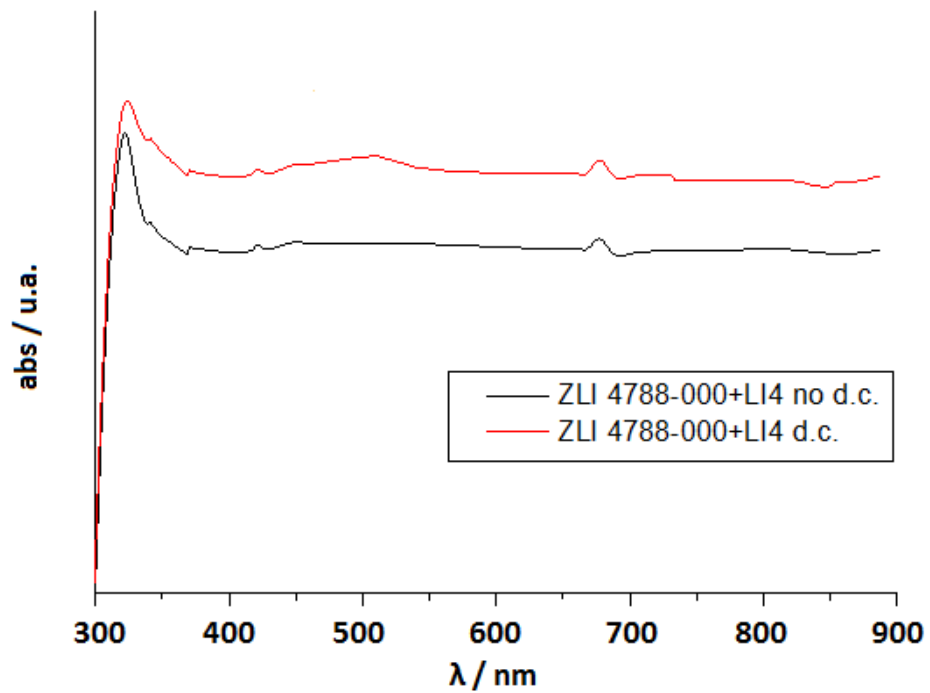


Fig. 3.9 Difference between the curves in the graph of Fig. 3.8

As regards the mixture containing **ZLI4788-000/LI4**, the Fig 3.10 shows a visible peak when a dc field is applied, observed even through the difference of the two curves (Fig. 3.11).



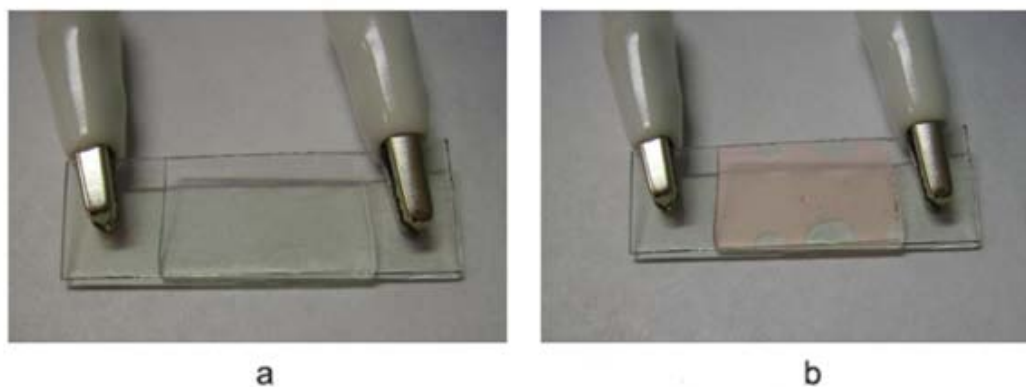


Fig. 3.10 Above: UV-Vis absorption spectrum of ZLI 4788/LI4; Below: Macroscopic observation of the color transition of the mixture ZLI 4788/LI4 when is applied (a) and not (b) a dc field

In this case are not observed any phenomena of scattering or opacification. The chromatic transition (gray to pink), due to the electrochromic molecules that change color when arrive to the electrode, it is clear and observable by naked eye or by spectrophotometer.

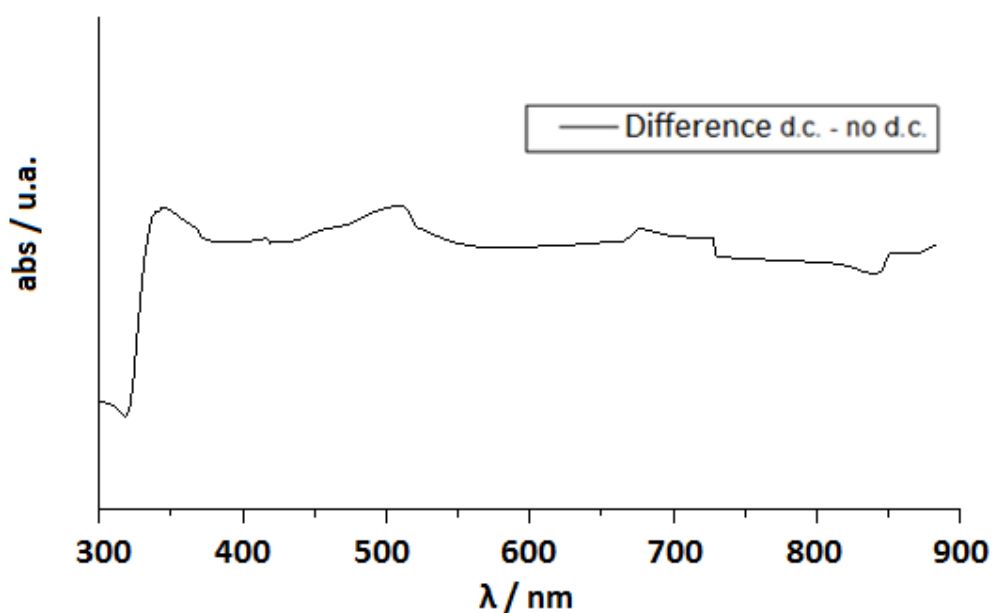


Fig. 3.11 Difference between the curves in the graph of Fig. 3.10

In Fig. 3.11, in fact, it sees a peak absorption around 510nm, which shows the absorption of the green and the appearance of pink.

Same goes for the mixture containing **ZLI4788-000** and **SA2**. The graph in Figure 3.12 shows an absorption of the color indicated by the trend curve where dc field is applied, even more clearly than the **ZLI4788-000** mixed with **LI4**.

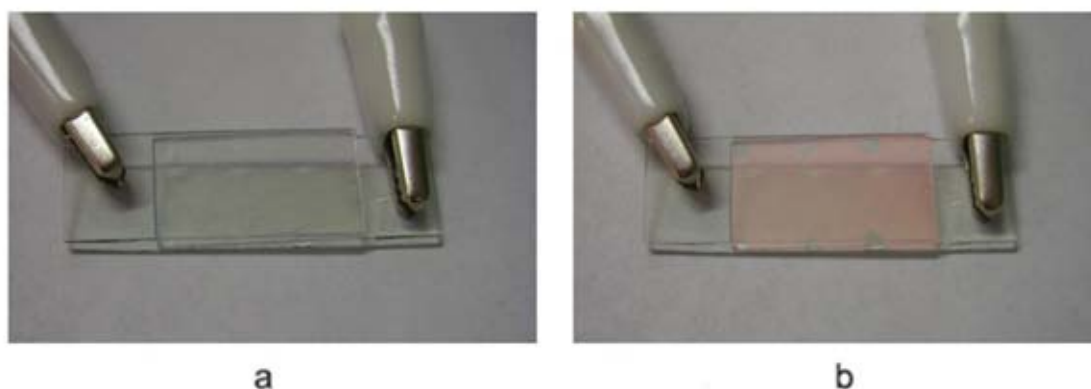
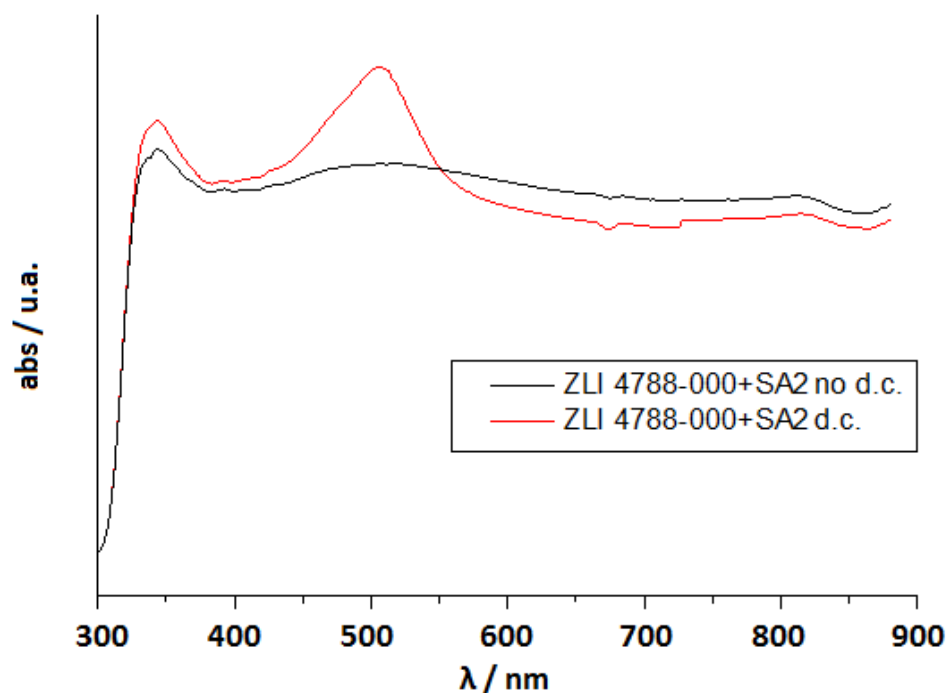


Fig. 3.12 Above: UV-Vis absorption spectrum of ZLI 4788/SA2; Below: Macroscopic observation of the color transition of the mixture ZLI 4788/SA2 when is applied (a) and not (b) a dc field

In fact, comparing the graph (Fig. 3.12) with the one where you see the subtraction of the curves (Fig. 3.13), it may notice a high peak around the wavelength of 510nm, due to a significant formation of color, linked to the electrochromic reactions at the electrodes as a result of migration of ions.

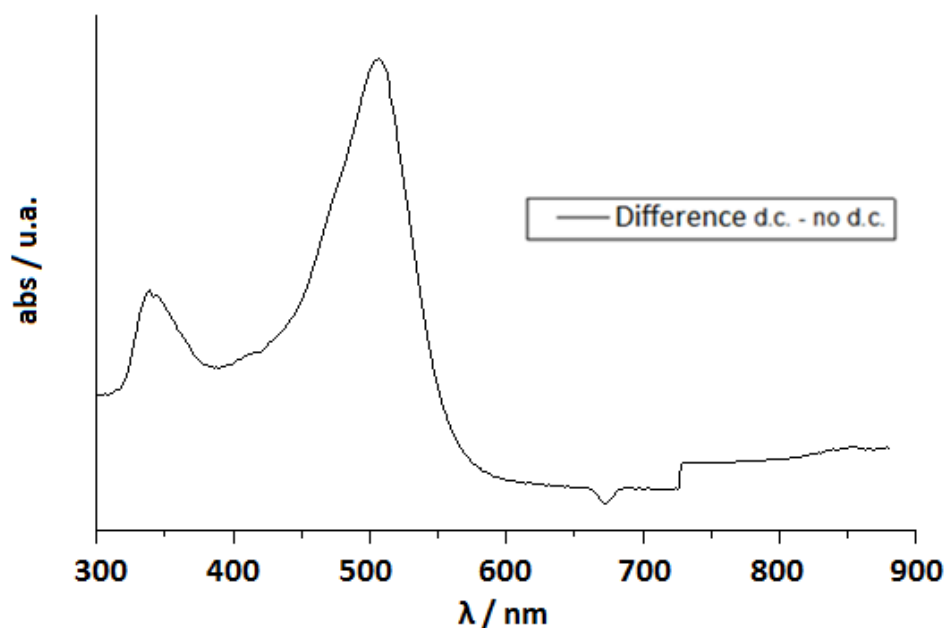


Fig. 3.13 Difference between the curves in the graph of Fig. 3.12

Verified the effective coloration of the samples by UV-Visible spectrophotometer, subsequent measures has focused on samples **ZLI4788-000 + LI4** and **ZLI4788-000 +SA2**.

To verify the effective release of pharmacologically active molecules, the two samples were observed in different alignments: homeotropic, planar and isotropic. These were obtained after surface treatment, high temperatures and at the intensity of external fields, with the intent to understand how the arrangement of the director may affect transport of molecules dissolved in the liquid crystal. Spectrophotometric measurements were carried out for each alignment, in order to observe the color changes of cells prepared thus determining the kinetics of transport of dissolved substances.

In the first series of measurements were performed test on mixture containing **ZLI4788-000/SA2** according to these possible alignments:

- *Planar*;
- *Homeotropic*, using cells treated on surface;
- *Isotropo*, at temperatures above T_{N-I} (98°C);

In all three cases, kinetic measurements were made using UV-Visiblespectrophotometer set to a wavelength of 510nm (where it is observed the absorption peak of the pink after the application of a dc electric field), to see how samples respond to electrical stimulation dc by calculating the time required to ensure that the sample becomes pink (saturation value), and that it takes to get it back to its initial value.

In Fig. 3.14 at room temperature and without surface treatment, the liquid crystal is *planar* in the alignment, the sample does not appear colored (maximum transmittance). After application of the electric field, there is an abrupt decrease of the curve due to electrode charging with the staining of the sample that becoming pink, increasing the absorption, and then reaches the steady state in around 100 seconds.

Note that, as a result of the pulse and time, slightly decrease of the maximum values of transmittance, showing that the sample does not return exactly to its initial state when the external dc field was switched off. This is due to the fact that the molecules after a certain time of exposure to an electric field, takes much more time to re-disperse spontaneously in the liquid crystal (150-200 seconds) (ie without a field guide) and cannot exclude the fact that a portion of the electrolyte remains anchored to the electrode that is partially colored.

Instead, the lower absorbance values, where occurs the saturation of the sample, remain almost the same since the sample may not exceed a certain degree of alignment and coloring. In addition, it can be seen how as a result of time, the curve tends to lower and to widen. These effects occur because the electrolytes in the sample take longer to return to its initial state, as if they memorize the number of cycles ON-OFF suffered. This performance is typical in many systems.^[24] The “spikes” observed at the top of the graph are due to ignition of the electric field that for a split second, destabilizing the internal field of the sample (Fig. 3.14).

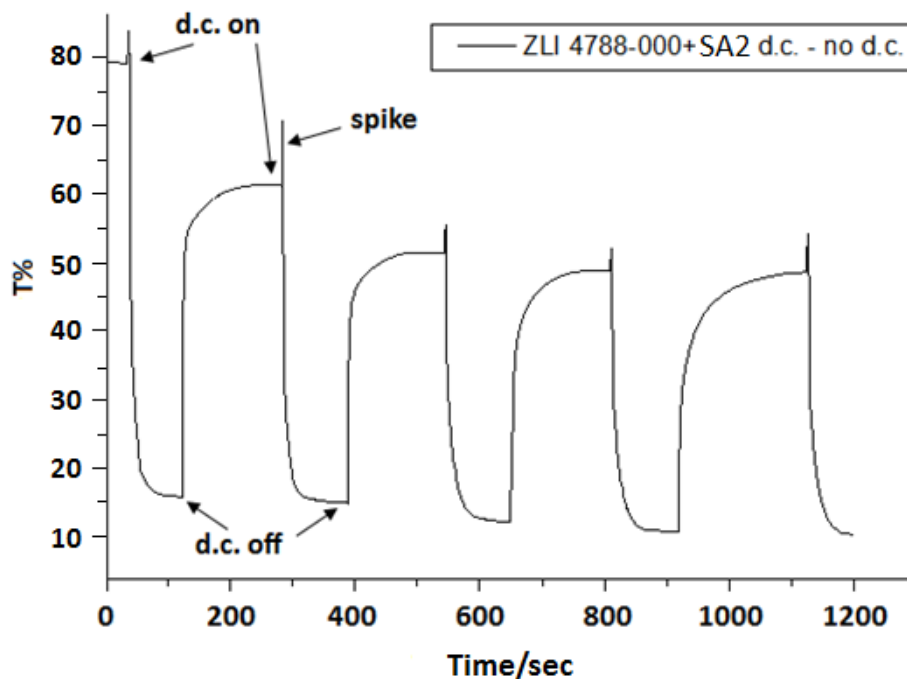


Fig. 3.14 Effect in the mixture planarly aligned of a dc field pulse train as function of time

In the case of the mixture included in a homeotropic cell, the sample takes about an hour to line up as verified by observations with an optical microscope.

As in the planar case discussed above, again, with the application of the field, we see a sharp decrease of the curve (Fig. 3.15). In this case, in contrast to the planar, exposure times are identical to the electric field, while they differ for those of restoring of the sample, which increase significantly. In the first case the falling time when there is an applied dc field were of the order of 150-200 seconds (with the formation of very narrow valley), in the homeotropic case, bleaching times are much longer, increasing to about 450 seconds. In addition, similarly to the planar case, we observe a lowering of the maximum values of transmittance and the saturation values (minimum transmittance) remain broadly the same, since the sample cannot exceed a certain color as mentioned in the previous case.

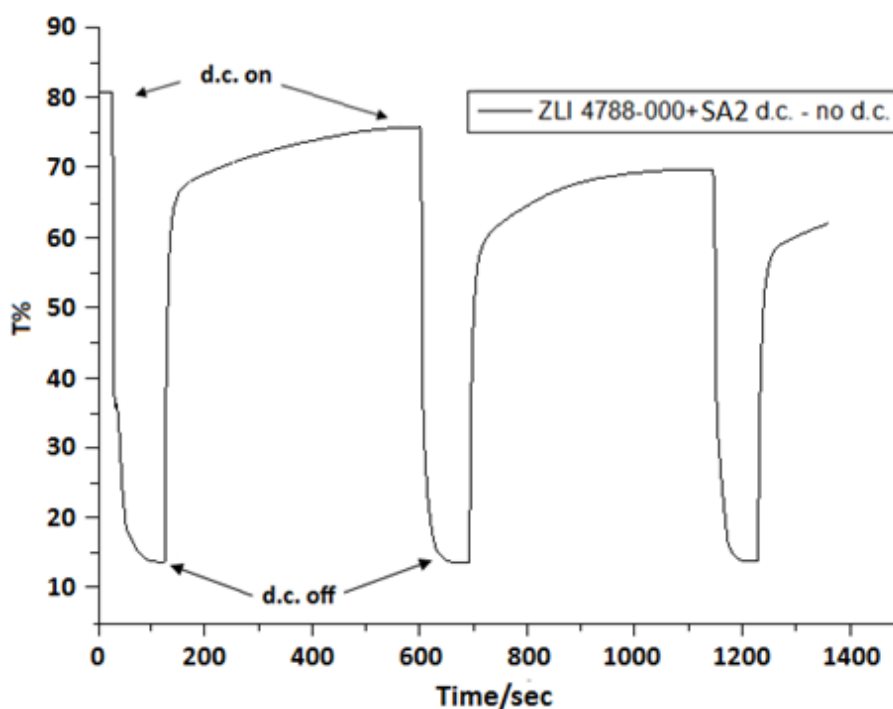


Fig. 3.15 Effect in the mixture homeotropically aligned of a dc field pulse train as function of time

To perform the measurements in the isotropic state, the sample was initially placed in the hot stage at a temperature of 98°C and the whole system was placed in the UV-Visible spectrophotometer.

The graph shown in figure 3.16 shows a strange behavior of the sample. Initially, the first plateau is due to a rearrangement of the system. Subsequently, the application of a dc field, due to the isotropic nature of the sample, causes a slow kinetics of the system that, with proper proportions, it never reaches saturation. In fact after 30 minutes, the sample has not reached a plateau. During the 30 minutes it turned off the electric field, but the system did not return to its original state, indeed the ignition of the electric field resumed the trend left. So it appears as an “one shot” system, where the electrolytes diffuse in only one direction, they anchor at substrate and hardly come back.

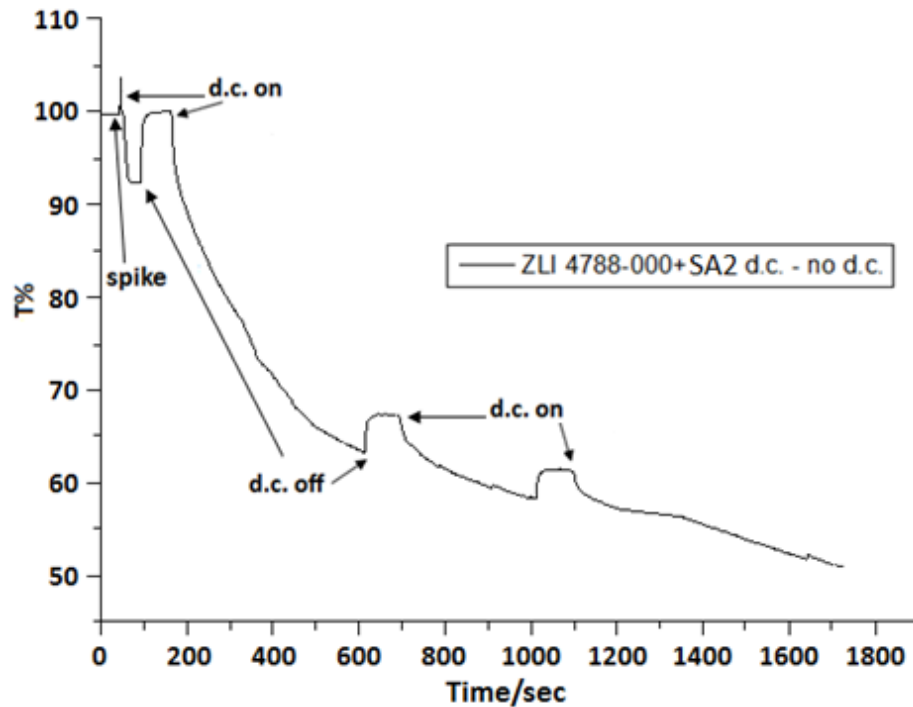


Fig.3.16 Effect in the mixture isotropically aligned of a dc field pulse train as function of time

The explanation of these phenomena observed from the spectrophotometric analysis are due to ion migration.^[25] Ion migration in a liquid crystal cell can have a significant influence on the electric field and this in turn on the LC director orientation, even when the ion concentration is low. On application of a voltage, charges migrate towards the electrodes and accumulate at the alignment layers, effectively reducing the applied potential across the cell and therefore modifying the director tilt.

A simple model can be used to describe the current flow^[26] and the ion diffusion in the liquid crystal sample. Two charge distributions of equal concentration (n_0) but opposite signs are assumed to exist within the cell. The mobilities of the positive and negative ions (μ_1, μ_2) are assumed to be single valued, but not necessarily equal. Many charge distributions with differing mobilities may exist in the cell, but it is instructive to fit to a model using two representative charge distributions.

Initially, the current declines linearly due to the movement of the faster of the ion distributions. Extrapolating this decline, a time is reached when the faster ions

have drifted to an alignment layer (abrupt decrease of the curve) and no longer contribute to the induced current. Subsequently, the current is dominated by the migration of the slower ion distribution. The current diminishes linearly once again, but with a lower gradient, until the slower ions have accumulated at the opposite alignment layer (steady state or plateau). If the two ion distributions are of equal mobility then a single linear decline of the current is observed.

When a field is switched off mutual repulsion of ions at the alignment layers gives rise to a potential barrier over which ions must first diffuse, before drifting towards the cell center under the influence of the charge separation field. This process causes the charge separation field to diminish, and finally, it falls below the switching threshold and the liquid crystal sample returns to a homogeneous state.

An algorithm developed at the University of Ghent^[27], Ghent, Belgium, calculates the migration of ionic impurities through the liquid crystal. A Monte Carlo approach is used to calculate drift and diffusion of the migrating ions.

Regarding the results shown by cells filled with a mixture containing **ZLI4788-000/LI4** depending on various alignments s observed a behavior very similar to the mix **ZLI4788-000/SA2**. This similarity of behavior is not surprising since the similarities in chemical and physical characteristics that the two molecules, SA2 and LI4, present.

To observe the reversibility and repeatability of this process, several cycles of alternating dc field exposure (ON-OFF) were performed in planar cell. In particular, it wanted to study the able of device to return in their original state.

For this reason it was decided to apply to the device dc short field pulses (5 seconds) to see if the device was able to return to its original state. Effectively, from the trend of the curves represented in Fig 3.17, is observed the sample returns to its initial state (in 20 seconds), but after each cycle there is a decrease of the maximum values of transmittance (red dotted line). This means that the sample remains slightly colored due to the fact that electrolytes remain anchored to the electrode.

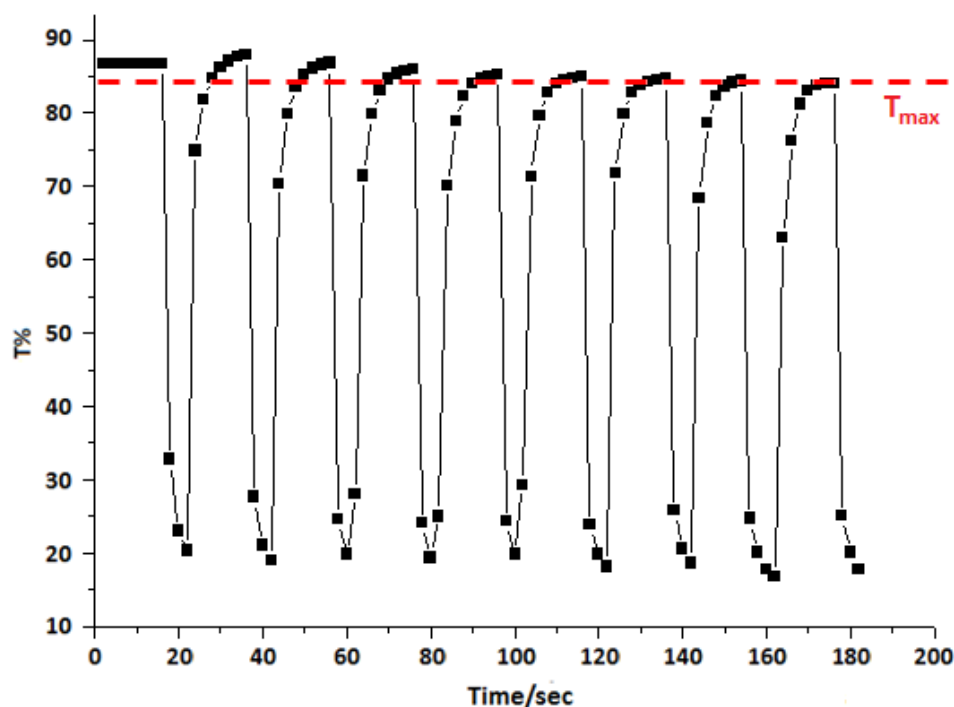


Fig.3.17 Fast cycles of dc field ON-OFF ($\tau_{ON}5s$, $\tau_{OFF}20s$) in the mixture planarly aligned

In the graph 3.18, has tried to determinate the minimum point of saturation of the sample, i.e., where the plateau starts (10 seconds), to see if with the increase of cycles is observed a deterioration of the device, resulting in sharp decrease of the minimum values of transmittance (blue dotted line).

As can be noted, the saturation values remain unchanged when applied a moderate dc field (enough to obtain the coloration of the sample), although it observes a lowering of the maximum values of transmittance (red dotted line) as in Fig. 3.17.

In the graph 3.19, it was decided to gradually increase the time of exposure to dc electric field, to see how the sample responded to stimuli. In particular, the sample was before observed at rapid ON-OFF cycles (τ_{ON} 5 seconds, τ_{OFF} 20 seconds) after it has been subjected to an electric field at different time intervals (60, 120 and 180 seconds) separated each other with a relaxation time (rise time) of 60 seconds, to determine the effective stability of the device, repeatability and transport efficiency.

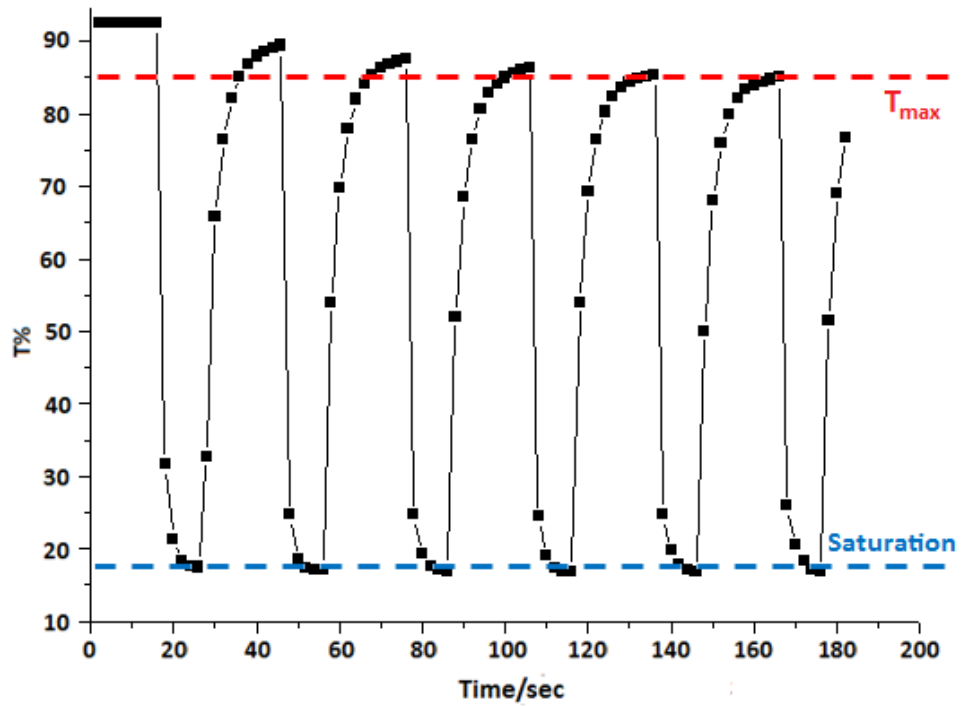


Fig.3.18 Fast cycles of dc field ON-OFF (τ_{ON} 10s , τ_{OFF} 20s)in the mixture planarly aligned

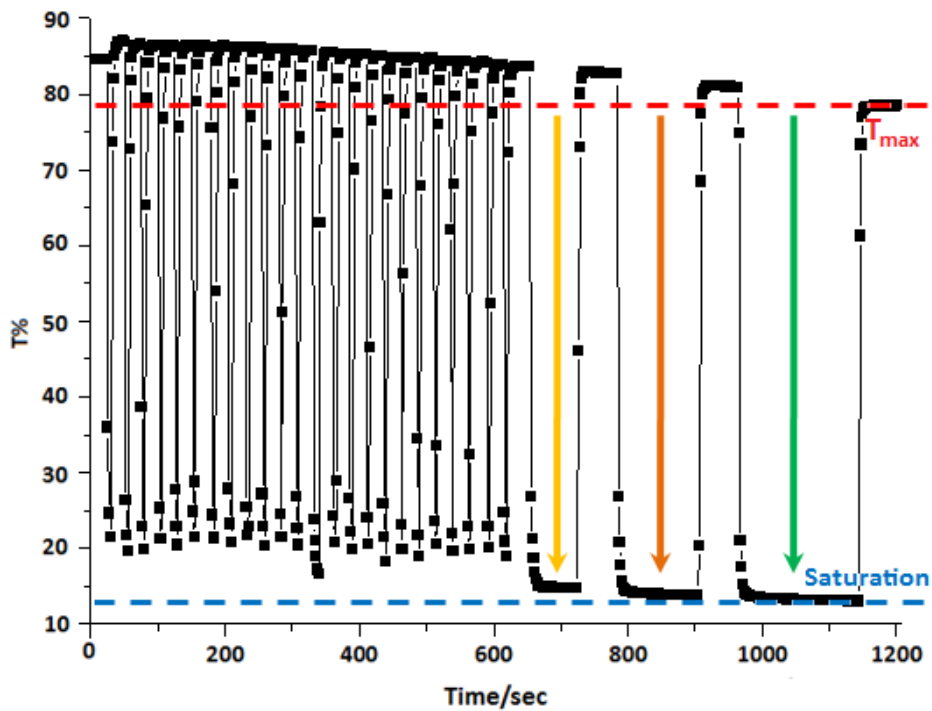


Fig.3.19 Fast cycles of dc field ON-OFF (τ_{ON} 5s , τ_{OFF} 20s), yellow arrow τ_{ON} 60s, orange arrow τ_{ON} 120s, green arrow τ_{ON} 180s spaced by a τ_{OFF} 60 seconds.

Rapid on-off cycles do not produce excessive saturation, due to the fact that they never reach the plateau, but as occurred in previous cases, resulting in slightly lower values of maximum transmittance (red dotted line).

This decrease of the maximum transmittance is best observed when the sample is subjected to a prolonged dc field. In fact, it can see a reduction of the maximum transmittance of about 10%, due to the electrolyte that under the action of an electric field strongly adhering on the wall of the substrate, generating on the electrode, several layers of electrolytes that hardly return in solution. This phenomenon is demonstrated by the fact that the saturation values (blue dotted line) is slightly lower, a sign that the device is subject to a sharp deterioration when exposed to long periods of electric fields.

3.1.3 Conclusion

In this work have been realized and studied the new drug delivery systems formed by thermotropic liquid crystals in which molecules were dispersed pattern of active ingredients. What model molecules were used electrochromic molecules, as capable of undergoing a change in color, and once arrived dielectric electrode, thus allowing an easy determination of their kinetics of transport through the device using UV-Vis spectroscopy, when subjected to fields dc electric.

The choice of **MBBA** as matrix liquid crystal for its nematic-isotropic transition temperature (T_{N-I}) next to human body temperature, did not lead to positive results for the onset of electrohydrodynamics instability that compete with the transport of electrochromic molecules .

In contrast, surveys, using the **ZLI4788-000** added to ionic liquids, have led to the creation of devices that transit from gray to pink, to witness the migration of the electrolyte. Through the various measures in different alignments, it was observed that the migration rate of the electrolyte varies with the alignment of liquid crystal.

It was determined the transport time and reversibility and repeatability of this process in several cycles of alternating dc field exposure (ON-OFF). Knowledge of these parameters and the difference that exists indifferent conditions can be very useful for modulating the amount of drug released over time, allowing the

creation of intelligent devices release of active ingredients based on thermotropic liquid crystals or *Smart Drug Delivery Systems (SDDS)*.

References

- [1] D.M. Hawcroft; *“Electrophoresis: The Basics”*; Oxford University Press, Oxford, (1997)
- [2] S.T. Wu and D.K. Yang; *“Reflective Liquid Crystal Displays”*; Wiley, Chichester, Chap. 1, (2001)
- [3] J.L. Fergason. U.S. Patent 4 435 047 (1984).
- [4] J.W. Doane, G. Chidichimo, N.A. Vaz. U.S. Patent 4 688 900 (1987).
- [5] H. Bunjes and T. Radehjj, *JPP* 57: 807-816, (2005)
- [6] M.G. Carr, J. Corish, O.I. Corrigan; *International Journal of Pharmaceutics* 157: 35-42, (1997)
- [7] F.T. M.C. Vicentini, R. Casagrande, W. A. Verri Jr., S. R. Georgetti, M. V. L. B. Bentley and M. J. V. Fonseca; *AAPS PharmSciTech*, Vol. 9, No. 2, (2008)
- [8] R.C. Pasquali, D. Chialifftta, M.F.G. Gamboa and C. Bregni; *Latin American Journal Of Pharmacy*, Vol. 26, 3, 387-393 (2007)
- [9] E. Farkas, D. Kiss, R. Zelkó; *International Journal of Pharmaceutics* 340, 71-75 (2007)
- [10] G. Zhang, X. Chen, Y. Xie, Y. Zhao and H. Qiu; *Journal of Colloid and Interface Science* 315, 601–606, (2007)
- [11] P. Saulnier, N. Anton, B. Heurtault and J.P. Benoit, *C.R. Chimie* 11, 221-228, (2008)
- [12] M. Malmsten, *“Soft drug delivery systems”*, RCS Publishing, (2006)
- [13] M. Malmsten, *“Drugs and Pharmaceutical Sciences”*, Vol. 122 (2002)

-
- [14] J.C. Shah, Y. Sadhale and D.M. Chilukuri; *Adv. Drug Delivery Rev.*, 47, 229–250, (2001)
- [15] S. Engström and L. Engström; *Int. J. Pharm*, 79, 113–122, (1992)
- [16] C.M. Chang and R. Bodmeier; *Int. J. Pharm*, 173, 51–60, (1998)
- [17] T. Uchida and H. Seki, “*Surface Alignment of Liquid Crystals*”, Chapter 5 of *Liquid Crystals: Applications and Uses*, vol. 3, edited by B. Bahadur, World Scientific, , pp. 21-25, 34, 44-45, 48-49, 60-63 (1995)
- [18] K. Nakamura, S. Kaneko, Y. Ito, H. Hirabayashi and K. Ogura; *J. Appl. Phys.*, 53, 17, (1982)
- [19] K. Nakamura, K. Nakada, Y. Ito and E. Koishi; *J. Appl. Phys.*, 57, 135, (1985)
- [20] Q. Yang, D.D Dionysiou; *Journal of Photochemistry and Photobiology, A: Chemistry*, 165(1-3), 229, (2004)
- [21] www.ionicliquids-merck.de
- [22] H.B. Zhang, X.H. Zhou, J.F. Dong, G.Y. Zhang e C.X. Wang; *Sci China Ser B-Chem*, Vol. 50, no. 2, 238-242, (2007)
- [23] M.D. Baumann, A.J. Daugulis, P.G. Jessop; *Appl Microbiol Biotechnol* 67, 131–137, (2005)
- [24] N.Liu, D.R. Dunphy, P. Atanassov, S.D. Bunge, Z. Chen, G.P. Lopez, T.J. Boyle and J. Brinker; *Nano Letters* vol.4, 4, 551-554 (2004)
- [25] R. James, G. Stojmenovik, C. Desimpel, S. Vermael, F.A. Fernández, S.E. Day and K. Neyts; *Journal Of Display Technology*, Vol. 2, No. 3, 237-246 (2006)
- [26] G. Stojmenovik, “*Ion transport and boundary image retention in nematic liquid crystal displays*” Ph.D., Ghent University, Ghent, Belgium, (2005)
- [27] S.Vermael, K. Neyts, C. Desimpel, D. de Boer, S. Day, F. Fernández, P. Trwoga, and F. Lanowith; in *Proc. 21st IDRC/the 8th IDW*, Nagoya, Japan, (2001)

3.2 Liquid crystals governing the diffusion of magnetic particles

One of the current trends in colloidal formulation is the design of “smart materials” associating two types of colloids. This hybrid systems consisting of a mixture of nanoparticles and organic molecules have been studied in an effort to produce stimuli responsive smart systems, for several area applications such as medicine, pharmaceuticals, biotechnology, nanotechnology and bioengineering.^[1,2]

In this context, suspensions of magnetic nanoparticles are of a great importance, as they enable the synthesis of new magnetic materials. They have thus been incorporated in systems as varied as polymeric gels,^[3,4] polymeric matrix,^[5] nematics,^[6] smectics,^[7,8] emulsions,^[9] liposomes,^[10] and vesicles^[11].

Today we can see magnetic forces being combined with microfluidics in an amazing variety of ways. Magnetic forces can not only be utilized to manipulate magnetic objects such as magnetic particles, magnetically labeled cells or plugs of ferrofluids inside a micro channel; they can also be used to manipulate non-magnetic, i.e. diamagnetic objects.

Magnetic forces are used for transport, positioning, separation and sorting of magnetic as well as non-magnetic objects.

These features are, for example, widely investigated for the development of magnetic drug delivery. Many studies have been conducted to better understand the benefits of magnetic nanoparticles, of how magnetic fields penetrate through human tissue and how the magnetic materials can be manipulated for their use in medicine.^[12]

Since time it was created the first magnetic carriers, in 1970, have been developed a variety of micro and magnetic nanoparticles as carriers to deliver drugs to specific sites in vivo. The optimization of these systems continues today.

Generally the magnetic component of the particle is coated with a biocompatible polymer, such as silica. The coating protects the magnetic particles from the attacks of the surrounding environment and can be functionalized, for example, with carboxylic groups and other molecules.^[13]

The therapy uses of magnetic nanoparticles is based on the formation of a complex in which the drug is associated with a magnetic nanoparticle that acts as a carrier. The complex drug/carrier is injected into the circulatory system of the subject by intra-arterial or intravenous injection, while an external magnetic field is used to focus and guide the drug in the affected area.^[14]

When the complex drug/carrier is focused on the target site the drug is released through changes in physiological conditions such as pH, osmolarity or temperature, or by enzymatic activity.^[15]

In the course of my research, it was observed the diffusion of magnetic particles under the action of a magnetic field in planarly and homeotropically aligned liquid crystal.

This work is a basic study, to observe the rate of diffusion of magnetic particles in the different alignments of liquid crystal and different direction of the magnetic lines of force, in order to exploit these features in a controlled drug delivery system.

3.2.1 Materials and Preparation of Sample

To perform these studies, was prepared a suspension of magnetic particles in a nematic liquid crystal. This suspension was prepared by adding through mechanical stirring 0.5 w/w% of Fe₃O₄ magnetic particles coated with a silica shell provided by Evonik, in **MLC-2079** provided by Merck

The sample cell consisted of two glass plates spaced by two Mylar strips ($d \approx 20 \mu\text{m}$). The cell surfaces were coated with transparent electrodes of indium tin oxide (ITO) and, in order to obtain homeotropic alignment, were treated by the surfactant **DMOAP** (*Dimethyloctadecyl [3 - (trimethoxysilyl) propyl] ammonium chloride*) as described in section 3.1.1. Then the cells were filled by capillary action with liquid crystal suspension.

In order to obtain a planar oriented director, an ac electric field (1 kHz, 4 Volt) was applied through the sample; so thanks to its negative dielectric anisotropy ($\Delta\epsilon < 0$) **MLC-2079** tilts perpendicular to the electric field (Table 3.8).

Liquid Crystal	MLC-2079
T_{S-N}	-
T_{N-I}	102°C
$\Delta\epsilon$ (1kHz, 20° C)	-6.1
ϵ_{\parallel} (1 kHz, 20° C)	4.1
ϵ_{\perp} (1kHz, 20° C)	10.2
Δn (+ 20° C, 589 nm)	0.15
n_o (+ 20° C, 589 nm)	1.6412
n_e (+ 20° C, 589 nm)	1.4912
Viscosity (cSt, 20°)	410
K_1 (20°C, 10^{-12} N)	15.9
K_3 (20°C, 10^{-12} N)	18.3

Table 3.8 Physic-chemical properties of MLC-2079

The samples prepared using the technique described above, were observed in a polarising microscope which was connected to an image acquisition system to observe the diffusion of magnetic particles

The experiments were conducted placing small commercial static magnet (10x20x40mm) to 12 mm from the edge filling of the cell. The magnet was positioned in different ways respect to the sample, in order to experience different lines of force depending on the direction of magnet.

It was placed in four directions respect the sample (Fig. 3.20):

- **Vertical**
- **Border**
- **Transversal**
- **Horizontal**

Furthermore, to verify the particle diffusion in a planar alignment of the liquid crystal, the sample was subjected to at a fixed sinusoidal electric field (1 kHz 4V).

All experiments were recorded by the camera placed on the optical microscope connected to computer. It was observed the spread of magnetic particles in a path of about 3 mm. The diffusion of the particles has been well

observed, thanks to the trail they left, due to “defects” generated by the movement of particles in the liquid crystal.

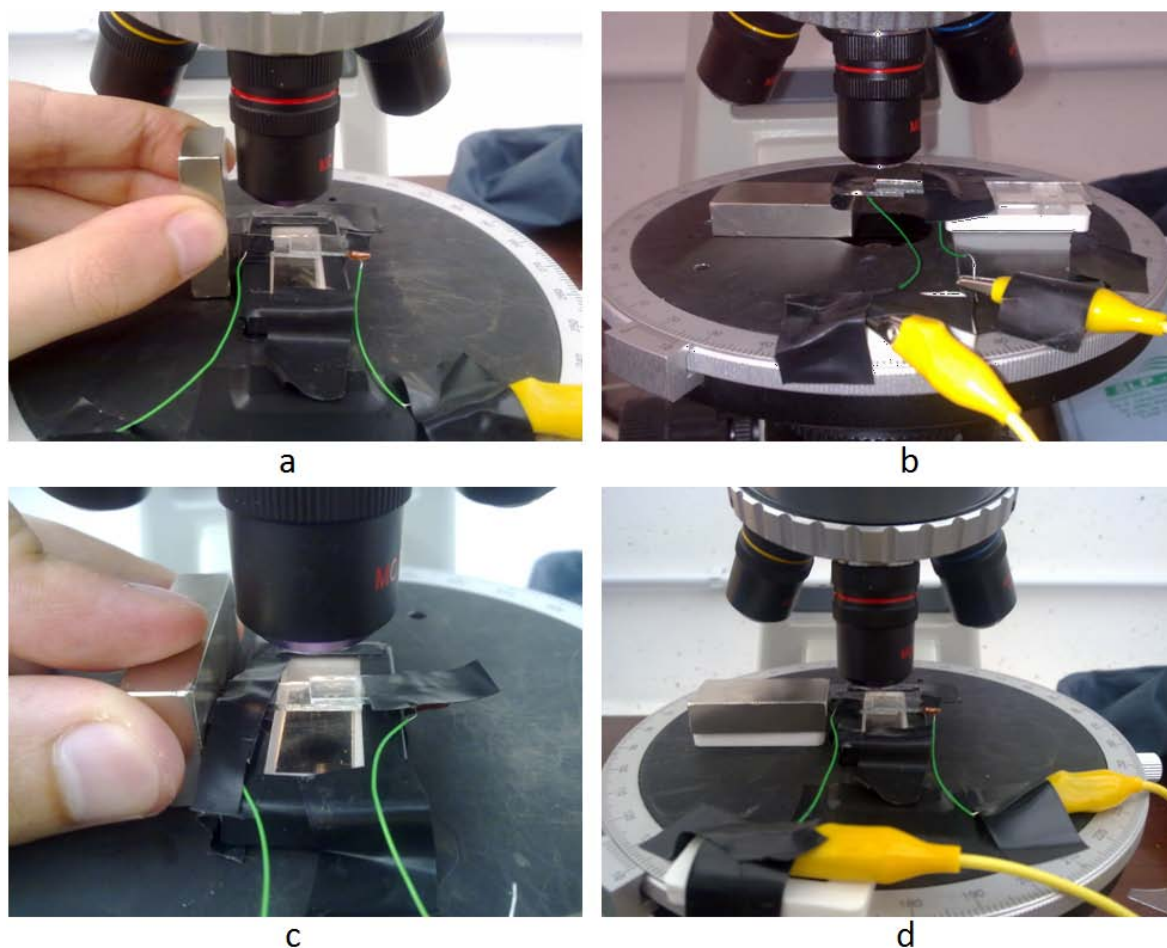


Fig 3.20 Orientation of magnet in experimental setup: a)Vertical; b)Border; c)Transversal; d)Horizontal

In order to obtain comparable values, all the measurements were conducted on the same sample, dragging back (thanks to a small magnet) the particles once each experiment ends.

For comparison, was used a suspension 0.5 w/w% of Fe_3O_4 coated silica, dispersed in paraffin oil.

All particles diffusion times were collected from video recorded, was extrapolated the averaged and then analyzed.

3.2.2 Results and discussion

The application of an external magnetic field acting on magnetic particles, causes their movement due to magnetization and resulting force acting on them

It is observed that the magnetic particles were moving in the liquid crystal at different speeds depending on: The orientation of the magnet, the liquid crystal alignment and the distance from the magnet.

Examining all videos for each sample was possible to enumerate a list of times related to the diffusion of magnetic particles in about 3 mm in length. This feature is important because from this can be obtained the different speed at which the particles move in the sample, and therefore the possibility to create a modulated delivery.

The first experiments were performed on the sample homeotropically aligned, then the same were performed in a planar way (Fig. 3.21).

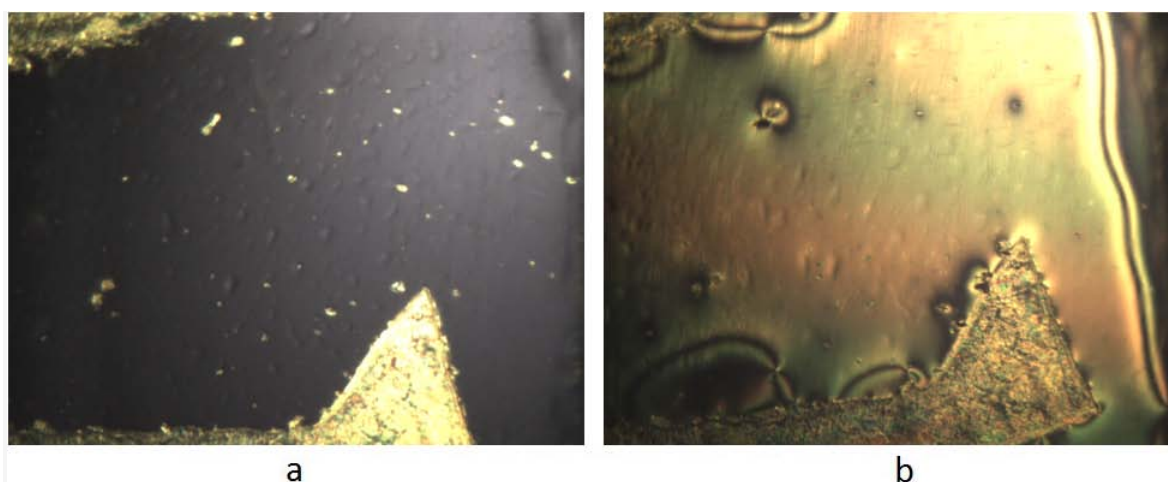


Fig 3.21 Orientation of liquid crystal sample: a) Homeotropic; b) Planar

The magnetic particles in the sample respond differently depending on the orientation of the magnet (Table 3.9).

When the sample is head to head with magnet (Fig. 3.22), the particles move very slowly due to the magnetic force that tends to push down them on the surface of the cell. The particles spread with different velocity. In homeotropic case the time of diffusion is 47 ± 10 minutes, in planar case 17 ± 7 minutes. This range of time depends on agglomeration of particles. In fact, even if they are silica coated, they can attract each other when are close, forming bigger particles that diffuse faster respect to the smallest, feeling more the lines of magnetic field.

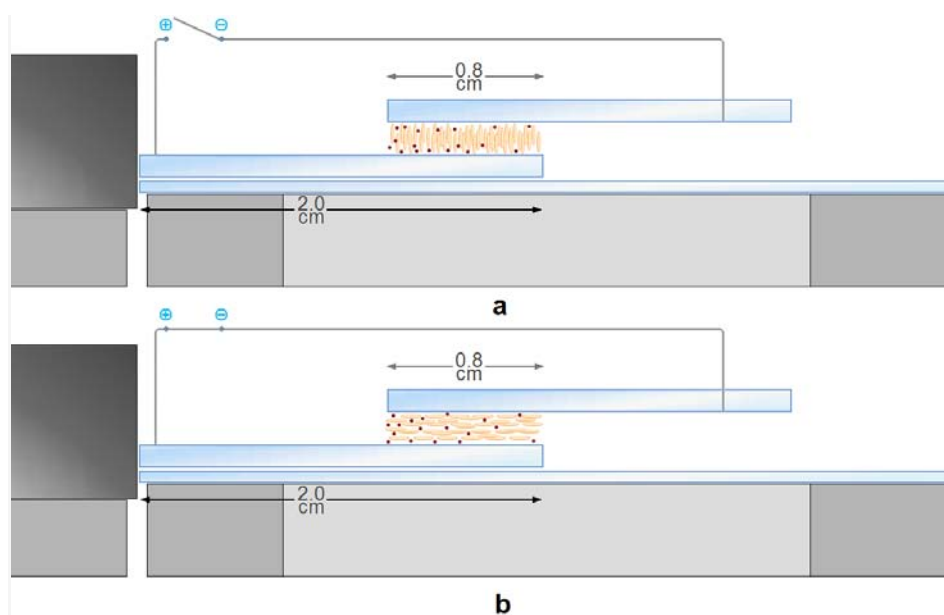


Fig 3.22 Arrangement of the system in horizontal mode: a) Homeotropic; b) Planar

When the magnet is in *border* mode (Fig. 3.23), the sample experiences weak lines of force. In this case it is observed that the particles move slowly. In the homeotropic case they run through 3 mm in 13 ± 7 minutes, in the planar case in 4.5 ± 2 minutes.

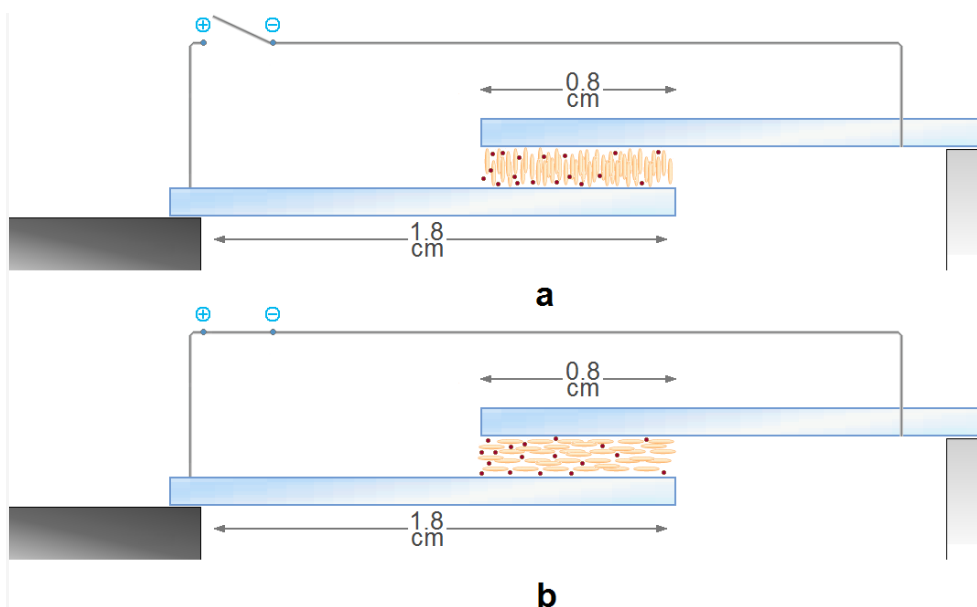


Fig 3.23 Arrangement of the system in border mode: a) Homeotropic; b) Planar

When the sample is in front of the magnet (Fig. 3.24 and Fig. 3.25), the particles move very fast, because they feel all lines of magnetic field strength. In the homeotropic case and with the magnet in *vertical* mode the particle spread in 5 ± 1

minutes while in *transversal* mode in 2.5 ± 0.5 minutes. In planar case in both mode it was register diffusion times about 2 minutes.

	HOMEOTROPIC	PLANAR (4Volt 1000Hz)
Horizontal	47 ± 10 minutes	17 ± 7 minutes
Border	13 ± 7 minutes	4.5 ± 2 minutes
Vertical	5 ± 1 minutes	2 minutes
Transversal	2.5 ± 0.5 minutes	2 minutes

Table 3.9 Diffusion times for homeotropic and planar case, in different position of magnet

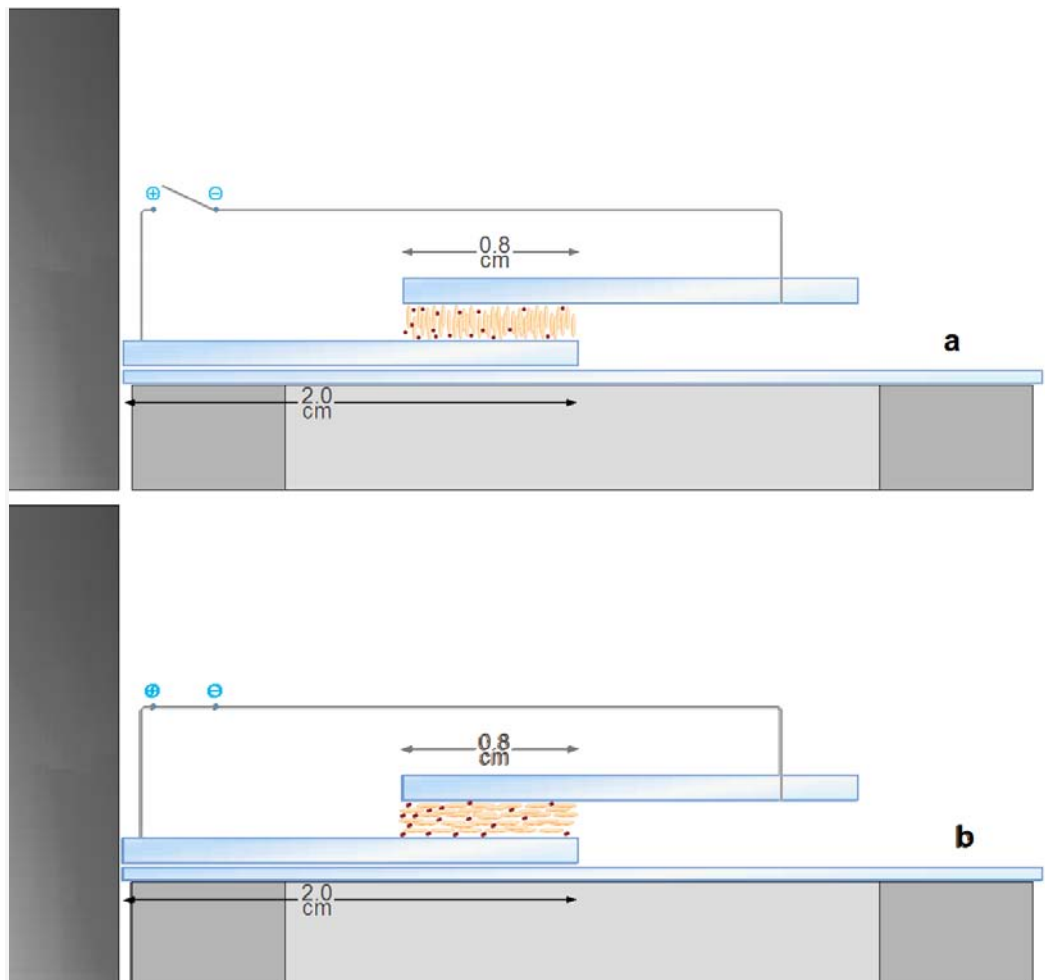


Fig 3.24 Arrangement of the system in vertical mode: a) Homeotropic; b) Planar

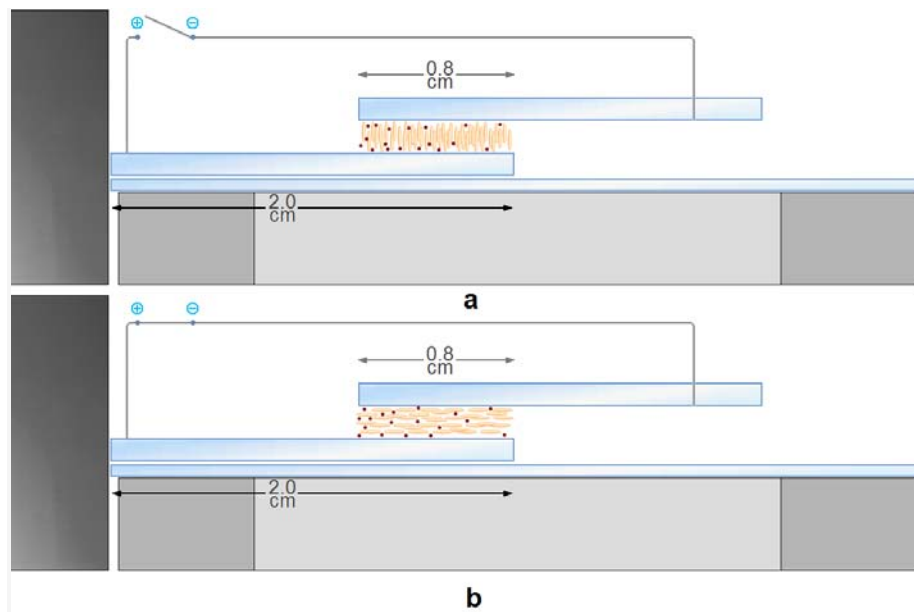


Fig 3.25 Arrangement of the system in transversal mode: a) Homeotropic; b) Planar

The difference between the *vertical* and *transversal* mode resides in the height of the magnet respect to the sample: if it is placed in the middle of magnet, when it is in *vertical* mode, will experience lines of force as in *transversal* mode; while when the sample is placed in the edge, will feel less lines of magnetic field (Fig. 3.26)

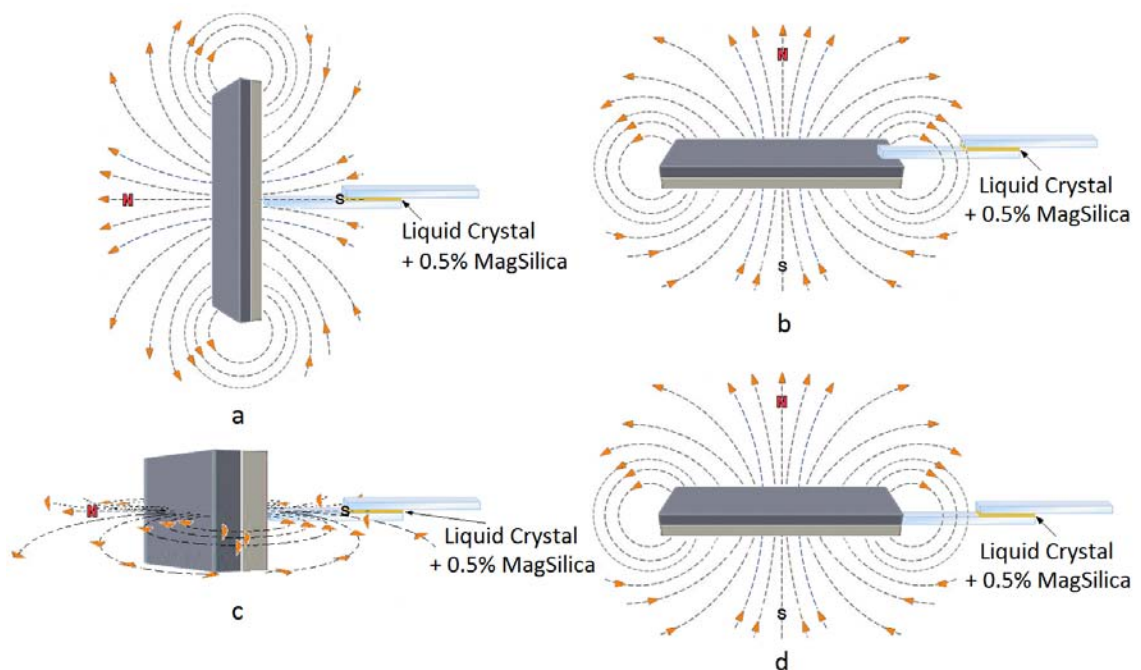


Fig 3.26 Lines of magnetic field acting on the sample in: a) Vertical; b) Border; c) Transversal and d) Horizontal

To compare the diffusion times values of particles in the liquid crystal with those of an isotropic medium, it was decided to perform the same experiment in paraffin oil (Table 3.10).

	PARAFFIN OIL
Horizontal	86 seconds
Border	38 seconds
Vertical	24 seconds
Transversal	22 seconds

Table 3.10 Diffusion times for paraffin oil, in different position of magnet

In this system the particles spread, as in liquid crystal, in different rate depending on the orientation of the magnet, but they but their diffusion times are much faster than those presented in the liquid crystalline suspension.

3.2.3 Conclusion

In this experiment have been realized and studied the behavior of magnetic particles in a unique scenery such as liquid crystals. The magnetic particles depending on the orientation of liquid crystal, the distance from the magnet and the orientation of the magnet itself, feel differently the lines of magnetic force, and therefore respond differently to external stimuli imposed. To have comparable values was used the same sample of suspension of magnetic particles in the **MLC-2079** (with negative $\Delta\epsilon$) in homeotropic cell. To realize the measurements with the sample planarly aligned was applied an ac field (1 kHz 4V).

It was observed that the magnetic particles spread faster in the sample planarly aligned, and also depending on the inclination of the magnet, they can move with times ranging from nearly an hour to few minutes.

For its behavior these particles silica-coated can be easily functionalized with e. g. specific drug, so the knowledge of these diffusion times can be helpful to

drive magnetically, specific molecules where and when needed, as a *Smart Drug Delivery Systems (SDDS)*.

References

- [1] J. W. Goodby; *Liq. Cryst.*, Vol. 24, 25 (1998);
- [2] Q.A. Pankhurst, J. Connolly, S.K. Jones, J. Dobson; *J. Phys. D.* 36, R167 (2003)
- [3] Z. Varga, G. Filipcsei, M. Zrinyi; *Polymer*, Vol.47, 227–233. (2006)
- [4] J. Galicia, O. Sandre, F. Cousin, D. Guemghar, C. Ménager, V.J. Cabuil; *Phys.: Condens. Matter*, 15, S1379-S1402 (2003)
- [5] J. Jestin, F. Cousin, I. Dubois, C. Ménager, J. Oberdisse, R. Schweins, F. Boué; *Adv. Mater.*, 20(13), 2533–2540 (2008)
- [6] V. Berejnov, J.C. Bacri, V. Cabuil, R. Perzynski, Y. Raikher; *Europhys. Lett.*, 41, 507–512 (1998)
- [7] P. Fabre, C. Casagrande, M. Veyssie, V. Cabuil, R. Massart; *Phys. Rev. Lett.*, 64(5), 539–542 (1990)
- [8] C. Ménager, V. Cabuil; *J. Colloid Interface Sci.*, 169, 251–253 (1995)
- [9] J. Bibette; *J. Magn. Magn. Mater.*, 122(1-3), 37–41 (1993)
- [10] C. Ménager, L. Belloni, V. Cabuil, M. Dubois, T. Gulik Krzywicki, T. Zemb; *Langmuir*, 12(14), 3516–3522 (1996)
- [11] S.B. Lecommandoux, O. Sandre, F. Checot, J. Rodriguez-Hernandez, R. Perzynski; *Adv. Mater.*, 17(6), 712 (2005)
- [12] M.R. Mourino; *Radiology*, 180, 593 (1991)
- [13] M. Koneracka, P. Kopcansky, M. Timko, C.N. Ramchand, A. Sequeira, M. Trevan; *J. Mol. Catalysis B. Enzymatic*, 18, 8 (2002)
- [14] J. Dobson; *Drug Development Research*, 67, 55 (2006)

- [15]** C. Alexiu, W. Arnold, R.S. Klein, F.G. Parak, P. Hulin, C. Bergemann, W. Erhardt, S. Wagenpfeil, A.S. Lubbe; *Cancer Res.*, 60, 8 (2000)

3.3 Liquid crystals that enhance the stability of surrounding environment (Fréedericksz Transition)

As described in the first chapter, the liquid crystal molecules are very sensitive to external stimuli. These lead to a destabilization of the liquid crystal that changes its properties depending on the external stimulus to which it is subjected.

In particular, nematic liquid crystals can be aligned along a well-defined direction either by treating the confining surface in a certain way^[1], or by applying an external electric (or magnetic) field.^[2] In the absence of an external field the director n coincides with the so-called “easy axis” whose orientation depends on the surface treatment. An additional electric (or magnetic) field can, depending on the LC's dielectric (magnetic) anisotropy, destabilize this orientation and the director n will deviate from the easy axis (Fréedericksz transition). Depending on the strength of that field, the anchoring is said to be weak or strong. Switching off the electric field from these states the previous alignment is restored in a few seconds. Using this feature of liquid crystals were realized over the years several optical devices.

In the last few years, electrodynamic instabilities in homeotropically oriented layers of negative dielectric anisotropy nematics have attracted the interest of a discrete number of authors^[3-7]; in fact, although the homeotropic orientation shows a less rich scenario it differs dramatically from the planar case. Furthermore, because at the Fréedericksz transition the nematic director spontaneously chooses a bend direction, a spontaneous breaking of the isotropic symmetry occurs, which makes possible a direct transition to the spatial chaos.^[6,8]

From a strictly phenomenological point of view, when a low frequency electric voltage is applied to a homeotropic sample of nematic liquid crystal with a negative dielectric anisotropy and positive conductive anisotropy, above a certain voltage threshold, the well-known Fréedericksz transition is observed.

Molecules or particles present in the liquid-crystal bulk influence the reorientation process at the Fréedericksz transition threshold, because they can

stabilize the system in a preferred alignment, preventing the tilt of the liquid crystal molecules.

In this section it presents an experimental study on the effects of different w/w% of liquid crystalline molecules and magnetic particles on the homeotropic nematic anchoring strength.

The use of homeotropically aligned MLC-2079 cells has the important advantage that in this geometry one can obtain the independent information about the surface anchoring strength from the Fréedericksz transition threshold. This is not possible in planar MLC-2079 cells as the electric field stabilizes the alignment in this case.

The aim of this experiments are to obtain the information about the surfaces anchoring strength and to stabilize and improve the homeotropic alignment with the use of additives, in order to obtain higher transparency for example in devices as smart windows.

3.3.1 Materials and Preparation of Sample

To study these effects were mixed by mechanical stirring with several new synthesized liquid crystalline stilbene derivates containing vinyloxyalkoxy chains^[9,10], liquid crystalline monomer or Fe₃O₄ magnetic particles coated with a silica shell provided by Evonik, in nematic liquid crystals.

The sample cell consisted of two glass plates spaced by two Mylar strips ($d \approx 20 \mu\text{m}$). The cell surfaces were coated with transparent electrodes of indium tin oxide (ITO) and, in order to obtain homeotropic alignment, were treated by the surfactant **DMOAP** (*Dimethyloctadecyl [3 - (trimethoxysilyl) propyl] ammonium chloride*) as described in section 3.1.1. Then the cells were filled by capillary action with nematic liquid crystal mixed with several liquid crystalline molecules in different w/w% (1.25, 2.5, 5) and magnetic particles (0.5 w/w%).

In order to obtain a planar oriented director when a definite electric field is applied through the sample, was chosen **MLC-2079** provided by Merck for its own negative dielectric anisotropy $\Delta\epsilon < 0$ (Table 3.8).

Since MLC-2079 has negative dielectric anisotropy the molecules want to orient perpendicular to the electric field, which is in conflict with the initial homeotropic alignment.

The liquid crystalline molecules are used as additives in MLC-2079 as a function of length of their alkyl chain (Table 3.11). In order to simplify the nomenclature these were named with abbreviations **LC** followed by number as showed in Fig 3.27.

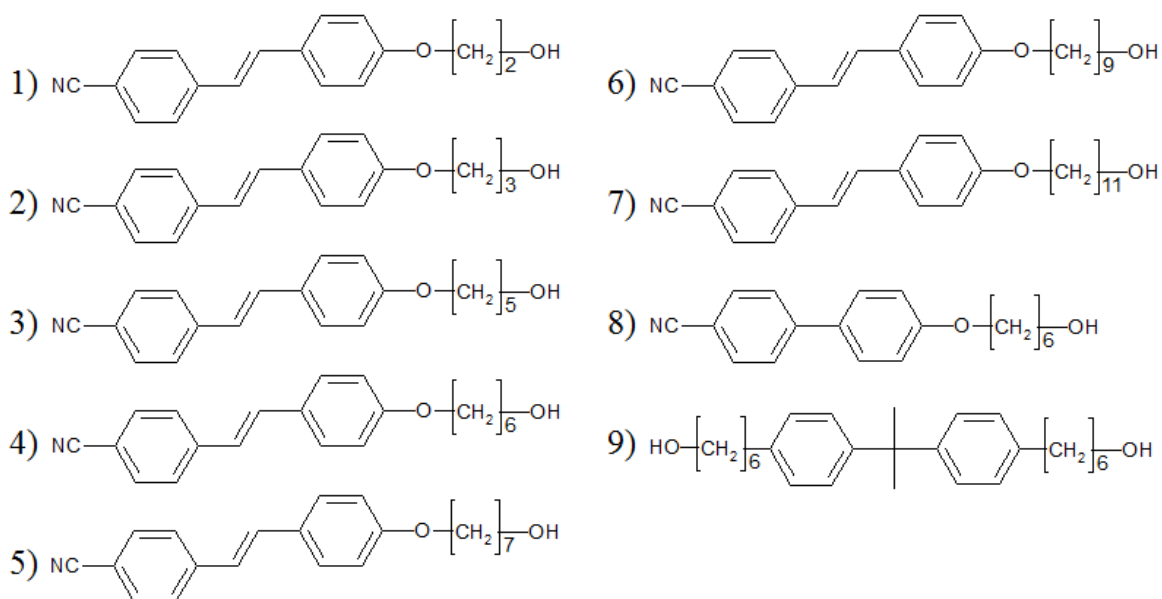


Fig 3.27 Structural formula of new synthesized liquid crystalline molecules used

LC	$T_{(K-S)}$	$H (Jg^{-1})$	$T_{(K-N)}$	$H (Jg^{-1})$	$T_{(K-I)}$	$H (Jg^{-1})$	$T_{(S-N)}$	$H (Jg^{-1})$	$T_{(S-N)}$	$H (Jg^{-1})$
1	-	-	166.1	(68.7)	-	-	-	-	170.5	(50.1)
2	-	-	86.9	(49.6)	-	-	-	-	100.3	(17.3)
3	88.8	(40.4)	-	-	-	-	94.9	(53)	104.8	(17.7)
4	-	-	127.9	(20.0)	-	-	-	-	131.0	(84.7)
5	-	-	83.4	(46.4)	-	-	-	-	91.3	(28.7)
6	-	-	91.0	(79.2)	-	-	-	-	98.4	(33.0)
7	-	-	98.2	(36.3)	-	-	-	-	101.2	(67.5)
8	-	-	88.3	(97.5)	131.6	(0.1)	-	-	112.8	(4.4)

Table 3.11 Transition temperature and related Enthalpy value for Liquid Crystalline molecules used and shown in Fig. 3.3.1

The experimental procedure consisted of two steps:

- to measure the threshold voltage for each mixture transition increasing step by step the voltage applied (manually) by the experimental setup shown in Fig. 3.28
- to measure the threshold voltage for each mixture by optical setup remotely controlled (automatically) as illustrated in Fig 3.29

The samples prepared using the technique described above, were observed in a polarising microscope which was connected to an image acquisition system to observe the correct homeotropic alignment of the samples.

In experimental setup manually controlled, a sinusoidal electric field was applied across the cells at fixed ac voltage frequency of 1 kHz, perpendicular to the glass plates, and the optical response was monitored on the oscilloscope.

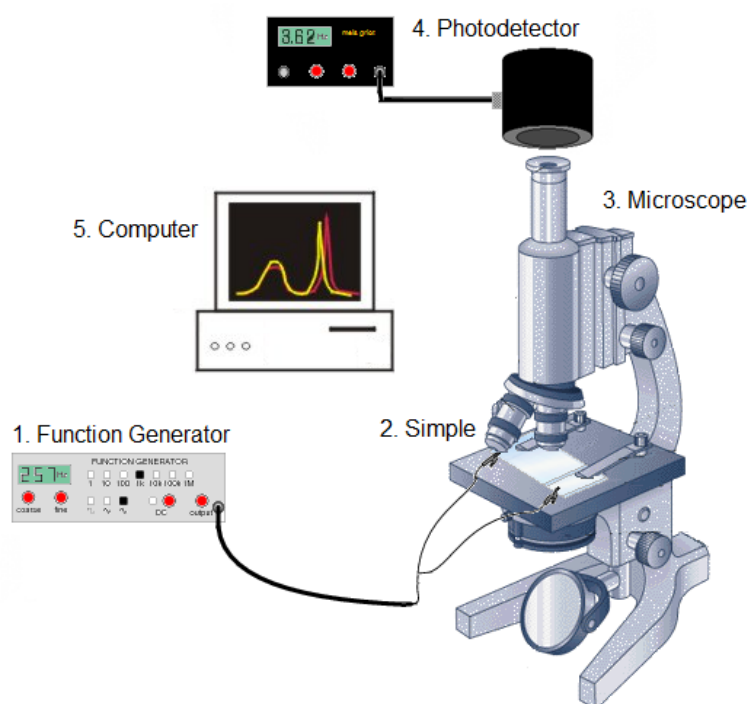


Fig. 3.28 Scheme of experimental setup manually controlled

All values recorded by the photodetector placed on the optical microscope were manually collected, elaborated and plotted by Origin software. In order to check the value of a threshold voltage for each samples, it was applied an

increasing voltage values up to 10V with a speed rate of 0.01V/min, so to be sure that the system be stable.

It defined as threshold field the one in which 10% and 90% of the saturated value of the transmitted light intensity was reached. All investigations have been performed at room temperature.

In experimental setup automatically controlled, a sinusoidal electric field modulated by an up ramp (10V, 2kHz) was applied across the cells and monitored on the oscilloscope. Photodetector receives the signal from the laser beam passing through the sample, recording the transmittance difference which is then sent through a lock-in to the computer to acquire the data.

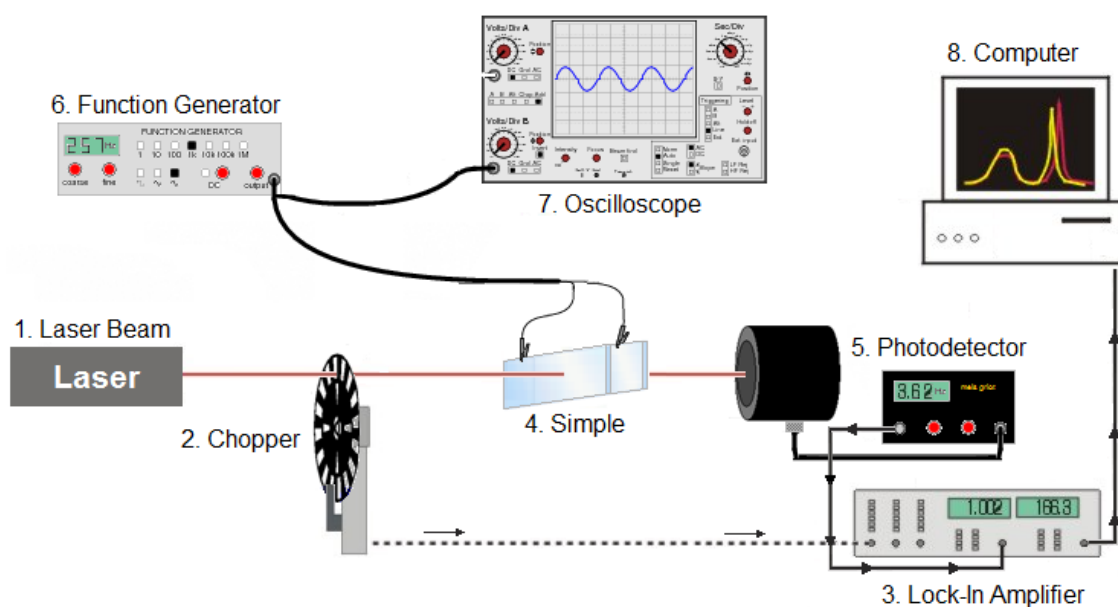


Fig. 3.29 Scheme of experimental setup automatically controlled

3.3.2 Results and discussion

The study of Fréedericksz transition of MLC-2079 is very important for the ability of additives to enhance the stability of surrounding environment and then improve the alignment of a liquid crystal device, also in order to obtain the information about the surface anchoring strength.

The observation through an optical microscopy of the behavior of homeotropically aligned MLC-2079 sample, under the effect of an ac electric field,

was carried out by gradually increasing the voltage until it reaches the threshold value (Fig. 3.30).

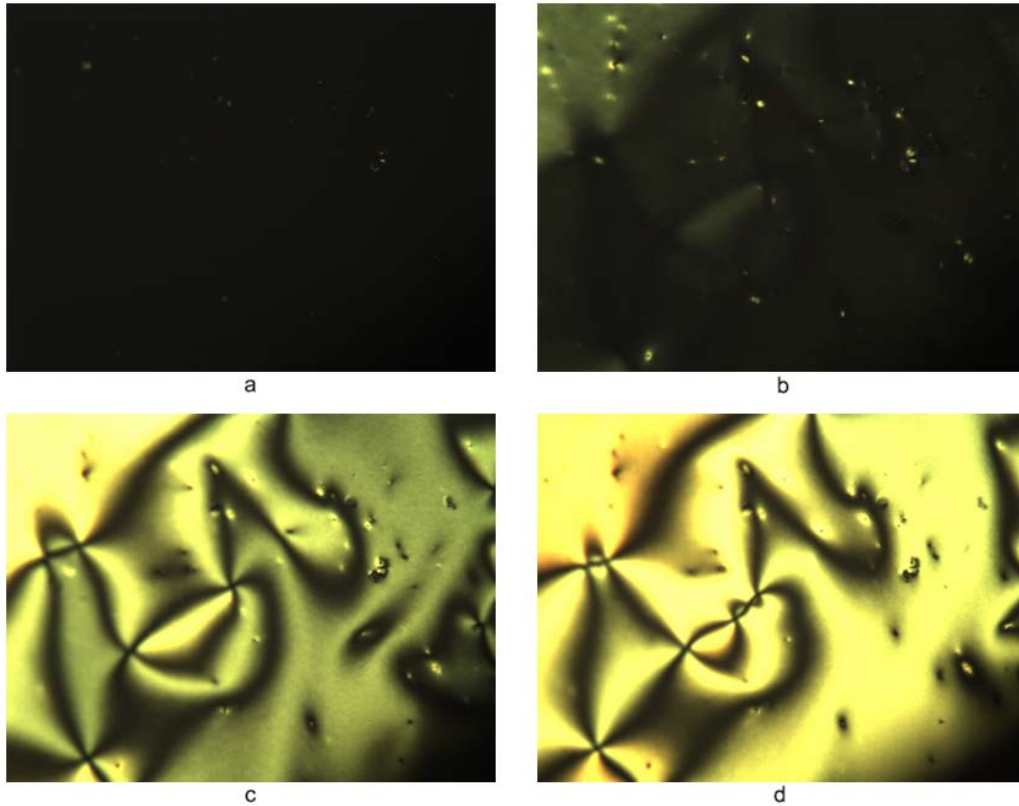


Fig. 3.30 Microscopic observation of MLC-2079 a) without ac field (Homeotropic), b) at V_{th} 10%, c) at V_{th} 90%, d) at the maximum voltage value (Planar)

It is observed that at relatively weak electric fields the Fréedericksz transition takes place. In fact as it can be seen in the graph in Fig. 3.30 the transition starts at $V_{th}10\% \approx 1.9$ and reaches a $V_{th}90\% \approx 2.6$. On increasing the voltage, the light transmittance has a sudden change in the slope at the voltage.

This is the normal behavior of a sample, which tends to align under the influence of an electric field. In fact, not finding impediments to the tilt of the liquid crystal molecules, they do not require a great current to guide its director.

From the electric-field threshold it is possible to calculate ^[11] the anchoring strength w of the nematic liquid crystal on the surface according to the equation:

$$w = qK_3 \tan\left(\frac{qd}{2}\right), \quad \text{with} \quad q = E\sqrt{\frac{|\Delta\varepsilon|\varepsilon_0}{K_3}}, \quad (10)$$

where d is the cell thickness, $\Delta\epsilon$ is the dielectric anisotropy, ϵ_0 is the vacuum dielectric constant, K_3 is the bend elastic constant, and E is the electric field threshold at which the Fréedericksz transition takes place. The anchoring strength was found to depend on the cell thickness.^[12,13]

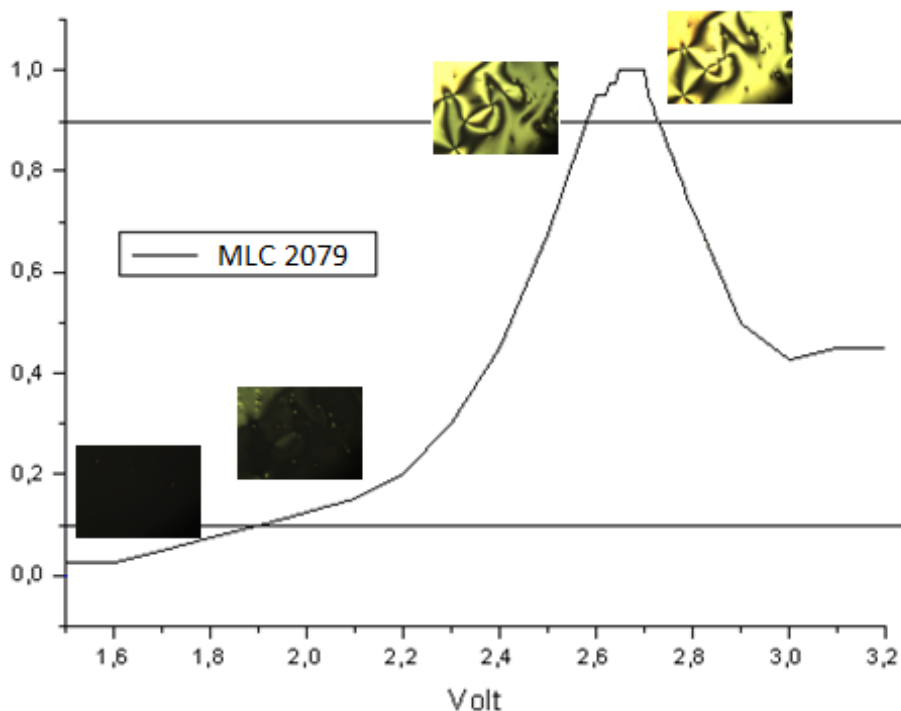


Fig. 3.30 Curve trend of MLC-2079 under the effect of an ac electric field

Just above the Fréedericksz transition threshold the director is essentially quasi-planar oriented.

According to the manual experimental setup described above, the ac electric field was increased very slowly, so that the Fréedericksz transition could fully develop.

The two experimental setups were used to be sure of the performed measures. Both carry out comparable results for all samples used, which leads to the deduction that the measurements are coherent.

To see if the effects of additives may influence the threshold value of the Fréedericksz transition, were added different liquid crystalline monomers in different weight percentages: 1.25, 2.5, 5 in MLC-2079. Indeed, increasing the

percentage of additive, there is an increase of the threshold electric field at which the transition occurs (Fig. 3.31).

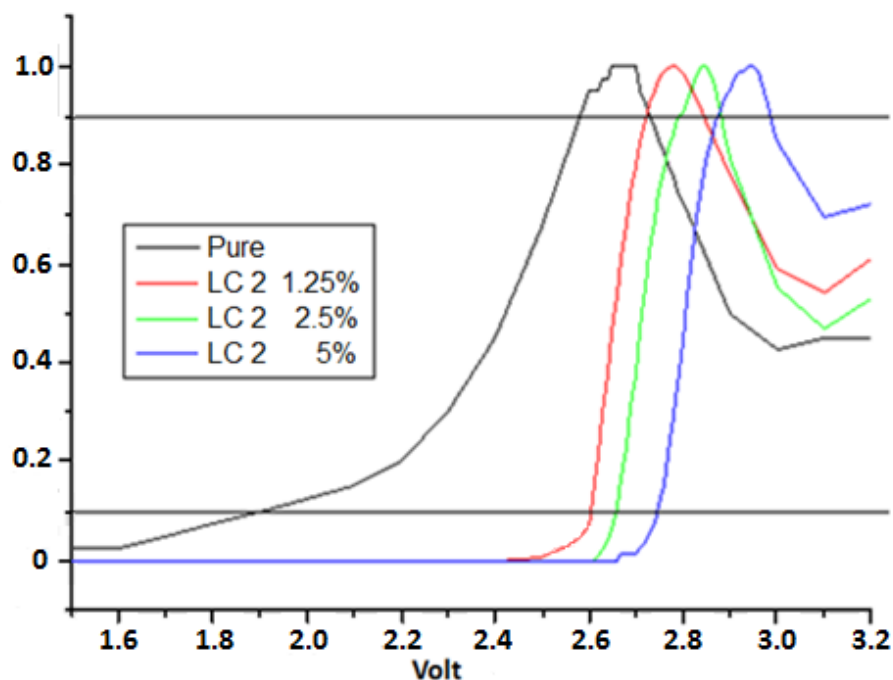


Fig. 3.31 Curve trend of MLC-2079/LC2 in different w/w% under the effect of an ac electric field

Once established that additives can improve the stability of the liquid crystal, the same measurements were repeated on samples of MLC-2079 mixed with the other LC. In particular, wants to observe is whether or not the alkyl chain affects the stability of the system. In fact, additives from 1 to 7 (LC1-LC7) are liquid crystalline stilbene derivates that differ only by the number of carbons in the alkyl chain. All mixtures gave satisfactory results at 10% and 90% of the threshold voltage

In the graphs in Fig 3.32 it can see as increasing the concentration of the additive, raises the 10% threshold voltage, except for samples with LC 4 and 5.

This phenomenon is most likely due to the inhomogeneity the sample that at low voltage does not follow the trend of other additives.

Moreover, does not observed an increasing stability by increasing the number of-CH₂-present as shown in Table 3.12.

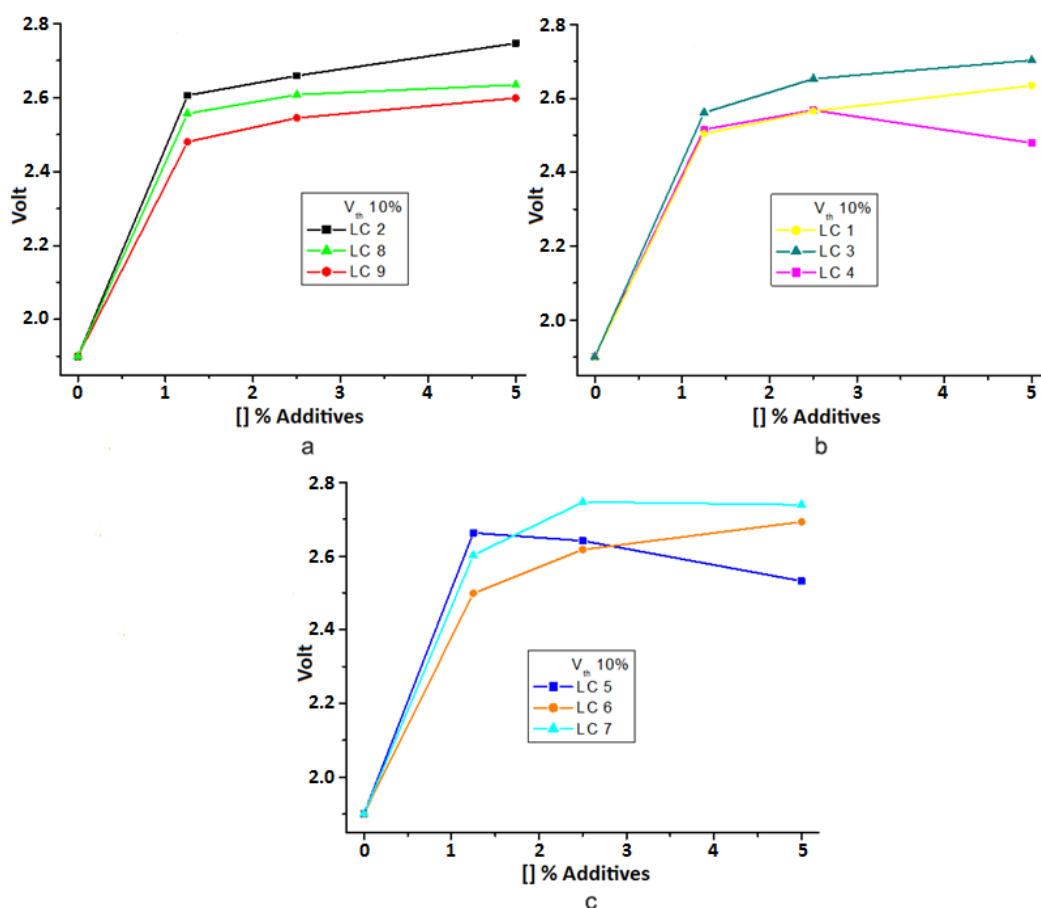


Fig. 3.32 Curve trend of $V_{th,10\%}$ of MLC-2079/LC_n in different w/w%

At 90% threshold voltage all additives increased the voltage threshold for the Frederiks transition and is observed an increase in values with increasing concentration (Fig. 3.33).

Different doping amount allows to reach voltage thresholds higher and higher increasing their concentration.

From the Table 3.12 appears that $V_{th,90\%}$ follows the number of $-CH_2-$ in alkyl chain, even if the voltage values are almost the same. This means that the alkyl chain does not play an important role for the stability of the molecule, although contributes in part.

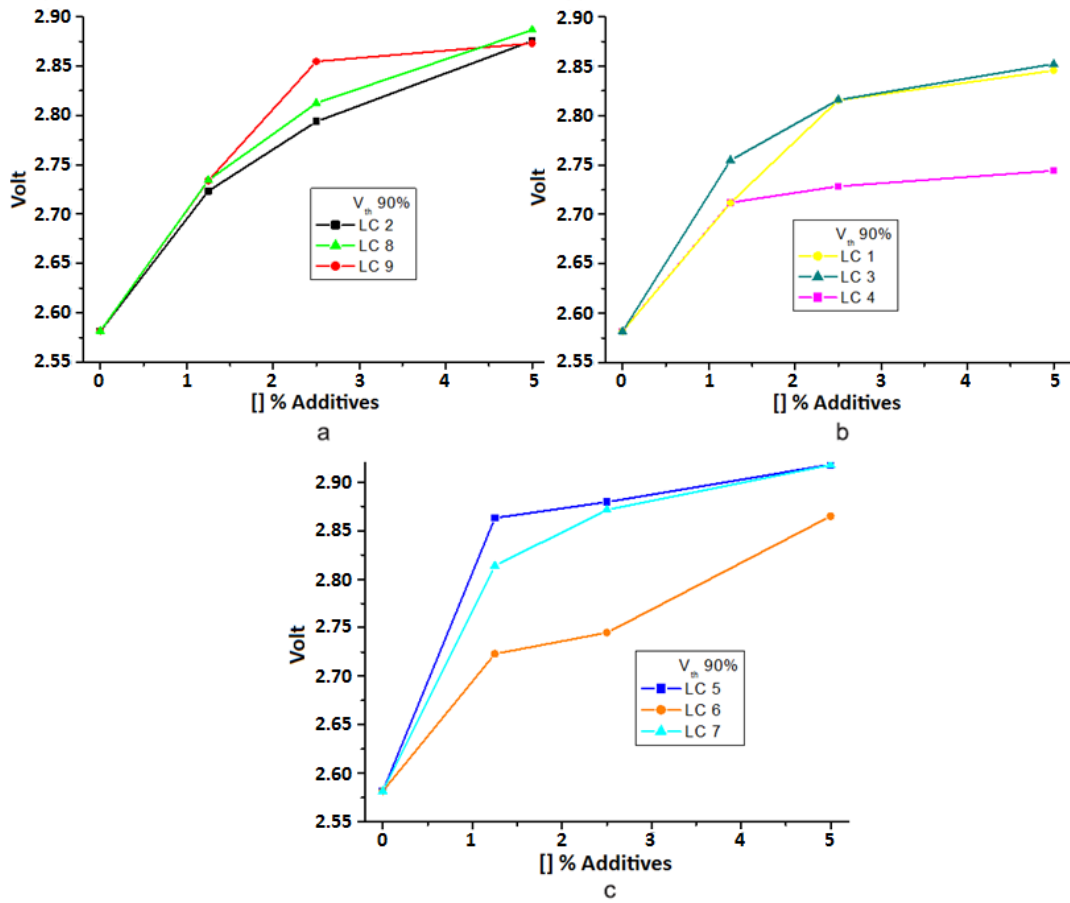


Fig. 3.33 Curve trend of $V_{th,90\%}$ of MLC-2079/LC_n in different w/w%

LC	0%		1.25%		2.5%		5%	
	$V_{th,10\%}$	$V_{th,90\%}$	$V_{th,10\%}$	$V_{th,90\%}$	$V_{th,10\%}$	$V_{th,90\%}$	$V_{th,10\%}$	$V_{th,90\%}$
1	1.9	2.582	2.504	2.712	2.565	2.816	2.635	2.846
2	1.9	2.582	2.605	2.723	2.659	2.794	2.746	2.875
3	1.9	2.582	2.562	2.755	2.653	2.816	2.703	2.852
4	1.9	2.582	2.516	2.712	2.568	2.729	2.479	2.744
5	1.9	2.582	2.663	2.863	2.641	2.880	2.532	2.918
6	1.9	2.582	2.499	2.723	2.618	2.745	2.693	2.865
7	1.9	2.582	2.602	2.814	2.747	2.872	2.740	2.918
8	1.9	2.582	2.556	2.734	2.608	2.813	2.634	2.887
9	1.9	2.582	2.480	2.734	2.545	2.855	2.599	2.873

Table 3.12 $V_{th,10\%}$ and $V_{th,90\%}$ of MLC-2079 in different LC_n w/w%

Was also expected to use the magnetic particles to see whether or not the influence the alignment of liquid crystal homeotropically oriented.

The idea to use magnetic particles in order to enhance the magneto-orientational response in liquid crystals was first proposed by Brochard and de Gennes in the 1970s^[14] and experimentally tested some years later. The as obtained doped nematic liquid crystals could be oriented by a magnetic field intensity 10^3 times smaller than usual.^[15,16] Since then, some experimental work has been dedicated to the better understanding of the phenomenon.^[17,18] Recently, it has been shown that the particle shape influences the value of the critical magnetic field necessary to align a thermotropic liquid crystal and in particular it has been underlined that elongated particles give the best results.^[19]

In this optic, was used magnetic particles to observe the Fréedericksz transition electrically induced.

Despite the small amount (0.5% w/w%) it has yielded significant results, compared to LC2 (Fig. 3.34). In fact w/w % higher than 0.5% generate disadvantages as aggregation of particles that consequently leads to inhomogeneous sample.

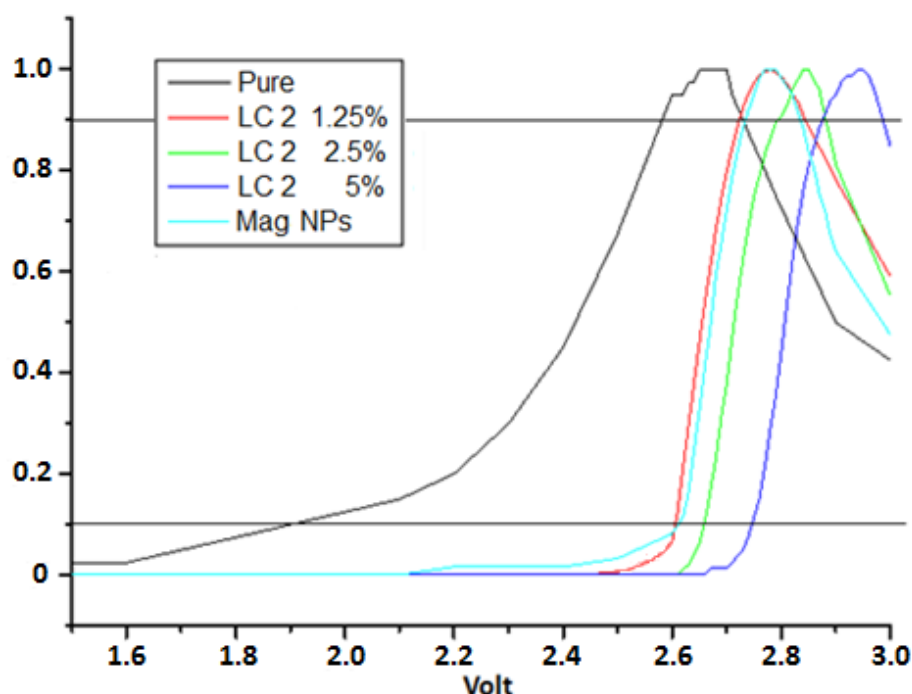


Fig. 3.34 Curve trend of MLC-2079/MNPs compared with MLC-2079/LC2

Although magnetic particles is in lower percentages, it increases the voltage threshold for the Fréedericksz transition, with comparable values to 1.25% of a LC additive.

3.3.3 Conclusion

It was studied an electric-field-induced alignment transition due to the breaking of the surface anchoring in initially homeotropic MLC-2079 mixed with several liquid crystalline molecules.

It was observed that increasing the concentration of these liquid crystalline molecules, there is an increase in anchoring force which increases the threshold voltage 10% and 90%. This is due to the fact that the additives have a long alkyl chain that prevent the tilt of the director since interpose themselves between the various molecules of the liquid crystal.

In addition it was observed that magnetic particles are able to increase the stability of the system with values comparable to the threshold voltage of 1.25% crystalline liquid additive used. These properties can be very useful for systems where there is need to maintain a stable orientation of liquid crystal, ie, where low values of voltage does not cause instability in the system, so this study can be used in applications such as *LCD* or *smart windows*.

References

- [1] B. Jerome, *Rep. Prog. Phys.*, 54, 391 (1991)
- [2] P.G. de Gennes; *The Physics of Liquid Crystals*, Oxford University Press (1974)
- [3] Y. Hidaka, J. Huh, K. Hayashi, S. Kai, M.I. Tribelsky; *Phys. Rev. E* 56, R6256 (1997)
- [4] H. Richter, N. Klopper, A. Hertrich, A. Buka; *Europhys.Lett.* 30, 37 (1995)
- [5] H. Richter, A. Buka, I. Rehberg, *Phys. Rev. E* 51, 5886 (1995)
- [6] A.G. Rossberg, A. Hertrich, L. Kramer, W. Pesh; *Phys.Rev. Lett.* 76, 4729 (1996)

-
- [7] A. Hertrich, W. Decker, W. Pesh, L. Kramer; *J. Phys. II* 2, 1930 (1992)
- [8] M.I. Tribelsky, K. Tsuboi, *Phys. Rev. Lett.* 76, 1631 (1996)
- [9] G. Chidichimo, G. Salerno, L. Veltri, B. Gabriele, F.P. Nicoletta; *Liquid Crystals*, Vol. 31, No. 5, 733–737, (2004)
- [10] G. Chidichimo, G. De Filpo, G. Salerno, L. Veltri, B. Gabriele, F.P. Nicoletta; *Mol. Cryst. Liq. Cryst.*, Vol. 465, pp. 165–174, (2007)
- [11] A.A. Sonin; “*The Surface Physics of Liquid Crystals*”, Gordon and Breach (1995)
- [12] A.L. Alexe-Ionescu, G. Barbero, A.G. Petrov; *Phys. Rev. E*, 48 R1631 (1993)
- [13] G. Barbero, G. Durand; *J. Phys.*, 51, 281 (1990)
- [14] F. Brochard, P.G. de Gennes, *J. Phys.*, 31, 691–708 (1970)
- [15] S.-H. Chen, N.M. Amer, *Phys. Rev. Lett.*, 51, 2298–2301 (1983)
- [16] A.M.F. Neto, M.M.F. Saba; *Phys. Rev. A: At., Mol., Opt. Phys.*, 34, 3483 (1986)
- [17] V. Berejnov, V. Cabuil, R. Perzynski, Y. Raikher, *J. Phys. Chem. B*, 102, 7132–7138 (1998)
- [18] C. Da Cruz, O. Sandre, V. Cabuil; *J. Phys. Chem. B*, 109, 14292–14299 (2005)
- [19] P. KopCansky, N. TomasoviCova, M. Koneracka, V. Zavisova, M. Timko, A. Dzarova, A. Sprincova, N. Eber, K. Fodor-Csorba, T. Toth-Katona, A. Vajda, J. Jadzyn, *Phys. Rev. E: Stat., Nonlinear, Soft Matter Phys*, 78, 011702 (2008)

3.4 Liquid crystals that improve the conductivity through the visible light

The target of the experiment described in this section is to produce glass device able to change their optical property as a result of external factors, like electric fields or sunlight. In fact, *smart windows* is an application referred to electrically switchable glass or glazing which changes light transmission properties when voltage is applied. This glass device can be used in building and automotive applications in order to control the incident day light and glare ^[1-3] according to occupant comfort. Certain types of smart glass can allow users to control the amount of light and heat passing through: with the press of a button, it changes from transparent to translucent, partially blocking light while maintaining a clear view of what lies behind the window. Another type of smart glass can provide privacy at the turn of a switch. (Fig. 3.35)



Fig. 3.35 Example of Smart Windows

The control of sunlight can be achieved by electrically switchable chromogenic materials (**see Chapter 2**), which are glazing devices able to change either their colour or transmittance when external stimulus occurs. They are mainly based on electrochromic systems, which change their colour as a consequence of REDOX reactions, and liquid crystal systems that allow controlling their transmittance by the electrical-driven director reorientation.

For example, electrochromic windows are the most popular electrically switchable Chromogenic materials;^[4,5] they change light transmission properties in

response to voltage and thus allow control over the amount of light and heat passing through. In electrochromic windows, the electrochromic material changes its “opacity”: it changes between a colored, translucent state (usually blue) and a transparent state. A burst of electricity is required for changing its state, but once the change has been effected, no electricity is needed for maintaining the particular shade which has been reached. Electrochromic glass provides visibility even in the darkened state and thus preserves visible contact with the outside environment.

On the contrary, the physical principle used in nematic liquid crystal-based systems is the electrically-driven reorientation of the liquid crystal director, which results in a change of their transmittance.^[6] Recently, Gardiner et al.^[7] have presented an interesting device based on an alternative electro-optical effect, which they observed in the smectic A phase. Upon application of a low-frequency voltage, the motion of ionic additives generates highly scattering focal conic textures in the device, becoming opaque. Then, the application of a larger frequency voltage turns the device in the clear state.

Among liquid crystal-based systems polymer-dispersed liquid crystals (PDLCs) deserve particular mention. They are composite materials, which show both the advantages of a solid polymer and a fluid liquid crystal. In fact, they are formed by either micron-sized liquid crystal droplets embedded in a polymer matrix (“Swiss cheese” morphology), or by liquid crystal that fills the voids and crevices of a polymer network (“polymer ball” morphology), which give them a solid-like nature.

Typically, the liquid mix of polymer and liquid crystals is placed between two layers of glass or plastic that include a thin layer of a transparent, conductive material followed by curing of the polymer, thereby forming the basic sandwich structure of the smart window. With no applied voltage (OFF state), the liquid crystals are randomly arranged in the droplets, resulting in scattering of light, and it appears translucent white.

Upon application of a suitable electric field, the molecular reorientation will change the refractive index of liquid crystal domains allowing light to pass through the droplets with very little scattering and the device will appear transparent in the ON state if the optical matching condition is fulfilled. The degree of transparency can be controlled by the applied voltage. This is possible because at lower voltages, only a few of the liquid crystals align completely in the electric field, so only a small portion of the light passes through while most of the light is scattered. As the voltage is increased, fewer liquid crystals remain out of alignment, resulting in less light being scattered.

The reorientation electric fields are dependent on several parameters including droplet size and shape, size distribution, anchoring effects at polymer boundary, liquid crystal dielectric and conductive anisotropy, polymer molecular weight and chemical nature.

To enhance these devices and especially to improve utilization with a less environmental impact, recently it was observed that by adding small amounts of conductive molecules in the polymer matrix, the electrical conductivity can be finely adjusted, affect strongly the electro-optical response of PDLCs.^[8] In this way the electric field across the nematic liquid crystal droplets can be increased with a consequent large reduction in the reorientation fields and relaxation times.

In this section it will describe the development of a device capable to have a low environment impact, in order to realize a energy saving system (to lower the demand on precious no-renewable fuels for lighting and cooling) and allows a controlled comfort from daylight. In fact, the use of smart glass can save costs for heating, air-conditioning and lighting and avoid the cost of installing and maintaining motorized light screens or blinds or curtains.

In this optics it was prepared PDLCs reverse mode, able to reach a transparent OFF-State and an opaque ON-State (Very important for energy saving). They allow overcoming some drawbacks of direct mode PDLCs such as opaque unpowered state and large values of haze. In addition, these devices are doped with photoconductive molecules able to tune the film conductivity under daylight and

ensure an automatic opacity because is able to self-increase its scattering as a function of the impinging light intensity.

3.4.1 Materials and Preparation of Sample

Reverse mode shutters have been obtained by using dual-frequency addressable liquid crystals^[9,10], by polymerizing nematic emulsions^[11], by functionalizing the liquid crystal/polymer matrix interface^[12], and by means of rough surfaces^[13].

Nematic emulsion were prepared in vials by mixing the appropriate amounts of liquid crystalline monomer (*1,4-bis {4-[6-(acryloyloxy) hexyloxy] benzyloxy} benzene*, 16w/w% and synthesized in agreement with Ref. [16]), and the eutectic nematic mixture **ZLI 4788-000** ($\Delta\epsilon = -5.7$, 84 w/w%, $\sigma_{\text{avg}} = 2.35 \times 10^{-8} \Omega^{-1} \text{m}^{-1}$), doped with different percentages (up to 10w/w%) of a dispersion of *zinc phthalocyanine* in ionic liquid (**ZP/IL**) in the weight ratio 0.5:100 (*1-hexyl-3-methylimidazolium bis (trifluoromethylsulfonyl) imide*, Merck). Such composition was chosen after a set of trials involving other lipophilic ionic liquids, photoconductive and photochromic molecules, and different concentrations.

After stirring at 100°C, emulsion were introduced by capillarity into homemade cells whose thickness was set to be 30µm by glass spheres. Glass substrates had a 120nm indium tin oxide conductive layer (Balzers) with an average roughness of 2.6nm, which are known^[13] to align liquid crystalline mixtures perpendicularly (homeotropically) to them. After having checked the homeotropic alignment of mixtures by polarizing optical microscope, cells were exposed at a controlled temperature (80°C) to UV light for 15min (average power 10mW/cm²) in order to induce the phase separation between liquid crystal and polymer. As the polymerization processes are rather sensitive to thermal fluctuations only samples, which kept a good homeotropic alignment after polymerization process, were considered for the subsequent electro-optical characterization. Obviously, an improvement in the final degree of alignment can be gained by covering glass substrates with alignment promoters as polyimide layers. The electro-optical

properties of samples were measured by means of laser beam optical setup^[14] equipped with a white light source (Linios 1000, Laser point, maximum power output $10\text{mW}/\text{cm}^2$) for the measurements under irradiation. Briefly, a He–Ne laser light beam passed through a chopper and a beam expander. The beam diameter was set to be 0.8 mm by a variable iris before impinging on the sample. Then, light coming out from the sample was collected by a high-speed detector with an acceptance angle equal to 2.51. The sample was mounted on a computer-controlled rotatable stage to vary the incident angle. The intensity of the incident laser light measured through an empty cell was assumed to be full-scale intensity. The ON and OFF response times, τ_{ON} and τ_{OFF} , defined, respectively, as the time required to drop to 10% of the maximum transmittance and to reach 90% of the optical response after the external field is removed, were determined by monitoring the drive signal ($\nu=1\text{ kHz}$, $E_{\text{pp}}=3\text{V}\mu\text{m}^{-1}$) and the response of the photodiode using a digital storage oscilloscope. Conductivity measurements were carried at 1kHz, which is the typical drive frequency of PDLCs, with a LCR meter (Hewlett Packard4284A).

3.4.2 Results and discussion

1,4-bis{4-[6-(acryloyloxy)hexyloxy]benzoyloxy} benzene is known to allow and keep after the polymerization, a good homeotropic alignment of liquid crystal on rough substrates covered by indium tin oxide.^[13,15,16] The alignment is achieved through typical grooves present in the substrates, which promote an excellent alignment and an easy axis almost perpendicular to the cell glass plates.

Such preferential alignment can be stored if cross-linkage of the polymerizable component is performed. Thanks to this it is possible to obtain transparent films after a polymerization process. Highly transparent (OFF state transmittance, τ_{OFF} , larger than 70%) PDLC films were obtained after the polymerization-induced phase separation process at all doping percentages of ZP/LI mixture. Fig. 3.36 shows the typical field dependent transmittances, which are left shifted as the weight percentage of zinc phthalocyanine/ionic liquid mixture is increased. The electro-

optical left shift is easily explained by an increase of cell conductivity as a function of the weight percentage of ZP/IL mixture, which results in a decrease of the reorientation fields, required to make the device opaque.^[17]

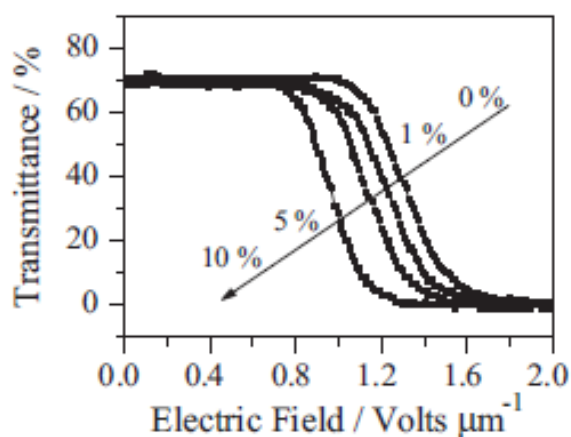


Fig. 3.36 Transmittance dependence on the applied electric field for increasing percentages of ZP/IL mixture in dark conditions.

Scanning electron microscopy confirmed the presence of a polymer ball morphology in all our samples: small polymer balls (average radius about 100nm) merging in a network structure, whose voids and crevices are filled by liquid crystal (Fig. 3.37).

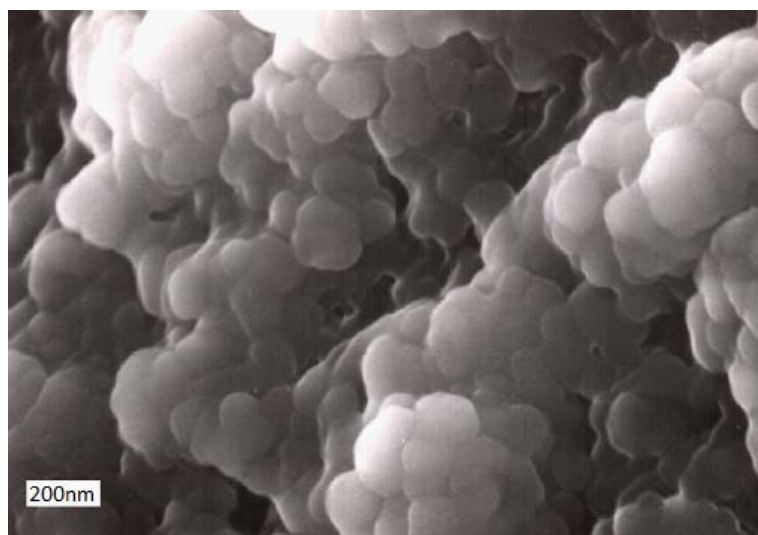


Fig. 3.37 SEM picture of sample morphology. The average radius of polymer balls is 100nm.

Such a structure allows a large viewing angle as the thin liquid crystal layers around the polymer droplets do not give rise to a sufficient phase shift of the light,

as confirmed by the measurements of transmittance as a function of the cell tilt angle (Fig. 3.38).^[18]

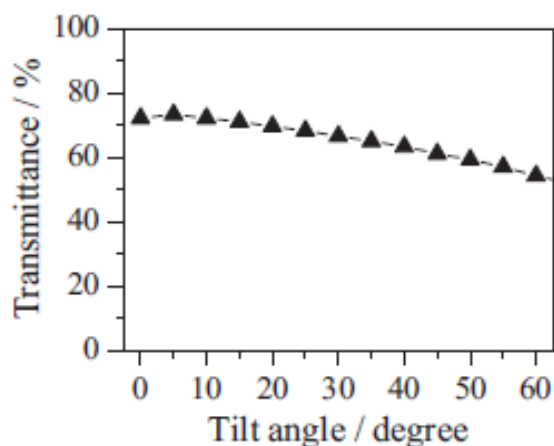


Fig. 3.38 Typical behavior of transmittance as a function of the cell tilt angle.

If an ac external field is applied to cells in dark conditions ($\nu=1$ kHz), liquid crystal directors will reorient perpendicularly to the field direction because of its negative dielectric anisotropy, increasing the light scattering and reducing the transmittance values (about 1% for an electric field of $1.8 \text{ V}\mu\text{m}^{-1}$). Fig. 3.39 reports the typical field-dependent transmittance of a cell in a conventional reverse mode PDLC. It is possible to distinguish three different regimes: (1) a lower electric field range ($E < 1.0 \text{ V}\mu\text{m}^{-1}$) where the films appear transparent, (2) a larger electric field range ($E > 1.6 \text{ V}\mu\text{m}^{-1}$) in which the cells look opaque, and, finally, (3) an intermediate range ($1.0 \text{ V}\mu\text{m}^{-1} < E < 1.6 \text{ V}\mu\text{m}^{-1}$) where one can tune the value of transmittance as a function of impinging radiation intensity.

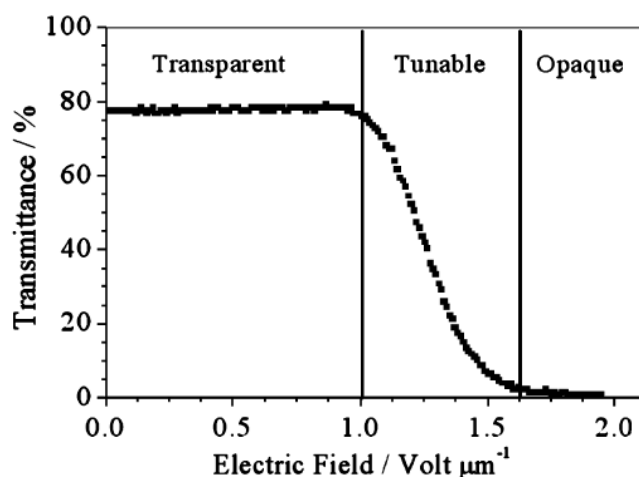


Fig. 3.39 Typical electric field-dependent transmittance of reverse mode PDLCs

The highly transparent state is a consequence of both the polymer ball morphology of samples and the good match between the polymer matrix refractive index and liquid crystal ordinary one. If the external field is removed, the restoring forces acting at polymer and substrate interfaces will cause the homeotropic reorientation of directors (Fig. 3.40). Both τ_{ON} and τ_{OFF} values are of the order of few milliseconds ($\tau_{ON} \approx 30\text{ms}$ and $\tau_{OFF} \approx 4\text{ms}$).

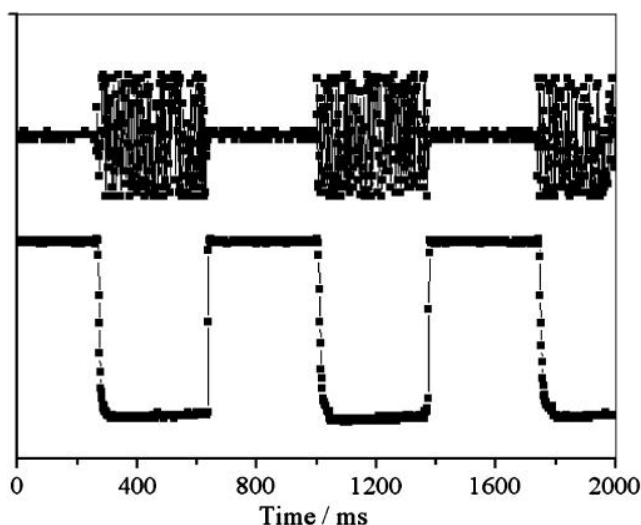


Fig. 3.40 Electro-optical response to an ac field. Both ON and OFF response time values are of the order of few milliseconds

For the sake of completeness, we mind that liquid crystals are anisotropic materials but, being PDLCs rather complex heterogeneous systems and since a complete description of their electrical properties is not known, we have considered PDLCs just as isotropic media (to a first approximation^[19]). The measurements of the average conductivities performed on liquid crystal-saturated polymer matrix (liquid crystal 75w/w% and monomer 25 w/w%, which is the weight ratio for the onset of an electro-optical response^[19]), and liquid crystal with different weight percentages of ZP/IL mixture are reported in Fig. 3.41a and b. They show that the polymer matrix and liquid crystal conductivities increase after doping and under irradiation, and that the polymer matrix conductivity values are generally one order of magnitude lower than the liquid crystal ones. It is possible to observe that both liquid crystal-saturated polymer matrix and liquid crystal conductivities increases monotonically (see values at 0 mWcm^{-2}) for increasing

w/w% of zinc phthalocyanine/ionic liquid mixture, allowing consequently a fine adjustment of PDLCs conductivity. If polymer matrices and liquid crystal cells are exposed to increasing light powers, we observe an increase in their conductivities due to the photoconductive effect of zinc phthalocyanine. As shown in Fig. 3.41c, the conductivities of polymer matrix, liquid crystal, and PDLC at 1kHz increase as a function of irradiation power.

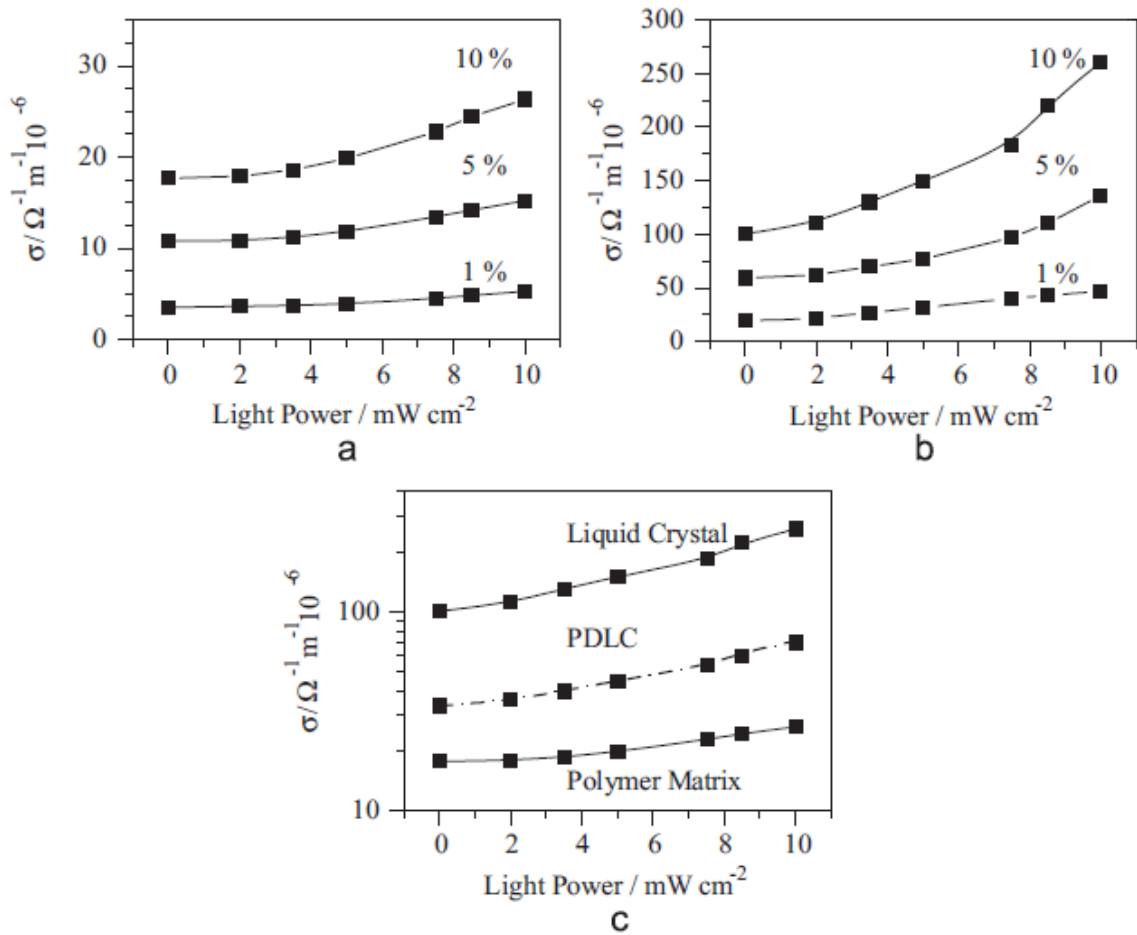


Fig.3.41 Average conductivity of: a) liquid crystal-saturated polymer matrix, b) liquid crystal as a function of the applied light power at the drive frequency of 1 kHz for different amounts of ZP/IL; c) comparison of average conductivities at 10w/w% of ZP/IL mixture. Solid lines are just a guide for eyes, dotted line is obtained by using Eq.(2)

The PDLC conductivity values reported in Fig.3.41c can be obtained from the polymer matrix, σ_{matrix} , and liquid crystal, σ_{LC} , ones by the following simple weight average:

$$\sigma_{\text{PDLC}} = 0.80 \sigma_{\text{matrix}} + 0.20 \sigma_{\text{LC}} \tag{11}$$

Keeping in mind the onset of phase separation (the saturated liquid crystal matrix needs an amount of 25w/w% monomer and 75w/w% liquid crystal), 16w/w% of the monomer, used in the PDLCs composition, is able to form a 64w/w% saturated liquid crystal polymer matrix. If one considers that we used a simple additive law for conductivities, neglecting the possible shift in the phase separation onset due to the presence of ionic liquid (which could enhance the mutual solubility between the polymer and the liquid crystal), such a value (64w/w%) can be accepted as close to the experimental 80w/w% value used in Eq.11.

The optical control of the light scattering properties of polymer dispersed liquid crystals can be achieved by fine tuning of the cell electrical properties under light irradiation. In fact, measurements under irradiation were performed in the steady-state regime after 10 min of turning on the lamp. This further increase in film conductivity is expected to result in a further left shift of PDLC electro-optical response when exposed to light irradiation. Indeed, if one considers the PDLCs doped with 10w/w% of ZP/IL mixture (see Fig. 3.42) it is possible to observe such shift, which causes lower switching fields and sharper line shapes.

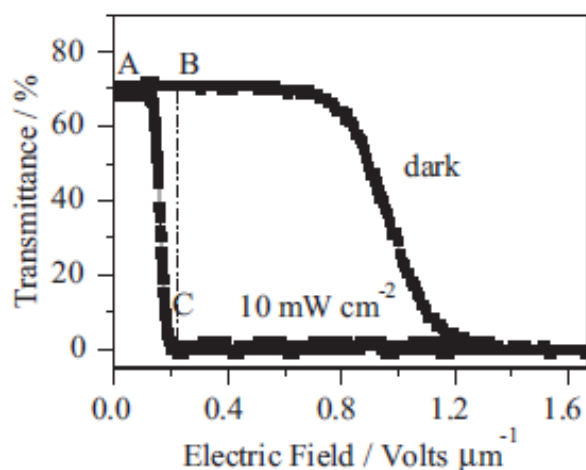


Fig. 3.42 Transmittance dependence on the applied electric field in dark and under irradiation (10mWcm^{-2}) conditions. A, B, and C, are the initial transparent state, the biased transparent state, and their radiated opaque state, respectively.

Such behavior is more evident in Fig. 3.43a, where the threshold and saturation fields of the PDLCs doped with 10w/w% of ZP/IL mixture are reported as

a function of the impinging power (full lines are linear fits of experimental data). The increase in the polymer matrix conductivity affects both the OFF and ON times as shown in Fig. 3.43b. We observe a linear decrease of both τ_{ON} and τ_{OFF} times.

Such results are in agreement with previous observations indirect mode operating and “Swiss cheese” PDLCs doped with conductive oligomers.^[8] Such results open the opportunity to manufacture smart windows able to self-adjust their transmittance as a function of daylight and glare. In fact, if one biases the previously described cells with an electric field lower than the threshold value, i.e. the device is still in a fully transmissive state, the increase in the impinging light power will left shift the device electro-optical response with a consequent reduction of its transmittance.

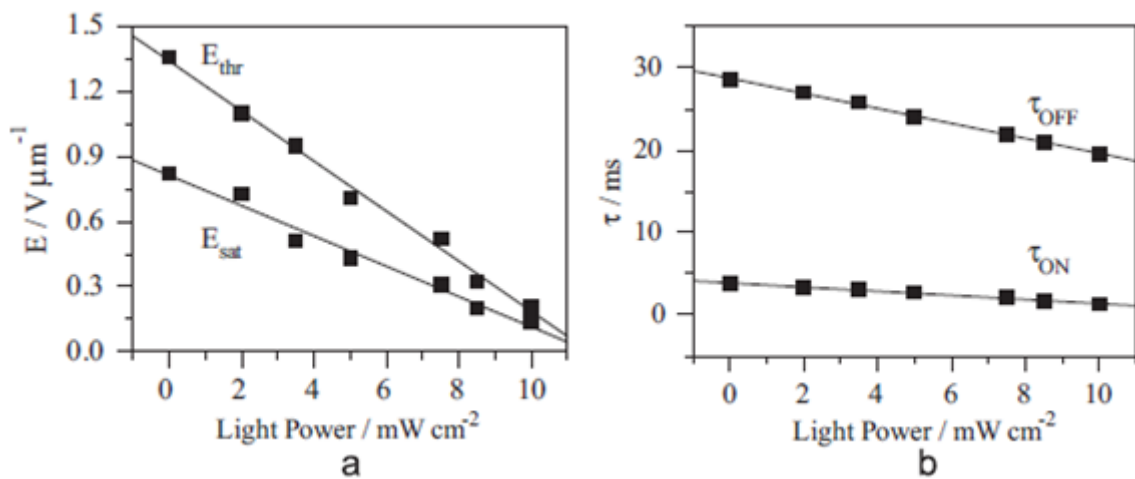


Fig. 3.43 Behaviour of a) the threshold and saturation fields and b) the electro-optical response times for a PDLC doped with 10w/w% of ZP/IL mixture as a function of the applied light power. The lines are linear fits of experimental data.

To better clarify the device mechanism let's consider Fig. 3.42 where it is reported the electro-optical responses of a PDLC doped with 10w/w% of ZP/IL mixture in dark and under irradiation ($10\text{mW}/\text{cm}^2$) conditions and three different states: **A** is the initial transparent state, **B** is the biased transparent state, and **C** is the irradiated opaque state. In dark conditions and with no electric field applied, the device is in the transmissive state **A**. If it is biased with an electric field of $0.2\text{V}/\mu\text{m}^{-1}$ or larger (up to $0.8\text{V}/\mu\text{m}^{-1}$), the device moves to the state **B**, which is still highly transmissive since the applied field is lower than the threshold field. If the

device is exposed to light irradiation, 10mW cm^{-2} in the case shown in Fig. 3.42, the electro-optical response changes and the film reduces its transmittance to that of state **C**, which is strongly opaque. Such opaque state is persistent until the light irradiation and bias are present and a transmissive state (**A** or **B**) can be easily gained either by switching off the lamp (path **C-B**) or by turning off the electric bias (path **C-A**). Both state **A** and **B** are equivalent for their transmittance values, but are quite different in their response times. Indeed, the transition **C-A** requires a time interval equal to the OFF response time, τ_{OFF} , which is of the order of few tens of milliseconds (see Fig. 3.43b), while the time for the transition **C-B** is limited by the recombination time of zinc phthalocyanine in dark conditions. In order to quantify the response of our PDLCs to the optical stimulus, we measured the transmittance as a function of time in cells biased with an electric field lower than E_{thr} and under repeated light beam square steps (light power 10mWcm^{-2}) as shown in Fig. 3.44. In the dark the applied field is notable to “switch off” the device as the strength of the applied field is lower than E_{thr} . Under light irradiation the doping molecules become conductive increasing the conductivity of the polymer matrix, and thus the switching field is strongly reduced allowing the bias field to make the PDLC opaque with in a time scale of some minutes (about 3 min for the 90%–10% transition). If the light beam is turned off, the doping molecules relax to their initial non-conductive state in a slightly larger time interval (about 5 min for the 10–90% transition) within which the device recover sits original transparency. It should be noted that under different light powers and doping percentages the films are able to reach intermediate steady-state values of transmittance, while the setting of bias value (lower than $0.2\text{V}\mu\text{m}^{-1}$ in the example of Fig. 3.42) allows one to choose the final degree of opacity.

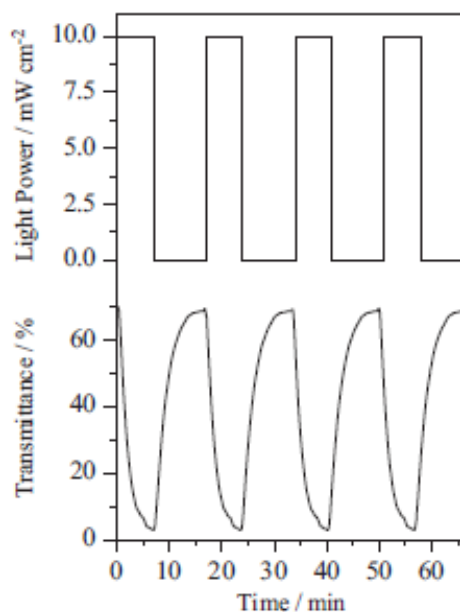


Fig. 3.44 Time-dependent transmittance of a PDLC doped with 10w/w% of ZP/IL mixture.

The device stability was checked under repeated light beam square steps. In particular, after 100 irradiation cycles we did not observe any change in the initial and final values of transmittance, and there was no burn-in or fade effect associated with the use of additives.

3.4.3 Conclusion

In this work we have shown the preparation and characterization of self-adjusting chromogenic cells suitable for external glazing. We have homeotropically aligned liquid crystalline mixtures by rough surfaces. The mixtures were formed by a low molecular mass liquid crystal with a negative dielectric anisotropy, a liquid crystalline monomer, and a dispersion of photo-conductive molecules in ionic liquid. The obtained reverse mode operation PDLC is able to control its light-scattering properties as a function of irradiation conditions by simply applying an electric field lower than the threshold one. In the dark, the field applied across the film is not able to reorient the liquid crystal directors, and, consequently, the cell is transparent. In steady-state irradiation conditions, the change in the electrical properties of the polymer matrix enhances the effective field acting on the liquid crystal, making the film opaque. The device can gain the initial transmittance value either, in few milliseconds, by turning off the bias electric field or, in few minutes,

by removing the light source. A different bias value or doping amount allow one to select the wanted degree of opacity. Such *smart window* are able to self-control the incident daylight and glare as a function of incident intensity both in building and automotive applications. In addition, the use of rough surfaces allows an easier and faster preparation with no limit theoretically imposed on the cell dimensions as in other liquid crystal devices.

References

- [1] C.M. Lampert, C.G. Granqvist (Eds.), *“Large-area Chromogenics: Materials and Devices for Transmittance Control”*, SPIE Optical Engineering Press, Bellingham, WA, (1990)
- [2] C.M. Lampert; *Sol. Energy Mater. Sol. Cells* 76, 489–499 (2003)
- [3] G.P. Smestad, C.M. Lampert; *Sol. Energy Mater. Sol. Cells*, 91 440–444 (2007)
- [4] G.G. Wallace, G.M. Spinks, L.A.P. Kane-Maguire, P.R. Teasdale, *“Conductive Electroactive Polymers”*, CRC, Boca Raton, (2003)
- [5] P.M.S. Monk, R.J. Mortimer, D.R. Rosseinsky, *“Electro-chromism: Fundamentals and Applications”*, VCH Inc., Weinheim, (1995)
- [6] J.W. Doane, G.Chidichimo, N.A. Vaz, US Patent 4688900, (1987)
- [7] D.J. Gardiner, S.M. Morris, H.J. Coles; *Sol. Energy Mater. Sol. Cells*, 93, 301–306 (2009)
- [8] D. Cupelli, F.P. Nicoletta, G. De Filpo, G. Chidichimo, A. Fazio, B. Gabriele, G. Salerno; *Appl. Phys. Lett.* 85, 3292–3294 (2004)
- [9] P. Nolan, D. Coates; *Mol. Cryst. Liq. Cryst. Lett.* 8, 75–83 (1991)
- [10] T. Gotoh, H. Murai; *Appl. Phys. Lett.* 60, 392–394 (1992)
- [11] F.P. Nicoletta, G. De Filpo, J. Lanzo, G. Chidichimo; *Appl. Phys. Lett.* 74, 3945–3947 (1999)
- [12] Y.D. Ma, B.G. Wu, G. Xu; *Int. Soc. Opt. Eng.* 1257, 46–57 (1990)

- [13] M. Macchione, D. Cupelli, G. De Filpo, F.P. Nicoletta, G. Chidichimo; *Liq. Cryst.* 27, 917–920 (2000)
- [14] G. Chidichimo, Z. Huang, C. Caruso, G. De Filpo, F.P. Nicoletta; *Mol. Cryst. Liq. Cryst.*, 299, 379–387 (1997)
- [15] R.A.M. Hikmet; *J. Appl. Phys.*, 68, 4406–4412 (1990)
- [16] R.A.M. Hikmet, B.H. Zwerver; *Liq. Cryst.*, 12, 319–336 (1992)
- [17] B.G. Wu, J.H. Erdmann, J.W. Doane; *Liq. Cryst.*, 5, 1453–1465 (1989)
- [18] M. Macchione, D. Cupelli, G. De Filpo, F.P. Nicoletta, G. Chidichimo; *Liq. Cryst.* 27, 1337–1341 (2000)
- [19] P.S. Drzaic, *“Liquid Crystal Dispersions”*, World Scientific, Singapore, (1995)

3.5 Lyotropic Liquid crystals and Ferrofluids in nonlinear optics

The search for new nonlinear optical (NLO) materials with high optical nonlinearities is gaining interest both from the research as well as industrial point of view. For this reasons in the latest years many studies were involved on very smart materials, thanks to their physical-chemical properties: complex fluids^[1]. Ones of them are Liquid Crystals, Polymers and Ferrofluids.

The use of nanoemulsions as drug delivery vehicles for the treatment of proliferative inflammatory diseases, such as cancer and atherosclerosis, has been increasingly studied.^[2-4]

In search of more efficient drug delivery devices, the systematic modification of the composition of those nanoemulsion systems to optimize the pharmacologic properties of the drug-vehicle association is an important research pathway

It has been showing that cholesteryl ester-rich nanoemulsions resembling the structure of lipoproteins can function as drug-targeting devices^[5-7] to carry drugs to tumors^[8] or atheromatous lesions.^[9] Nonprotein nanoemulsions resembling low-density lipoproteins (LDL) can pick up apolipoprotein E (apo E) in contact with plasma and bind to LDL receptors using this apolipoprotein as a ligand.^[10] The properties of LDL or other lipoprotein-binding receptors are interesting in terms of drug delivery.

Magnetic fluids or ferrofluids are colloidal suspensions of magnetic nanoparticles, dispersed in a liquid carrier^[11]. They have attracted great interest in health and new technology areas^[12-22]. Ferrofluid is used in many magneto-optical devices which use physical characteristics of the magnetic colloid such as field-induced birefringence and controlled modulation of the optical transmission, among others.

Exploiting the capabilities of the LDE to bind specific receptors that are over-expressed in certain diseases (like cancer) and the ability of magnetic particles, as ferrofluids, to drive in a specific site and act against the tumor itself (hyperthermia), it could create an excellent way to reach and destroy cancer cells

The purpose of this work is to observe the nonlinear optics behavior of these materials, in order that they can exploit these features, for potential future use in optics and advanced biotechnology.

3.5.1 Materials and Preparation of Sample

The study developed at the Universidade de Sao Paulo, in Brazil is based on studies of nonlinear optics and is divided into two parts.

In the first were studied nonlinear optical properties of the Fe_3O_4 ferrofluids. In the second have been analyzed different optical responses of lipoproteins.

The magnetic colloids used were the oil-based surfacted ferrofluid **EMG911** (Fig.3.45) and the water-based ferrofluid **EMG509** from Ferrotec. The magnetic grains' typical diameter is 10 nm coated with an anionic surfactant.



Fig. 3.45 Oil-based EMG911

The samples used in this work were encapsulated between glass plates separated by a $L=50\mu\text{m}$ and $200\mu\text{m}$ spacers, filled respectively with 0.36% and 0.09% of ferrofluid compound in synthetic isoparaffinic solvent (for oil-based EMG911) and Milli-Q water (for water-based EMG509). The absorption spectra of EMG911 and EMG509 (Fig.3.46) show significant absorptions, over a broad wavelength region, below 550 nm.

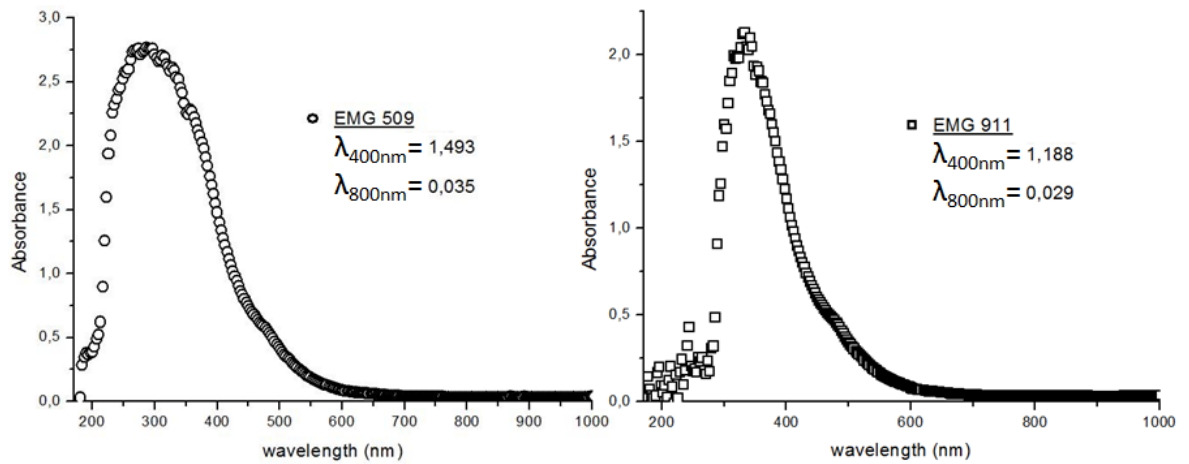


Fig. 3.46 Absorption spectra of Ferrofluids

All lipoproteins used are provided by the INCOR (Instituto do Coração) in São Paulo/SP. In particular was used LDL, LDLox and LDE (Fig. 3.47).



Fig. 3.47 LDE sample

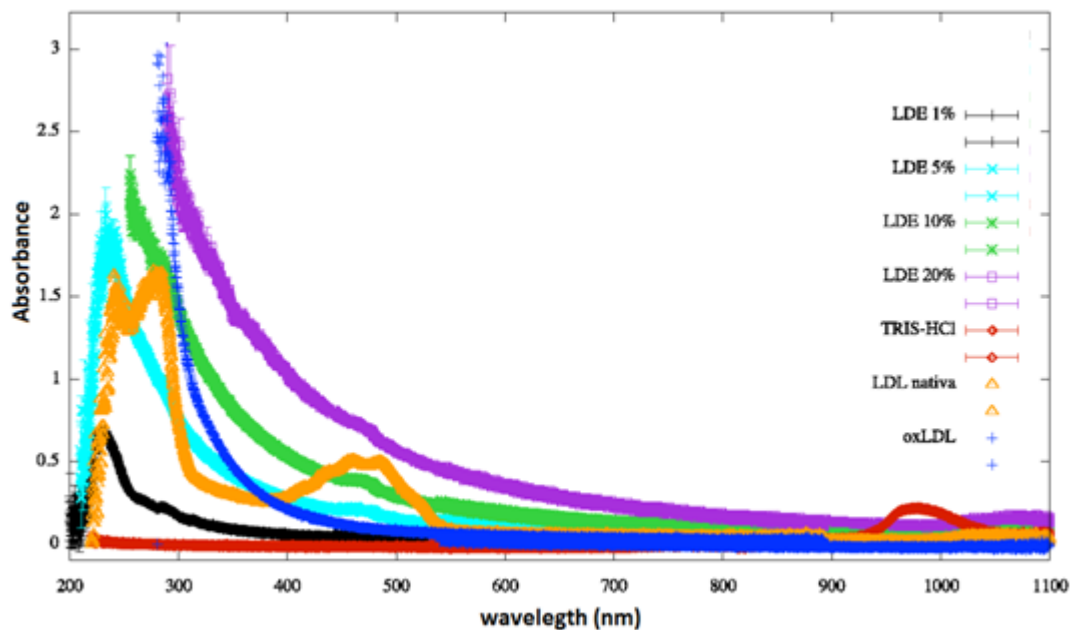


Fig. 3.48 Absorption spectra of Lipoproteins

The samples used in this work were placed in a L=1mm quartz cuvettes. The absorption spectra was measured (Fig.3.48); **TRIS** (*2-Amino-2-hydroxymethyl-propane-1,3-diol*) was used as solvent.

3.5.2 Theoretical Background

3.5.2.1 Electronic nonlinear optical process

To evaluate a material for the above applications, one must characterize its index of nonlinear refraction (NLR) and nonlinear absorption (NLA) coefficient. Especially for NLA we focused our study only on Two Photon Absorption (TPA) effects.

Two-photon absorption (TPA) is the simultaneous absorption of two photons of identical or different frequencies in order to excite a molecule from one state (usually the ground state) to a higher energy electronic state.

The physical processes that give rise to NLA and the accompanying NLR include “ultrafast” bound electronic processes and “excited state” processes, where the response times are dictated by the characteristic formation and decay times of the optically induced excited states. Excited-state nonlinearities can be caused by a variety of physical processes including absorption saturation ^[23], excited-state absorption in atoms and molecules ^[24] or free-carrier absorption in solids ^[25,26], photochemical changes ^[27], as well as defect and color center formation ^[28].

Several different experimental techniques can be employed to measure TPA and NLR coefficients and for the most cases, the optical nonlinearities are detected under the excitation of laser pulses. Among these techniques, the Z-scan technique, which was first introduced by Sheik-Bahae ^[29,30] is an appropriate method to measure them.

Sheik-Bahae’s theory, are applied in two different situations: open-aperture (**OA**) and closed-aperture (**CA**) Z-scan method. From this two kind of method we can determine the nonlinear refractive (n_2) and the nonlinear absorption (β) index.

First of all we consider the nonlinear refractive index (n_2). Considering total refractive index (n) we can write:

$$n = n_0 + n_2 I_0 \quad (12)$$

Where n_0 is the linear refractive index, n_2 is the nonlinear one and I is the light intensity.

Assuming a Gaussian beam with a beam waist radius w_0 traveling in the $+z$ direction, we can write E as:

$$E(z, r, t) = E_0(t) \frac{w_0}{w(z)} \cdot \exp\left(-\frac{r^2}{w^2(z)} - \frac{i \pi r^2}{\lambda R(z)}\right) e^{-i\phi(z,t)} \quad (13)$$

where the beam radius is:

$$w^2 = w_0^2 \left[1 + \left(\frac{z}{z_0}\right)^2\right] \quad (14)$$

the radius of curvature of the wavefront at z is:

$$R(z) = z \left(1 + \frac{z_0^2}{z^2}\right) \quad (15)$$

the diffraction length of the beam is:

$$z_0 = \frac{\pi w_0^2}{\lambda} \quad (16)$$

Considering that the sample length is small enough ($L \ll z_0$) that changes in the beam diameter (w) within the sample due to either diffraction or nonlinear refraction can be neglected.

If we consider that the medium have a area where its refraction index is different of the all bulk. Passing through this area, the wave front will undergo a shift phase depending on difference between the refraction index in irradiating area and whole. This phase shift at the focus is:

$$\Delta\Phi_0(z, t) = \frac{2\pi}{\lambda} \Delta n_0(t) L_{eff} \quad (17)$$

Where:

$$\Delta n_0 = n_2 I_0 \quad (18)$$

and

$$L_{eff} = \frac{1 - e^{-\alpha_0 L}}{\alpha_0} \quad (19)$$

with L the sample length and α_0 the linear absorption coefficient.

Following Sheik-Bahae's theory ^[30], now will describe process for β index determination.

The TPA mechanism occurs when the photon energy, $h\omega$, is larger than one-half the band-gap energy, E_g ($E_g < 2h\omega < 2E_g$).

The equation describing TPA (a third order response) of a beam of irradiance I_0 as a function of depth z in a material is

$$\frac{dI}{dz} = -(\alpha_0 + \beta I) I_0 \quad (20)$$

where β is the TPA coefficient, and the equation includes residual linear absorption of coefficient α_0 . Once absorption has taken place, electrons are excited across the energy gap and are available to subsequently absorb linearly.

The coefficients of nonlinear absorption can be easily calculated from transmittance curves.

In fact, for a Gaussian beam we can obtain the transmitted intensity (eq. 20) for sample; this will be proportional to transmitted power ^[30]:

$$P(z, t) = P_i(t) e^{-\alpha L} \frac{\ln [1 + q_0(z, t)]}{q_0(z, t)} \quad (21)$$

For normalized transmittance we have:

$$T(z) = \frac{\ln[1 + q_0(z)]}{q_0(z)} \quad (22)$$

For $|q_0| < 1$, this transmittance can be expressed in terms of the peak irradiance in a summation form more suitable for numerical evaluation:

$$T(z) = \sum_{n=0}^{\infty} \frac{[-q_0(z, 0)]^n}{(n+1)^{3/2}} \quad (23)$$

Where

$$q_0(z) = \frac{\beta I_0 L_{eff}}{1 + \left(\frac{z}{z_0}\right)^2} \quad (24)$$

Thus, once an open aperture Z-scan is performed, the nonlinear absorption coefficient β can be clearly determined.

M. Yin et al.^[31], have described a theory in which, even if that both open- and closed-aperture Z-scans must be performed, it is possible to gain NLR index (n_2) and TPA coefficient (β) only from a single closed-aperture Z-scan.

They have found that, for laser beams with circular symmetry and low irradiances, the normalized transmittance $T(z)$ can be expressed, by

$$\begin{aligned} T(z) &= \frac{\int_{-\infty}^{\infty} dt \int_0^{r_a} |E_d(z, r, t)|^2 r dr}{\int_{-\infty}^{\infty} dt \int_0^{r_a} |E_d(\Delta\Phi = 0, \Delta\Psi = 0)|^2 r dr} \\ &= 1 + \frac{\int_{-\infty}^{\infty} |E_{d0}(t)|^2 f(t) dt \int_0^{r_a} T_1 r dr}{\int_{-\infty}^{\infty} |E_{d0}(t)|^2 dt \int_0^{r_a} T_0 r dr} \Delta\Phi_0 \\ &\quad + \frac{\int_{-\infty}^{\infty} |E_{d0}(t)|^2 f(t) dt \int_0^{r_a} T_2 r dr}{\int_{-\infty}^{\infty} |E_{d0}(t)|^2 dt \int_0^{r_a} T_0 r dr} \Delta\Psi_0 \\ &= 1 + T_{\Delta\Phi}(z) + T_{\Delta\Psi}(z) \end{aligned} \quad (25)$$

where $T_{\Delta\Phi}$ originating from NLR is an odd function of z ; and $T_{\Delta\Psi}$ caused by TPA is an even function of z .^[31] By considering the on-axis Z-scan, and Gaussian beam in the low-irradiance limit, the two nonlinear terms in eq. 25 can be expressed as:

$$T_{\Delta\Phi}(x) = - \frac{4x}{(x^2 + 9)(x^2 + 1)} \Delta\Phi_0 \quad (26)$$

$$T_{\Delta\Psi}(x) = - \frac{2(x^2 + 3)}{(x^2 + 9)(x^2 + 1)} \Delta\Psi_0 \quad (27)$$

where $x = z/z_0$ and

$$\Delta\Psi_0 = \frac{\beta I_0 L_{eff}}{2} \quad (28)$$

so replacing eq. 17 and 28 to eq. 26 and 27, we obtain eq. 25 as:

$$T(x) = 1 - \frac{8\pi}{\lambda} \frac{n_2 I_0 L_{eff} x}{(x^2 + 9)(x^2 + 1)} - \frac{2\beta I_0 L_{eff} (x^2 + 3)}{(x^2 + 9)(x^2 + 1)} \quad (29)$$

3.5.2.2 Thermal Lens

When a light beam illuminates an absorbing medium, radiationless process, with characteristic time of ms, converts the absorbed light into heat. The refractive index depends, among other factors, on temperature.

An increment ΔT of the temperature induces a change $\Delta n = (dn/dT) \Delta T$ in the refraction index^[32], where the parameter dn/dT is the thermo-optical coefficient.

In this framework, a beam with a Gaussian-shaped intensity profile induces a thermal lens in the medium. The characteristics of this lens depend on the medium, particularly the thermal conductivity and the thermo-optical coefficient. Although other techniques were used to study nonlinear optical effects of thermal origin, the single-beam Z-scan technique is attractive because of its simplicity and sensitivity in measuring both, the magnitude and sign of the thermo-optical coefficient and the thermal conductivity. In this technique, a polarized Gaussian beam is focused to a narrow waist by a lens and a sample is moved through the focal point. The transmittance T of an iris, centered in the z-axis (propagating axis of the laser beam) in the far field, is measured as a function of the position of the sample along the z-axis. In the parabolic approximation of the induced thermal lens^[33], the amplitude of the Z-scan signal is given by the dimensionless parameter θ written as

$$\theta = \frac{2.303 P A}{\lambda \rho C_p D} \left(-\frac{dn}{dT} \right) \quad (30)$$

where P is the power of incident laser beam (W), A is the linear optical absorption, D is the Thermal diffusivity, λ is the laser wavelength (nm), ρ is the density (g/cm^3) and C_p is Specific heat ($\text{J/g}\cdot\text{K}$). The formation of the thermal lens is characterized by the time constant t_c given by

$$t_c = \frac{\omega^2}{4D} \quad (31)$$

where ω is the waist of the laser beam in the sample's position, D is the Thermal diffusivity, respectively.

3.5.3 Experimental setup: The Z-scan technique

All the following measurements for the determining of the TPA and NLR have been carried out with Z-scan technique.

In this technique, a polarized Gaussian laser beam, propagating in the z -direction, is focused to a narrow waist. The sample is moved along the z -direction and the transmitted intensity is measured through a finite aperture *in the far field* as a function of the sample position z ; measured with respect to the focal plane. As the sample moves through the beam focus (at $z = 0$), self-focusing or -defocusing modifies the wave front phase, thereby modifying the detected beam intensity (Fig. 3.49)

To figure out how the Z-scan transmittance as a function of z is related to the nonlinear refraction of the sample, let us assume a medium with a negative nonlinear refraction index and a thickness smaller than the diffraction length of the focused beam. This can be considered as a thin lens of variable focal length. Beginning far from the focus ($z < 0$), the beam irradiance is low and nonlinear refraction is negligible. In this condition, the measured transmittance remains constant (i.e., z -independent). As the sample approaches the beam focus, irradiance increases, leading to self-lensing in the sample. A negative self-lens before the focal plane will tend to collimate the beam on the aperture in the far field, increasing the transmittance measured at the iris position. After the focal plane, the same self-defocusing increases the beam divergence, leading to a widening of the beam at the iris and thus reducing the measured transmittance. Far from focus ($z > 0$), again the nonlinear refraction is low resulting in a transmittance z -independent. A pre-focal transmittance maximum (peak), followed by a post-focal transmittance minimum (valley) is a Z-scan signature of a

negative nonlinearity. An inverse Z-scan curve (i.e., a valley followed by a peak) characterize a positive nonlinearity (Fig.3.49).

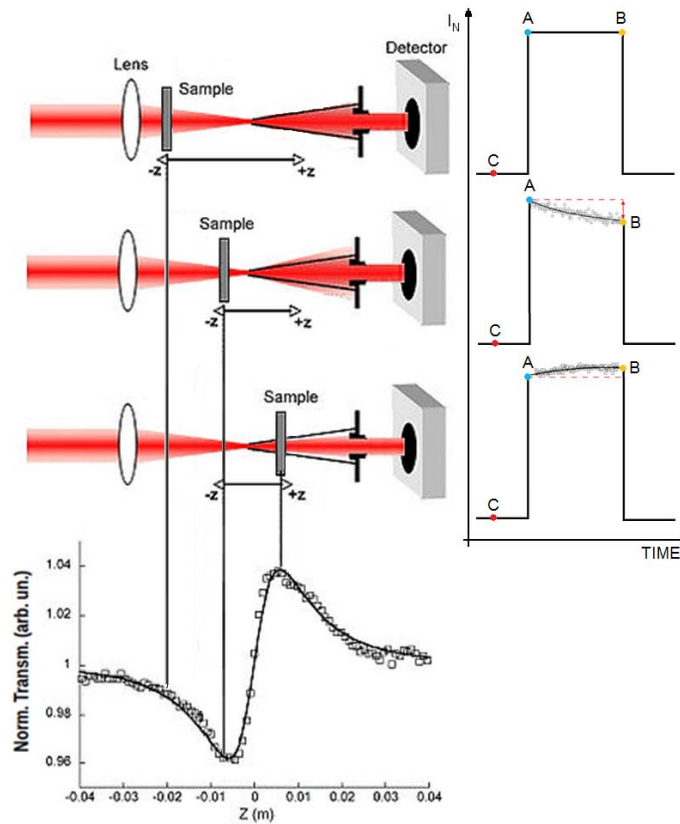


Fig. 3.49 Z-scan (CA)mode, in positive nonlinearity

Beside is possible to observe how the transmittance change as a function of z , following this equation:

$$T_N(z) = \frac{T_B(z) - T_C}{T_A(z) - T_C} \quad (32)$$

Z-scan can be performed in two ways. In the open-aperture (OA) Z-scan method, which is only sensitive to nonlinear absorption, all the transmitted light is measured by detector (Fig. 3.50). In the closed-aperture (CA) Z-scan version, which is sensitive to nonlinear absorption as well as the nonlinear refractive index, only part of the transmitted light is detected by detector (Fig. 3.49). To extract the NLR index, one must take the NLA value that is obtained from an open-aperture Z-scan, into the account in the closed aperture Z-scan modeling.

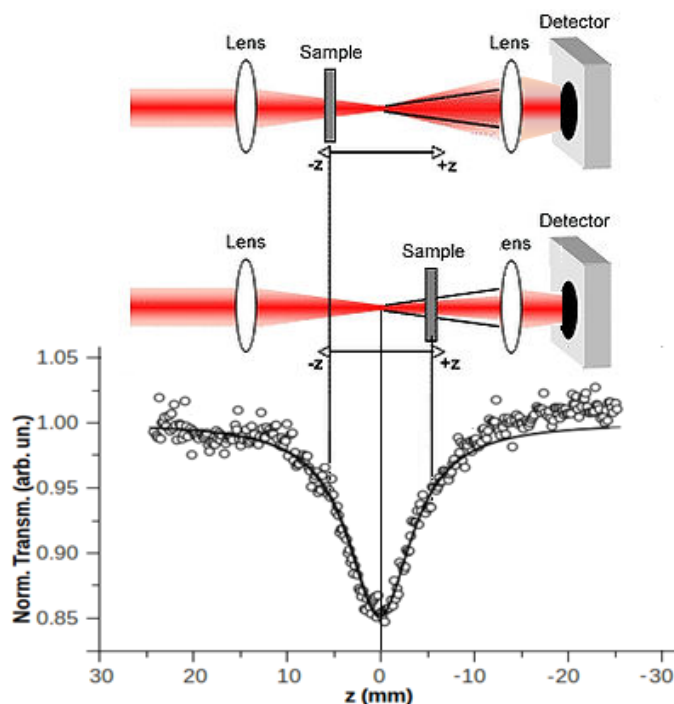


Fig. 3.50 Z-scan (OA) mode

The Z-scan experiment was performed with a mode-locked Ti:Sapphire laser (Chameleon Ultra II, Coherent) as a light source. The beam wavelength and pulse width were $\lambda=800\text{nm}$ and $\tau=280\text{fs}$, respectively. The on-axis peak intensity at focus was $I_0=11\text{GW}/\text{cm}^2$ and the beam waist was $\omega_0=20\mu\text{m}$. The system generates the femtosecond pulses at a frequency of 80 MHz. A Pockels cell based pulse picker (model 305, Conoptics) was used to reduce the pulse frequency to the range from 100 Hz to 1 MHz.

The on-axis transmitted light was collected by the 0.4 mm diameter aperture of an ultra fast photodetector (SV2-FC, Thorlabs) to conduct the closed aperture Z-scan configuration experiment. The open aperture configuration experiment was performed using a focusing lens to converge all the transmitted light to inside the aperture of the ultra fast photodetector (Fig. 3.51).

All the experiments were performed at $T=22^\circ\text{C}$, and the absorption spectrum of the sample was obtained by spectrophotometry.

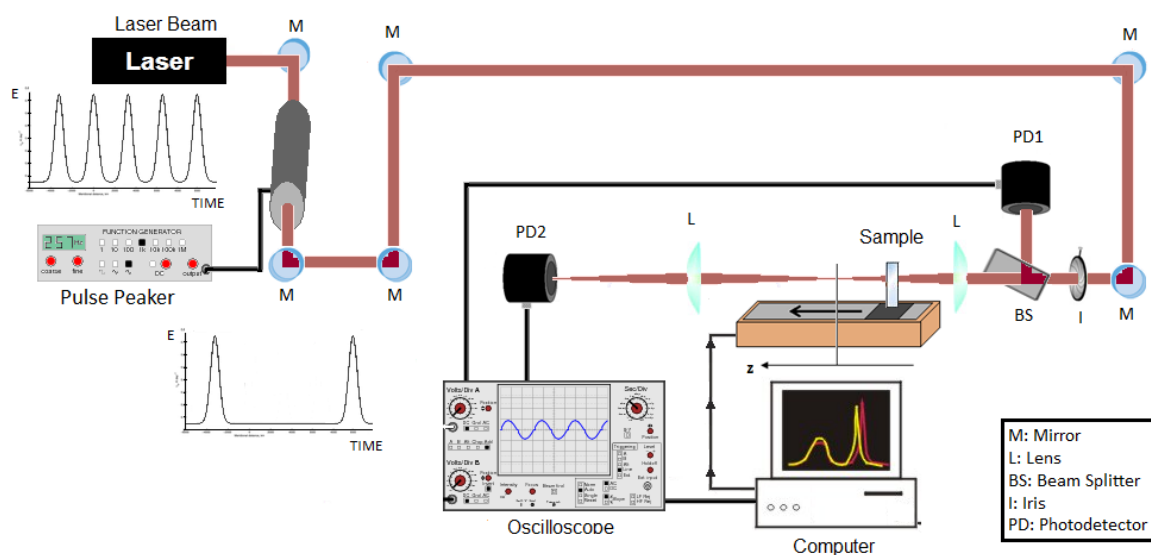


Fig. 3.51 Experimental configuration of Electronic Z-scan technique

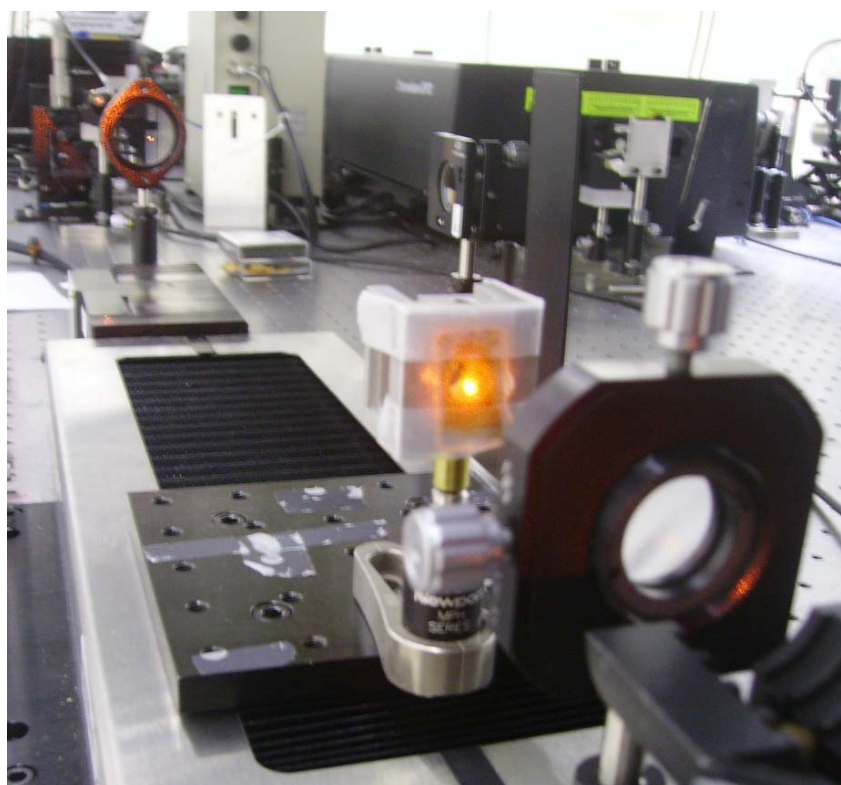


Fig. 3.52 Sample in Electronic Z-scan technique

The Z-scan apparatus used here is the usual one described elsewhere. ^[34,35] Our setup uses two laser beams ($\lambda=532\text{nm}$ and $\lambda=405\text{nm}$). For 532nm measurements was used a cw Millennia II laser from Spectra Physics ($\lambda= 532 \text{ nm}$) (Fig. 3.54). For 405nm was used CUBE 405-100C from Coherent ($\lambda=405\text{nm}$).

A mechanical chopper is used to modulate the laser beam incident on the sample. The beam waist of the laser at focus ω_0 was about $30\mu\text{m}$ and the power of the laser incident on the sample was 167 mW for 532nm and 64 mW for 405nm .

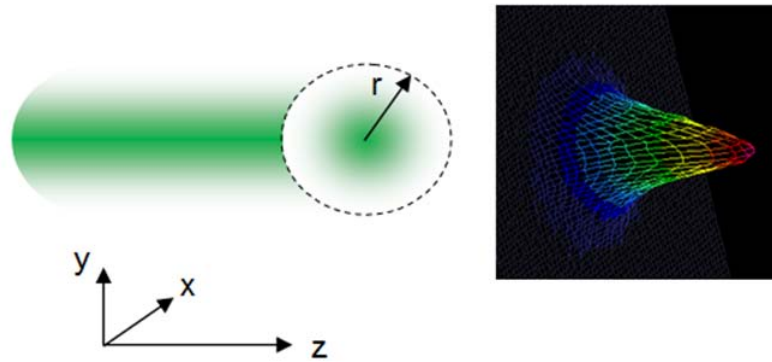


Fig. 3.53 Gaussian profile

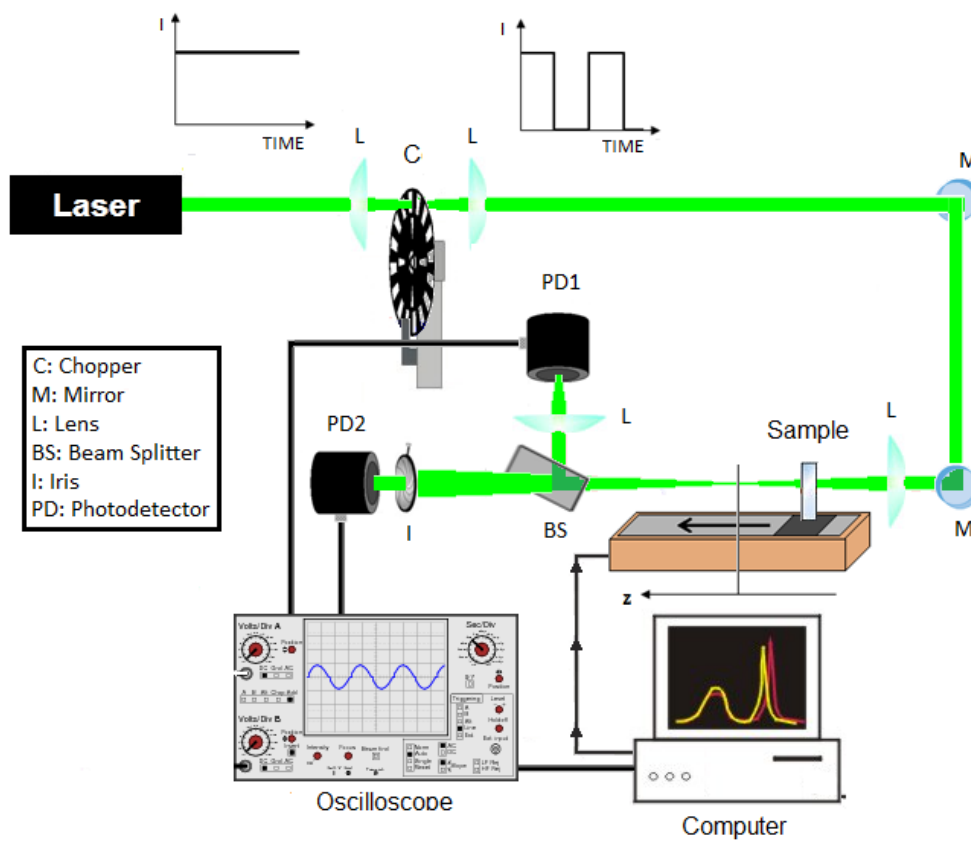




Fig. 3.54 Experimental configuration of Thermal lens in Z-scan technique

3.5.4 Results and discussion

Although light absorption is a local process, the diffusion of heat gives rise to a nonlinear optical phenomenon. This indirect nonlinear phenomenon is common to all absorbing materials. In fact the energy absorbed is immediately converted into heat and when itself is transferred to the sample gives rise of nonlinear values.

In the first part will be taken account nonlinear optical study of ferrofluids, then move on to discussion of lyotropic systems based on cholesterol.

Femtoseconds pulsed laser, mainly generate electronic nonlinear optical phenomena, in which there are basically “ultrafast” electronic bound process and “excited state” processes. NLA and NLR are well observed in this kind of arrangement.

The choice of the incident laser wavelength is critical to obtain reliable values of nonlinear optical parameters, in fact it can't observe TPA where linear absorption exist (higher Energy). Observing the absorption spectrum of oil- and water-based ferrofluids, it possible to note that at 800nm the linear absorption of the samples is small, so the TPA occurs near the maximum of the absorbance curve (400nm) (Fig. 3.46).

In search of the optimal experimental conditions to obtain the relevant data it was decided to observe the behavior of ferrofluids, in samples with $L=50\mu\text{m}$ filled with 0.36% of Water and Oil-based ferrofluid, misured in a OA mode.

Fig. 3.55 show at high pulsed frequency, respectively little (water-based) and huge (oil-based) β values. It means that for EMG 509 samples, we have to use high rate pulse to observe small variations. So in the next measurements, it will considered only the oil-based EMG911 ferrofluid

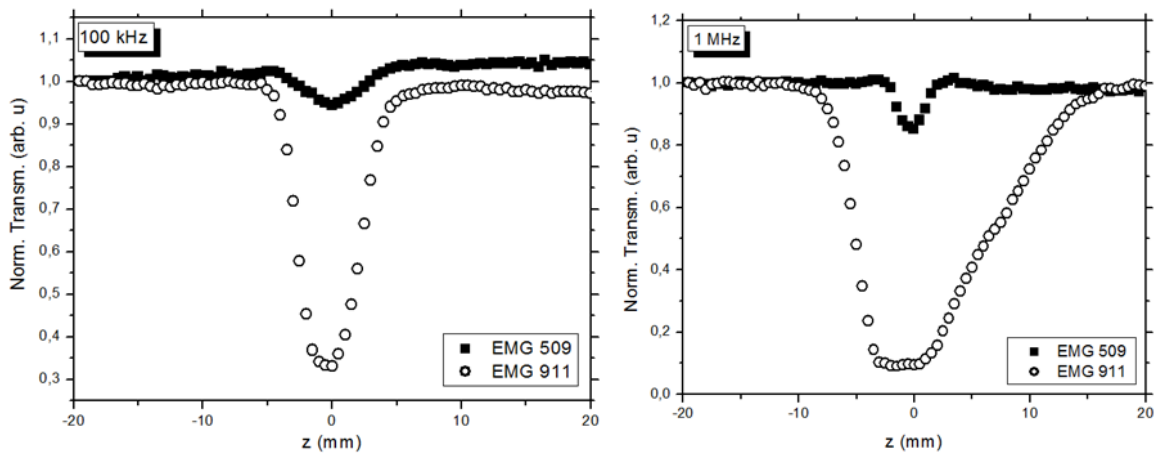


Fig. 3.55 Comparison of TPA measurements of EMG509 and EMG911 at 2 frequency pulses

In figure 3.56a and 3.56b shown typical results of the z-scan measurement which corresponds to the far-field normalized transmittance as a function of the distance from the lens focus of a ferrofluid sample respectively in OA and CA Z-scan method. The open-aperture curve in figure 3.56a exhibited a normalized transmittance valley, indicating the presence of nonlinear absorption in the solution. The data were analyzed by using the procedure described above and the nonlinear absorption coefficient β is obtained by fitting (solid line) the experimental z-scan plot to equation 23. The obtained value of nonlinear absorption coefficient β (extract from equation 28), is 2,85 cm/GW.

The glass substrate had negligible nonlinear optical response at 800 nm, which was measured by the same method and hence the nonlinear response observed, resulted from the ferrofluid sample.

The closed-aperture curve in figure 3.56b, exhibited a peak-to-valley shape, indicating a negative value of the nonlinear refractive index n_2 . The nonlinear refractive index is estimated by theoretically fitting the experimental data. The solid curve in figure 3.56b is the theoretical fit and the nonlinear refractive index n_2 , evaluated using equations 17, is $-2.95 \times 10^{-14} \text{ cm}^2/\text{W}$.

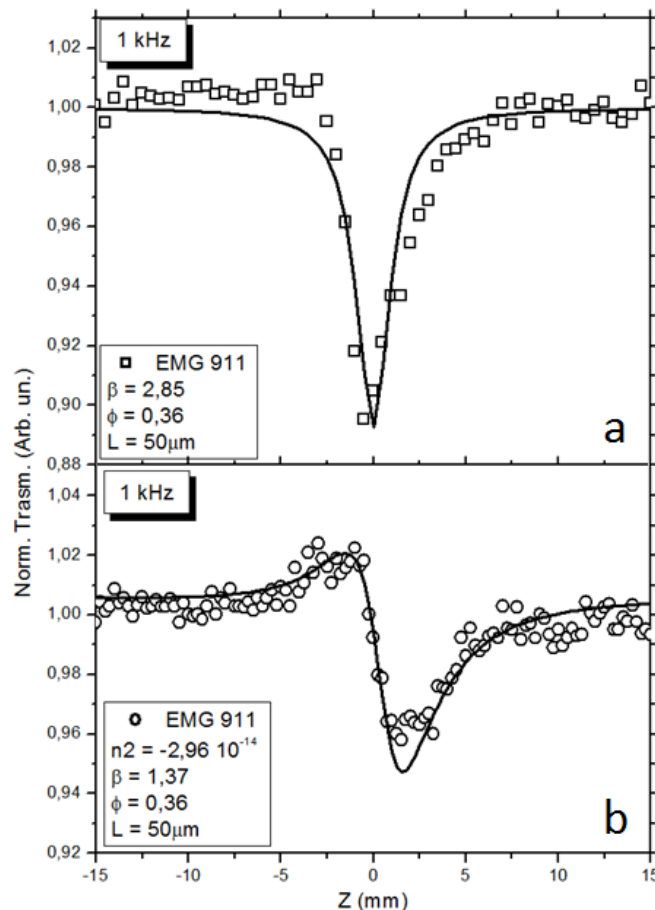


Fig. 3.56 Z-scans transmittance curves for oil-based Ferrofluid EMG 911. Square (a) and circle (b) points represent experimental data obtained with 1kHz pulse rate respectively for TPA and NLR. Solid line represents the fit curve assuming $z_R=1,7\text{mm}$ and $1,2\text{mm}$.

For samples with sizeable refractive and absorptive nonlinearities, closed-aperture measurements contain contributions from both the intensity-dependent changes in the transmission and in refractive index^[30,31], as shown in eq. 29. It may be noted that the α value used in the experiments is $5,23 \text{ cm}^{-1}$ and ΔZ_{p-v} are between 1-2 z_0 , that are reasonable experimental values.

Considering only the TPA in EMG911 sample, it was measured the nonlinear absorption at different frequencies of pulse (from 100Hz to 1MHz) (Fig. 3.57a).

It was observed that high pulse rate, generate pronounced valleys and then huge values of TPA index (β). Experimental data show, in fact, that for $T_N < 0.6$ not only electronic effects occurs.

This phenomena was confirmed by Fig 3.57b where at frequency lower than 10kHz, the values of nonlinear absorption are almost the same. Increasing the frequency of pulses (up to 1000 kHz), the β values increased rapidly, due to thermal effect.

The mechanisms responsible for this trend are maybe due to Soret effect ^[36-38], Thermal effects^[33] (because high repetition frequency slowly heating the focal region with a subsequent decrease in the density of the medium and in the refractive index) or Free Carrier Absorption (**FCA**) ^[39].

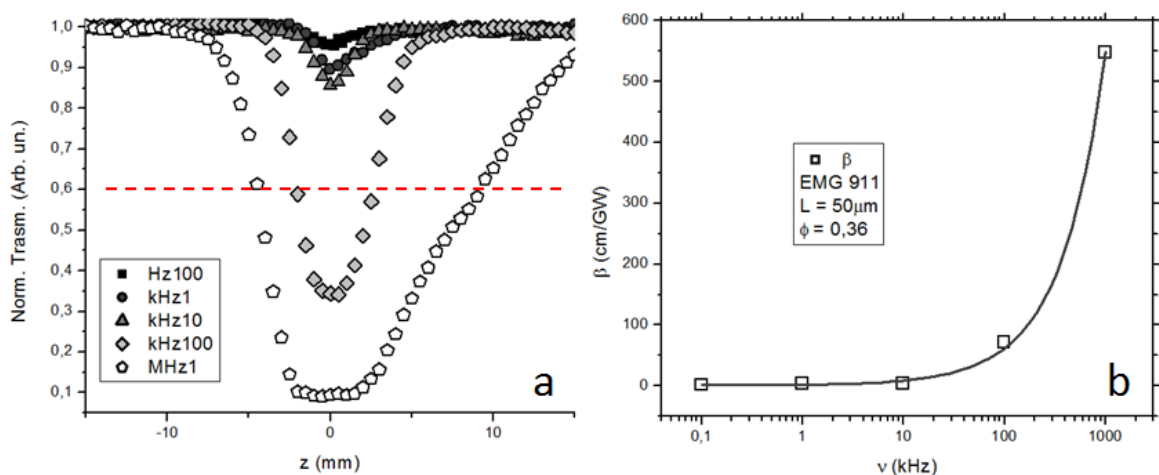


Fig. 3.57 a) Z-scans transmittance curves for different rate pulses of oil-based Ferrofluid EMG 911; b) β values for different rate pulses

To better observe the characteristics of ferrofluid solutions in a wide frequency range, we have used 200 μm samples thickness with 4 times diluted solutions (0.09%). In this way, we have studied the solution behaviors in a different pulsed frequency (from 40kHz to 460kHz) and evaluate its β and n_2 values. The nonlinear indices of the other sample have been measured in the same approach described previously.

In the series of experimental investigations of the optical nonlinearities of the ferrofluid solution described below, we used radiation with a low pulse repetition

rate to exclude the effect of the thermal storage or FCA processes that were observed in the case of pulses with a high repetition frequency.

Figure 3.58a shown that increasing the frequency of pulse from 40kHz up to 460kHz the T_N was above 0.6.

Observing β data for different rate pulse (Fig. 3.58b), we can note how, raising repetition pulse frequency from 40kHz to 460kHz, there are a low increase of β values. In the first column of Table 3.13 (No A) are summarized β values plotted in Fig. 3.58b.

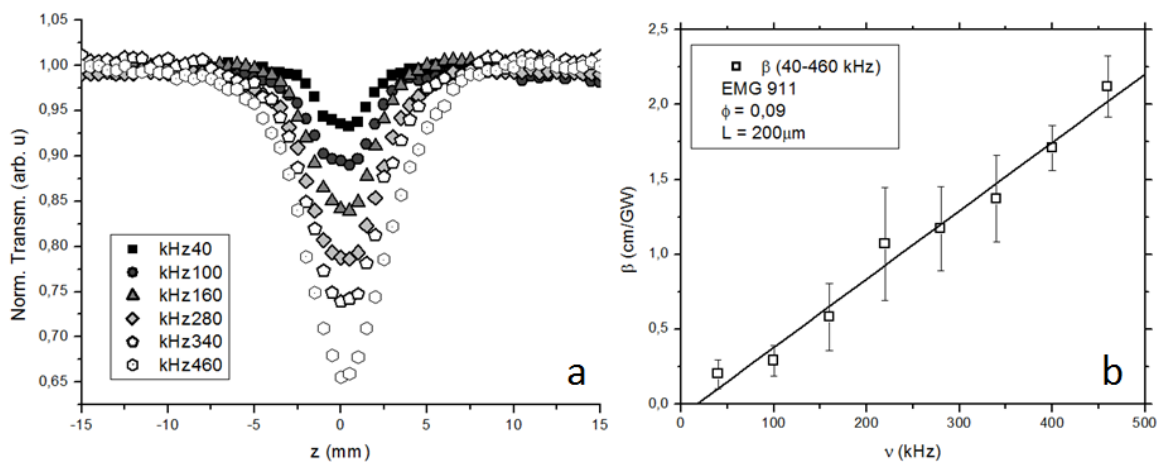


Fig. 3.58 a) Z-scans transmittance curves for different rate pulses of oil-based Ferrofluid EMG 911; b) β values for different rate pulses ($L=200\mu\text{m}$ $\phi=0.09\%$)

To verify if that graphic trend is only due to a thermal effect, we have done the same experiment placing in front of the sample different optical filter (from 0.1% to 0.35%), so that reduce partially the incident light on the sample (from 10.67 GW/cm^2 to 5.54 GW/cm^2) and avoid warm phenomena on irradiating area.

Graph in figure 3.59 shown how for same pulse rate, reducing the incident light on sample, the β values are almost invariable; this linear tendency keep on increasing the pulse frequency. The results are summarized in Table 3.13.

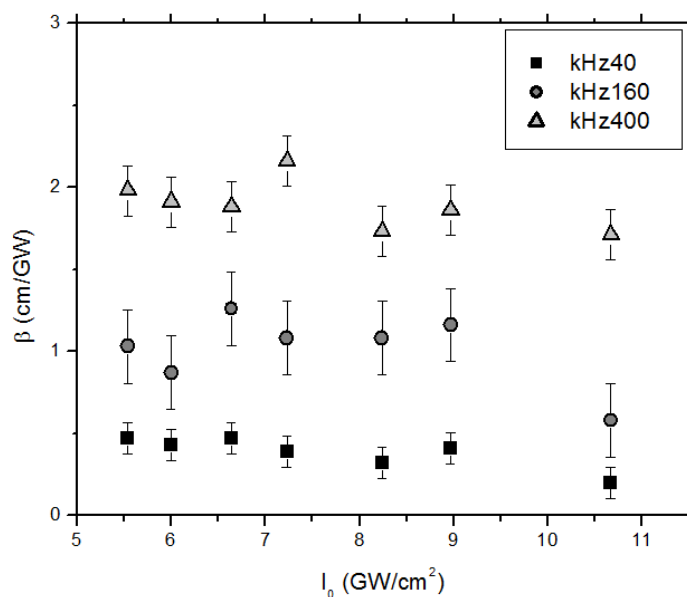


Fig. 3.59 β data for different rate pulses and values of incident light

I_0 V_{pulse}	No A	A 0.1	A 0.15	A 0.2	A 0.25	A 0.30	A 0.35
	10.67 (GW/cm ²)	8.97 (GW/cm ²)	8.24 (GW/cm ²)	7.23 (GW/cm ²)	6.64 (GW/cm ²)	6.00 (GW/cm ²)	5.54 (GW/cm ²)
40 kHz	0.2	0.41	0.32	0.39	0.47	0.43	0.47
100 kHz	0.29	0.52	0.47	0.39	0.47	0.52	0.6
160 kHz	0.58	1.16	1.08	1.08	1.26	0.87	1.03
220 kHz	1.07	1.51	1.71	1.80	1.81	2.00	2.26
280 kHz	1.17	1.68	1.71	1.51	1.41	1.65	2.07
340 kHz	1.37	1.86	1.83	1.40	1.65	1.22	1.98
400 kHz	1.71	1.86	1.73	2.16	1.88	1.91	1.98
460 kHz	2.12	2.61	2.59	2.67	2.43	2.43	2.73

Table 3.13 Different values of β as a function of pulse frequency and the incident light

With regard the experiments with cholesterol were used continue laser beams, that work at wavelengths lower than the previous experiment. In particular the aim is to study the thermal properties (thermal diffusivity) of materials and how these will vary at different wavelengths.

As already observed in previous studies^[29], LDL, through thermal-lens z-scan technique thanks to its own characteristics, exhibit a signal characteristics of absorbing media with negative thermo-optical coefficient, while oxidized LDL did not show any effect in the same conditions. (Fig. 3.60a)

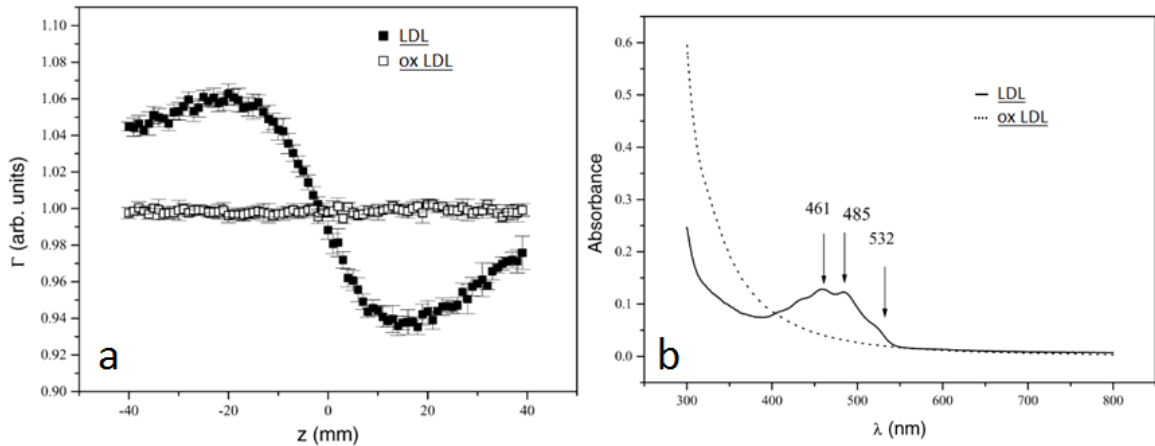


Fig. 3.60 a) Z-scans transmittance curves and b) Absorption spectra for LDL and oxLDL

These results could be partially justified observing the absorption spectra (Fig. 3.60b). LDL exhibits a broad absorption band with two peaks at 461nm and 485nm and a shoulder at about 532nm, while oxLDL does not exhibit any particular absorption peak (3.60b).

To observe if LDE show also similar characteristics to LDL, it was subjected to spectrophotometric analysis. The graph in Fig. 3.61 shows that at 405nm to 532nm there is a slight linear absorption of the sample. Therefore it was decided to measure the thermal diffusivity of the LDE sample, in these two wavelengths

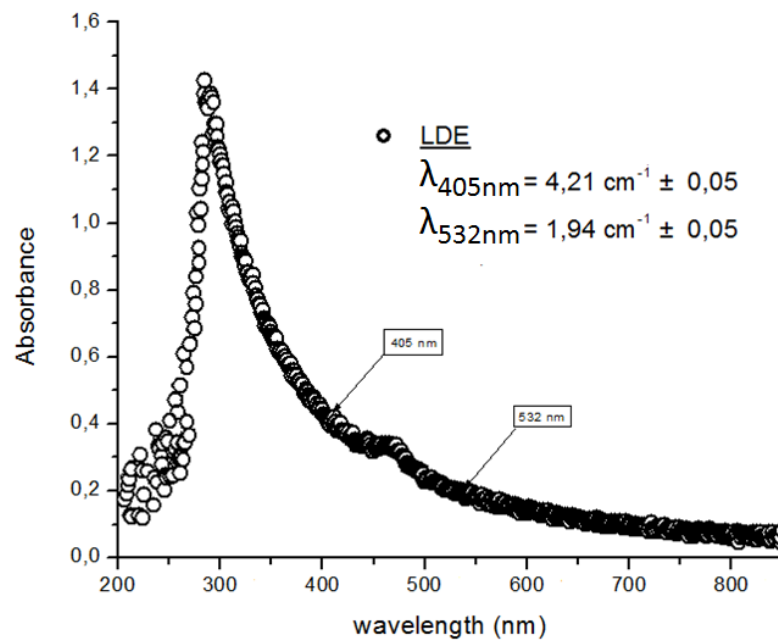


Fig. 3.61 Absorption spectra for LDE

Before to conduct the experiments this sample was kept in the dark, at controlled temperature to avoid degradation due to light or high temperature stress. For these reasons the experiments were done separately and the time exposure of the sample to the laser beam was just enough to conduct the experiments. This result shows that the time evolution of θ observed in experiments is not due to eventual long-term sample degradation induced by the interaction with the laser beam.

Experiments conducted at a wavelength of 405nm (Fig. 3.62) and 532nm (Fig. 3.63) gave small signals, but nevertheless may be useful to determinate thermal diffusivity values.

They show a characteristics Z-scan signal with negative (dn/dT).

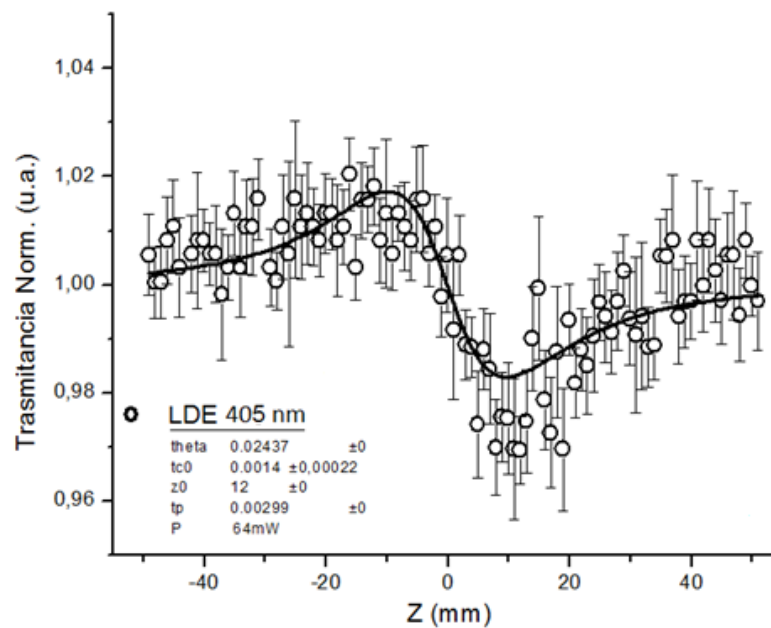


Fig. 3.62 Z-scan signal for LDE at 405nm

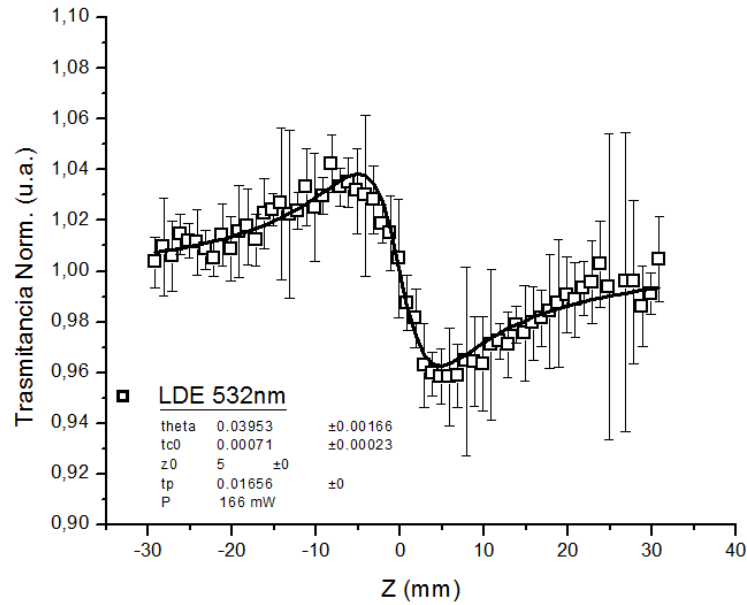


Fig. 3.63 Z-scan signal for LDE at 532nm

Extracting the values of theta from the curves, knowing the values from the experimental conditions and of the intrinsic material (Table 3.14), and then substituting the values into the equation 30 we have the experimental value of thermal diffusivity. For comparison, we extracted the theoretical value of thermal diffusivity using the equation 31.

LDE	θ	Pot (W)	Abs	dn/dT (K^{-1})	λ (cm)	ρ (g/cm^3)	C_p (J/gK)	tc_0 (s)	ω_0 (cm)	tp (s)
405 nm	0.024	0.064	0.421	$-1.50 \cdot 10^{-4}$	$4.05 \cdot 10^{-5}$	0.985	3.45	$1.4 \cdot 10^{-3}$	$3.93 \cdot 10^{-3}$	$2.99 \cdot 10^{-3}$
532 nm	0.0395	0.167	0.194	$-1.50 \cdot 10^{-4}$	$532 \cdot 10^{-5}$	0.985	3.45	$0.71 \cdot 10^{-3}$	$2.91 \cdot 10^{-3}$	$1.66 \cdot 10^{-3}$

Table 3.14 Experimental and intrinsic parameters for the determination of thermal diffusivity at 405nm and 532nm

Observing the experimental and theoretical values, extrapolated from the equations 30 and 31, is noted that they do not match. Therefore, further studies are needed to see if there are errors in the approach experimentally.

3.5.5 Conclusion

In summary, we have studied feature of the Z-scan curve of oil- and water-based ferrofluid (EMG911 and EMG509) under exposure of femtosecond laser pulses at 800nm, to determinate optical nonlinearities. We have found that water-based ferrofluid have small value compared to oil-based ferrofluid, and the last one for high frequency of pulsed light, considerable phenomena occurs (thermal or electronic) in thin sample. Using larger sample, it is possible to observe better electronic effects that takes place on ferrofluids in wide frequency range.

Especially it is revealed that measured values of β and n_2 are no due to light intensity coming on the sample, but are originated to frequency rate pulse that no allows relaxing of samples. For this reason the excited electrons remain in a upper energy level (or intermediate one), for pulses faster and faster in time.

Furthermore, it was observed that samples of LDE show a small characteristics Z-scan signal with negative (dn/dT). Therefore, it is possible to extract the value of thermal diffusivity experimental and theoretical, that require further investigation. These systems can be used in the foreseeable future as a **DDS**.

References

- [1] S. Safran, N.A. Clark; *“Physics of Complex and Supramolecular Fluids”*, EXXON Monograph Series; Wiley: New York, (1987).
- [2] R.C. Maranhão, B. Garicochea, E.L. Silva; *Cancer Res.*; 54:4660–4666 (1994)
- [3] A.M. Carmona-Ribeiro; *Int J Nanomedicine*;5: 249–259. (2010)
- [4] R.C. Maranhão, E.R. Tavares, A.F. Padoveze, C.J. Valduga, D.G. Rodrigues, M.D. Pereira; *Atherosclerosis.*; 197:959–966 (2008)
- [5] R.C. Maranhão, S.R. Graziani, N. Yamaguchi; *Cancer Chem Pharmacol.* 49:487–498 (2002)
- [6] L.A. Pires, R. Hegg, C.J. Valduga, S.R. Graziani, D.G. Rodrigues, R.C. Maranhão; *Cancer Chemother Pharmacol.* 63:281–287 (2009)

- [7] M.L. Dias, J.P. Carvalho, D.G. Rodrigues, S.R. Graziani, R.C. Maranhão; *Cancer Chemother Pharmacol.*;59: 105–111 (2007)
- [8] S.R. Graziani, F.A.F. Igreja, R. Hegg; *Gynecol Oncol.*; 85:493–497 (2002)
- [9] I.J. Saremback; *Arterioscler Thromb Vasc Biol.* 28:1879–1881 (2008)
- [10] R.D. Hirata, M.H. Hirata, C.H. Mesquita, T.B. Cesar, R.C. Maranhao; *Biochim Biophys Acta.*, 1437:53–62 (1999)
- [11] R.E. Rosensweig; *Ferrohydrodynamics* (1997)
- [12] C. Scherer, A.M. Figueiredo Neto; *Braz. J. Phys.* 35, 718-727 (2005)
- [13] L.F. Gamarra, E. Amaro, S. Alves, D. Soga, W.M. Pontuschka, J.B Mamani, S.M. Carneiro, G.E.S. Brito, A.M.F. Neto; *J. of Nanoscience and Nanotechnology*, 10: 4145-53, (2010)
- [14] J.R. McCarthy, R. Weissleder; *Adv Drug Deliv Rev*, 60(11): 1241-51, (2008).
- [15] A. Jordan, R. Scholz, P. Wust, H.F. Hling, R. Felix; *J Magn Magn Mater*, 201: 413-19, (1999)
- [16] J. Andreas, S. Regina, M. Klaus; *J Magn Magn Mater*, 225: 118-26, (2001).
- [17] T.K. Jain, M.A. Morales, S.K. Sahoo, D.L. Leslie-Pelecky, V. Labhasetwar; *Molec Pharm*, 2: 194-205, (2005)
- [18] F.Q. Hu, L. Wei, Z. Zhou, Y.L. Ran, Z. Li, M.Y. Gao; *Adv Mater* 18: 2553-56, (2006)
- [19] C. Alexiou, R. Jurgons, R. Schmid, A. Hilpert, C. Bergemann, F. Parak; *J Magn Magn Mater*, 293(1): 389-93, (2005)
- [20] M.H. Kryder; *MRS Bull.*, 21 (9): 17-22, (1996)
- [21] D. Weller, A. Moser; *IEEE Trans. Magn.*, 35: 4423–39, (1999)
- [22] S. Sun, D. Weller; *J. Magn. Soc. Jpn.*, 25: 1434–40, (2001)
- [23] Y.R. Shen, “*The Principles of Nonlinear Optics*”, John Wiley and Sons, New York, (1984)

-
- [24] T.H. Wei, D.J. Hagan, E.W. Van Stryland, W.J. Perry, D.R. Coulter; *Appl. Phys. B* 54: 46 (1992)
- [25] T.F. Boggess, S.C. Moss, W. Boyd, A.L. Smirl; *Opt. Lett.* 9: 291-93, (1984)
- [26] A.A. Said, M. Sheik-Bahae, D.J. Hagan, T.H. Wei, J. Wang, J. Young, E.W. Van Stryland; *J. Opt. Soc. Am. B*, 9: 405 (1992)
- [27] D.R. Bosomworth, H.J. Gerritsen; *Appl. Opt.* 7: 95 (1968)
- [28] N. Mansour, K. Mansour, E.W. Van Stryland, E.W. Soileau; *Journal of Applied Physics*, 67: 1475-77 (1989)
- [29] M. Sheik-Bahae, A.A. Said, E.W. Van Stryland, *Opt.Lett.* 14: 955 (1989)
- [30] M. Sheik-Bahae, A.A. Said, T.H. Wei, D.J. Hagan, E.W. Van Stryland; *IEEE J. Quantum Electron.* 26: 760 (1990)
- [31] M. Yin, H.P. Li, S.H. Tang, W. Ji; *Appl. Phys. B*, 70: 587-91 (2000)
- [32] S.E. Braslavsky, G.E. Heibel; *Chem. Rev.* 92, 1381–1410 (1992)
- [33] C.A. Carter, J.M. Harris; *Appl.Opt.* 23, 476-481 (1984)
- [34] S.L. Gómez, F.L.S. Cuppo, A.M.F. Neto, T. Kosa, M. Muramatsu, R.J. Horowicz; *Phys. Rev. E* 59, 3059–3063. (1999)
- [35] S.L. Gómez, A.M.F. Neto; *Phys. Rev. E* 62, 675–680 (2000)
- [36] C. Soret; *Arch. Sci. Phys. Nat.* 2, 48-61 (1879)
- [37] S.R. de Groot; “*L'Effet Soret, Diffusion Thermique dans les Phases Condensées*” (North- Holland, 1945)
- [38] S. Alves, A. Bourdon, A.M.F. Neto; *J. Opt. Soc. Am. B* 20, 713-718 (2003).
- [39] E.W. Van Stryland, M. Sheik-Bahae, D.J. Hagan; *Prog. Crystal Growth and Charact.* 27, 279-311 (1993)

3.6 Lyotropic liquid crystals as drug delivery system of doxorubicin

The idea to drive a drug within own body up to the target, was always a stimulant challenge for researchers. Thanks to new technologies, every years, new drug delivery systems are created and tested to treat faster and better diseases and so improve the life style.

Drug targeting is a method by which the distribution of drug in the organism is maneuvered in a manner such that its major fraction interacts exclusively with the target tissue at the cellular or subcellular level. This technique mainly is used when surgery may not be possible, for example depending on the location and the involvement of tumors with surrounding tissues. Therefore, the development of techniques that could selectively deliver drug molecules to the diseased site, without a concurrent increase in its level in the healthy tissues of the organism, is currently one of the most active areas of cancer research. In particular, magnetic micro- and nanoparticles are currently recognized as one of the most promising modalities of such carriers. The idea to apply extracorporeal magnets to direct drug-loaded magnetic particles to local sites in the body (a concept which is known as magnetic drug targeting, MDT) was conceived and investigated more than 30 years ago^[1,2]

This technology is based on binding established anticancer drugs with biocompatible magnetic nanocarrier (i.e. ferrofluids) injecting them in a blood stream then concentrate the drug in the area of interest (tumor site) by means the influence of magnetic fields.^[3,4] Besides drug targeting, as mediators for cancer magnetic hyperthermia, as MRI contrast agents, and in bioaffinity assays, magnetic nanospheres and ferrofluids have also been used in numerous biological fields including diagnostics, molecular biology and cell purification.^[5-12]

Magnetic nanoparticles (MNPs) are of relatively low toxicity; according to the literature results the concentration of MNPs equal to 5 mg/mL (10 times higher than any MNPs concentration foreseen to be used for ocular magnetic targeting) does not cause any toxic effect.

The benefits of magnetic drug targeting reside in a tissue-specific release of drugs, in a reduction of side effects and in a local drug action.^[10] The drug can then be released from the carriers either via enzymatic activity or changes in physiological conditions such as pH, osmolality, or temperature.

However, simple direct attachment of drug molecules to the surface of magnetic particles, either by physical adsorption or chemical bonding, can cause serious problems since the drug can be dissociated from the system and released in non-target areas. For these reasons the practice to encapsulated magnetic particles in a colloidal carrier loading^[13] a drug molecules has taken hold.

Among different carriers, magnetoliposomes and magnetic-niosome (magnetic particles encapsulated respectively within liposomes and niosome), mimic biological membranes to the same extent as classical liposomes, appear to be a versatile delivery system due to biocompatibility, chemical functionality and their potential for a combination of drug delivery and magnetic drug targeting.^[14-16]

Magnetically liposomes and niosomes, in fact, could be localized by an external magnetic field to the site whereby they could be successfully an effective targeted approach to cancer therapy.

As seen in chapter 2, liposomes are lyotropic liquid crystals composed mainly by one or more amphiphilic bilayers that form hollow. These liposomes are small deposits which may contain an antigen, an antibiotic, an allergen, a drug or a gene (gene therapy) and can be introduced into the body without causing immune rejection reactions. Naturally fat-soluble drugs will be accommodated in the double layer, water-soluble drugs into the liposome and drugs with mixed properties, between the double layer and the interior.

Magnetic-niosomes are used as drug carriers which can be accumulated in a target tissue by a strong permanent gradient magnetic field local hyperthermia or cancer therapy after intravenous injection.^[17]

The intend of this section is to describe a method for obtaining magneto-niosomes, in which both the magnetic material and Doxorubicin are incorporated into the aqueous space of the vesicles during their preparation. This method has a

number of advantages over above mentioned: it affords relatively high encapsulation efficiency and enables vesicles with magnetic properties.

3.6.1 Materials and Preparation of niosomes

Magnetic-Niosomes containing Doxorubicin were obtained using *a* nonionic surfactants of sorbitan ester class **Tween 60**, and **Pluronic L64**, a copolymers consist of *ethylene oxide* (EO) and *propylene oxide* (PO) blocks arranged in a tri-block structure provided by Sigma-Aldrich.

Doxorubicin was used as model drug and it was purchased from Sigma-Aldrich. The solvents are of high performance liquid chromatography grade.

EMG 707 purchased from Ferrotec was used as water soluble ferrofluid in which are dispersed nanoparticles of Fe_3O_4 with a diameter of 10nm.

For magnetite assay, were used *o-phenanthroline*, *Triton* and *hydroxylamine hydrochloride* purchased from Sigma-Aldrich and used with no further purifications.

Niosomes were prepared by thin film hydration method.^[18,19] Accurately weighed quantities of surfactant were dissolved in chloroform in a round-bottom flask. The chloroform was evaporated under reduced pressure and after its complete removal the hydration of the thin film was carried out under mechanical stirring at 50°C for 30 min with 5 ml of Doxorubicin solution (3.75×10^{-4}) and 5 ml of ferrofluid solution (5.38×10^{-7}). After preparation, the dispersion was left to equilibrate at room temperature overnight to allow the complete annealing and partitioning of the drug between the lipid bilayer and the aqueous phase.

Small unilamellar vesicles (**SUV**) were prepared starting from multilamellar vesicles (**MLV**) by sonication in an ultrasonic bath for 30 min at 50°C. The niosomes purification was also carried out by passing the niosomes suspension through a Sepharose CL-4B gel (Sigma).

The drug-entrapped vesicles were characterized for their shape, size, drug entrapment efficiency, magnetic particles content and in vitro drug release rate.

3.6.2 Qualitative/Quantitative measurement

3.6.2.1 Size and distribution analysis

To observe the particle sizes and polydispersity index of the niosomes were used Dynamic Light Scattering (DLS, 90 Plus Particle Size Analyzer, Brookhaven Instruments Corporation, New York, USA) at $25.0\pm 0.1^\circ\text{C}$ by measuring the autocorrelation function at 90° . The laser was operating at 658 nm. The mean size and standard deviation (\pm S.D.) was directly obtained from the instrument fitting data by the inverse “Laplace transformation” method and by Contin.^[20,21]

The polydispersity index discloses the quality of the dispersion, from values lower than 0.3 for suitable measurements and good quality of the colloidal suspensions. Each experiment was carried out in triplicate.

3.6.2.2 Transmission electron microscopy (TEM)

The morphology of hydrated niosome dispersions was examined by TEM. A drop of dispersion was stratified onto a carbon-coated copper grid and left to adhere on the carbon substrate for about 1 min. The dispersion in excess was removed by a piece of filter paper. A drop of 2% phosphotungstic acid solution was stratified and, again, the solution in excess was removed by a tip of filter paper. The sample was air-dried and observed under a ZEISS EM 900 electron microscope at an accelerating voltage of 80 kV.

3.6.2.3 Drug entrapment efficiency

The percent of Doxorubicin encapsulation efficiency (E%) was expressed as the percentage of the drug entrapped into purified niosomes referred to the total amount of drug that is present in the non-purified sample. It was determined by diluting 1 mL of purified and 1 mL of non-purified niosomes in 25 mL of methanol, followed by the measurement of absorbance of these solutions at the Doxorubicin wavelength. This procedure is necessary to break the niosomal membrane. Absorption spectra were recorded with a UV±VIS

JASCO V-530 spectrometer using 1 cm quartz cells. Each experiment was carried out in triplicate.

3.6.2.4 Assay of magnetite

The amount of encapsulated magnetite was determined based on ferrous ion by using *o*-phenanthroline as follows.^[22] A purified and non-purified niosomal samples (0.1 mL) was mixed with 0.1 mL of Triton X-100 solution (5%, v/v), before ionizing the magnetite by adding 0.5 mL of concentrated HCl; 0.5 mL of hydroxylamine hydrochloride solution (1.44 mol L^{-1}) was then added to reduce ferric ion. After 15 min, 1 mL of *o*-phenanthroline solution (12.6 mmol L^{-1}) was added, the mixture was neutralized with 0.25 mL of 12 mol L^{-1} NaOH, and the pH was adjusted to about 4.0 by adding the necessary volume of 50 mmol L^{-1} citrate buffer. Finally, the absorbance was read at 509 nm with a UV±VIS JASCO V-530 spectrometer.

3.6.2.5 In vitro release studies

The Doxorubicin magneto-niosomes were filled in a dialysis tube (Visking tubing 20/30), manipulated before use in according to Fenton's method.^[23] The niosomal formulations were placed in a beaker containing 50 ml of PBS (pH 7.4), stirred with a magnetic stirrer while keeping the temperature constant at $37 \pm 1^\circ\text{C}$ and samples were withdrawn at specific time intervals and analyzed using UV±VIS JASCO V-530 spectrometer using 1 cm quartz cells at wavelength of 480 nm, typical of Doxorubicin. To maintain a constant volume, an amount of medium equivalent to the volume of sample withdrawn was added to maintain the sink condition. The results were taken as mean values of three runs. The *in vitro* drug release profile of Doxorubicin was studied as control.

3.6.3 Results and discussion

In chemotherapy, the use of magnetic force for targeting a drug to a specific organ or tissue was first proposed on the assumption that magnetic fields are harmless to biological systems. In this light we decide to vehiculate Doxorubicin as

model drug in novel magneto-niosomes, suitable for the parenteral delivery, and to evaluate the physical-chemical properties and the *in vitro* release profile of the drug. Moreover the trypan blue dye exclusion assay and the MTT assay were performed to evaluate their degree of cytotoxicity in order to know the concentrations at which these systems could be used in the pharmaceutical applications.

All prepared niosomes were apparently opalescent, soft on and did not show any changes in appearance, homogeneity when loaded with Doxorubicin as model drug. All formulations were stable at room temperature over about 12 months. No sedimentation, creaming or flocculation can be inferred.

The total concentration of surfactant was 1×10^{-2} M for each formulation as shown in table 3.6-1, in which are resumed particles size and polydispersity index are for each composition.

As reported elsewhere, no cholesterol is required to form vesicles when Tween 60 and Pluronic L64 were used as surfactant.^[24,25] Tween 60 and L64 produced larger vesicles also if no drug was used in the preparation.^[25] In particular Tween 60-based niosomes are bigger than the L64-based ones and loaded vesicles are smaller than the empty ones (Tab 3.15). The presence of Doxorubicin in fact give a reduction in the case of L64-based vesicles: probably this is due to the better interactions between the niosomal matrix, rich of PEO-PPO groups, and the hydrophilic drug that involves an increase of bilayer cohesion and a strong reduction in the vesicles diameter.

Formulation Name	Surfactant (g)	Magnetic particles Mol	Doxorubicin Mol	Diameter (nm)	Polydispersity Index
T60	0.131	2.69×10^{-9}	-	379	0.284
T60-D	0.131	2.69×10^{-9}	1.87×10^{-6}	361	0.268
L64	0.290	2.69×10^{-9}	-	287	0.239
L64-D	0.290	2.69×10^{-9}	1.87×10^{-6}	147	0.254

Table 3.15 Composition, hydrodynamic diameter (nm) and polydispersity index of empty and loaded vesicular systems at 25°C. Values represent mean \pm S.D. (n = 3).

Table 3.15 also present the polydispersity index of different magneto-niosomes compositions. Both empty and loaded systems showed narrow peak, indicating that the vesicle population is relatively homogenous in size.

The Doxorubicin encapsulation efficiencies in magneto-niosomes were found to be about 64% and 55% for T60 and L64 formulations, respectively and were reported in table 3.16. The encapsulation percentage of ferrofluid were similar both for empty and loaded niosomes. The presence of ferrofluid give only a little decrease of the encapsulated drug amount in the niosomal matrix, probably due the a good electrostatic interaction between Doxorubicin and EMG707 ferrofluid.

Formulation Name	E% Magnetite	E% Doxorubicin
T60	98.31	-
T60-D	94.02	64.86
L64	90.01	-
L64-D	87.86	55.60

Table 3.16 Magnetite and Doxorubicin entrapment efficiency (%) of empty and loaded vesicular systems at 25°C. Values represent mean \pm S.D. ($n = 3$).

According to images obtained by TEM it can be inferred that ferrofluid is mainly located in the aqueous compartment of niosomes and that the vesicles were spherical and regular in shape as shown in Fig 3.64.

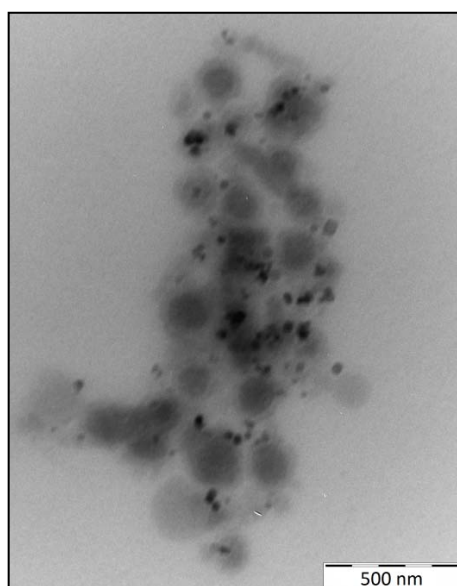


Fig.3.64 Photomicrographs of niosomal formulations as seen by TEM for the sample L64-D

The Doxorubicin release profiles from magnetic-niosomes are shown in Fig 3.65. The drug release behavior was investigated in PBS buffer at pH of 7.4 and temperature of 37°C to maintain the experimental conditions similar to body fluid.

In vitro studies revealed that the cumulative release rates of Doxorubicin from the formulations, in simulate plasmatic fluid, were significantly slower compared to free drug solution. By 3 h, about 94% of drug was released from free solution, while T60 and L64 niosomal formulations showed only about 26% and 39% of release, respectively. When the test is over, about 100% of drug was released from free solution while only 50% of Doxorubicin was released from niosomes.

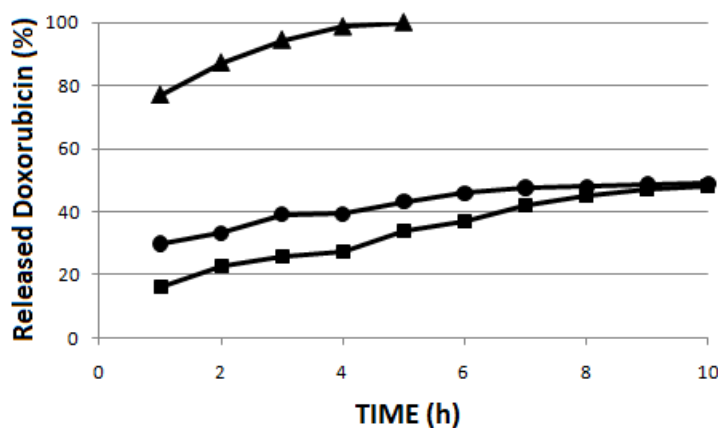


Fig. 3.65. Cumulative amount versus time of released 5FU: (▲) Drug solution, (●) L64-based niosomes, (■) T60-based niosomes

The release experiments clearly indicated that the amount of drug released from niosomal formulations is effectively retarded.

3.6.4 Conclusion

In this work it is described a method for obtaining magneto-niosomes, in which the magnetic material is incorporated into the aqueous space of the vesicles during their preparation (used for the encapsulation of water-soluble drugs). This method has a number of advantages over above mentioned: it affords increase of encapsulation efficiency of Doxorubicin and enables vesicles to be used for magnetic therapy. The presence of drug and ferrofluid in the aqueous core of the

vesicles result in a decrease of systems diameter. In addition being able to delay the release of the drug, it can be used in controlled drug delivery system.

References

- [1] K.J. Widder, A.E. Senyei, D.G. Scarpelli; *Proc Soc Exp Biol Med*, 158, 141 (1978)
- [2] K. Mosbach, U. Schroder; *FEBS Lett*, 102, 112 (1979)
- [3] A. Ito, M. Shinkai, H. Honda, T. Kobayashi, J. Biosci; *Bioeng.* 100, 1 (2005)
- [4] S. Mornet, S. Vasseur, F. Grasset, P. Veverka, G. Goglio, A. Demourgues, J. Portier, E. Pollert, E. Duguet; *Prog. Solid State Chem*, 34, 237 (2006)
- [5] J. Giri, P. Pradhan, V. Somani, H. Chelawat, S. Chhatre, R. Banerjee, D. Bahadur, *J. Magn. Magn. Mater*, 320, 724 (2008)
- [6] G. Schneider, G. Decher, *Nano Lett.* 4, 1833 (2004)
- [7] Y. Jun, Y.M. Huh, J. Choi, J.H. Lee, H.T. Song, S. Kim, S. Yoon, K.S. Kim, J.S. Shin, J.S. Suh, J. Cheon; *J. Am. Chem. Soc*, 127, 5732 (2005)
- [8] J.S. Kim, W. J. Rieter, K.M.L. Taylor, H. An, W. L. Lin, W.B. Lin; *J. Am. Chem. Soc.*, 129, 8962 (2007)
- [9] C. Gruttner, K. Muller, J. Teller, F. Westphal, A. Foreman, R. Ivkov; *J. Magn. Magn. Mater.* 311, 181 (2007)
- [10] T. Neuberger, B. Schopf, H. Hofmann, M. Hofmann, B. von Rechenberg; *J. Magn. Magn. Mater.* 293, 483 (2005)
- [11] X. Zhou, D. Xing, D. Zhu, L. Jia; *Electrochem. Commun*, 10, 564 (2008)
- [12] U.O. Hafeli, J.S. Riffle, L. Harris-Shekhawat, A. Carmichael-Baranauskas, F. Mark, J.P. Dailey, D. Bardenstein; *Mol. Pharm*, (2009)
- [13] F.H. Chen, L.M. Zhang, Q.T. Chen, Y. Zhang, Z.J. Zhang; *Chem. Commun*, 46 8633 (2010)
- [14] M. Gonzales, K.M. Krishnan; *J. Magn. Magn. Mater*, 293, 265 (2005)

-
- [15] P. Pradhan, J. Giri, R. Banerjee, J. Bellare, D. Bahadur; *J. Magn. Magn. Mater.* 311, 208 (2007)
- [16] D. Muller-Schulte, F. Fussl, H. Lueken, M. De Cuyper, In: U. Hafeli, W. Schutt, J. Teller, M. Zborowki, (Eds.), “*Scientific and Clinical Applications of Magnetic Carriers*”, Plenum, Plenum, New York, 517. (1997)
- [17] T. Kubo, T. Sugita, S. Shimose, Y. Nitta, Y. Ikuta, T. Murakami; *Int J Oncol.*, 17, 309 (2000)
- [18] A.D. Bangham, M.M. Standish, J.C. Watkins, *J Mol Bio* 13, 238 (1965)
- [19] L. Tavano, R. Muzzalupo, R. Cassano, S. Trombino, T. Ferrarelli, N. Picci; *Coll Surf B: Biointerfaces* 75, 319 (2010)
- [20] S.W. Provencher, *Comput Phys Commun*, 27, 213. (1982)
- [21] S.W. Provencher, *Comput Phys Commun*, 27, 229 (1982)
- [22] H. Kiwada, J. Sato, S. Yamada, Y. Kato; *Chem. Pharm. Bull.* 34, 4253 (1986)
- [23] R.R. Fenton, W.J. Easdable, H. Meng, E.S.M. Omara, M.J. Mckeage, P.J. Russel, T.W. Hambley, *J Med Chem*, 40, 1090 (1997)
- [24] I.F. Uchegbu, A.T. Florence, *Adv. Colloid Interface Sci.* 58, 1 (1995)
- [25] L. Tavano, R. Muzzalupo, S. Trombino, R. Cassano, A. Pingitore, N. Picci; *Coll Surf B: Biointerfaces* 79, 227 (2010)